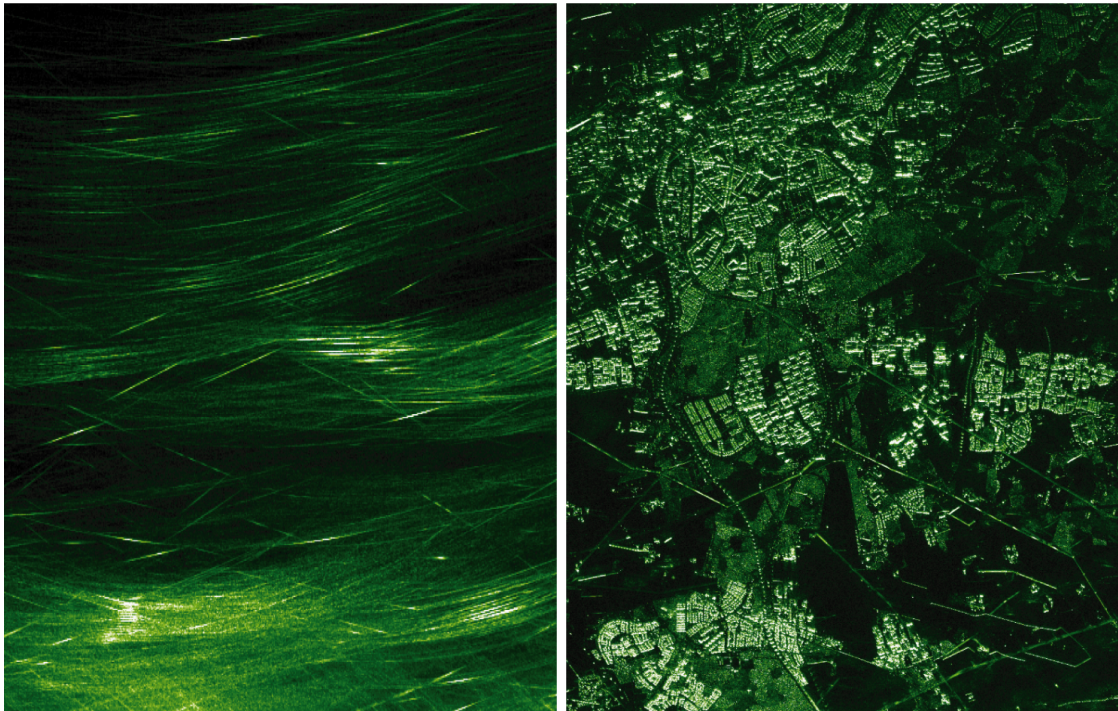




CHALMERS
UNIVERSITY OF TECHNOLOGY



GPS Based Flight Motion Capture

Development and evaluation of a high-performance standalone GPS navigation solution for an airborne radar system

Master's Thesis in Engineering Physics

JONATHAN ARVIDSSON

MASTER'S THESIS 2016

GPS Based Flight Motion Capture

Development and evaluation of a high-performance standalone GPS navigation solution for an airborne radar system

JONATHAN ARVIDSSON



CHALMERS
UNIVERSITY OF TECHNOLOGY

Department of Earth and Space Sciences
CHALMERS UNIVERSITY OF TECHNOLOGY
Gothenburg, Sweden 2016

GPS Based Flight Motion Capture
Development and evaluation of a high-performance standalone GPS navigation solution for an airborne radar system
JONATHAN ARVIDSSON

© JONATHAN ARVIDSSON, 2016.

Supervisor: Dr. Dammert Patrik, SAAB, Surveillance, Future
Examiner: Dr. Thomas Hobiger, CTH, Department of Earth and Space Sciences

Master's Thesis 2016
Department of Physics
Chalmers University of Technology
SE-412 96 Gothenburg
Telephone +46 31 772 1000

Cover: SAR image with the raw video used for creating it from from, FOI.

Typeset in L^AT_EX
Gothenburg, Sweden 2016

GPS Based Flight Motion Capture

Development and evaluation of a high-performance standalone GPS navigation solution for an airborne radar system

JONATHAN ARVIDSSON

Department of Earth and Space Sciences

Chalmers University of Technology

2016

Abstract

The objective of this study is to analyse Global Navigation Satellite System (GNSS) processing performance, to determine if it is possible, to capture the shape of a flight path of an airborne Synthetic Aperture Radar (SAR) radar, with a precision of less than 5 cm during the time it takes to record a SAR image, a SAR-run, without relying on a local reference receiver. The precision of position is achieved with the GNSS processing method Precise Point Positioning (PPP) which uses satellite information corrections and an extended Kalman filter. The data analysed were GPS observations from test flights with the Carabas 3 SAR helicopter including 12 flights with a total of 182 SAR-runs approximately 1 minute in length. The PPP processing was made by the position processing program RTKLIB. The PPP solution was compared with a Real Time Kinematics (RTK) solution. The average precision was 3.5 cm during a SAR-run. PPP is a precise technique with potential of capturing the flight movements. The implementation of a platform model and of Carrier Phase Ambiguity Resolution (CPAR) is expected to improve the performance.

Keywords: KPPP, PPP, RTKLIB, SAR, GPS, GNSS, Motion, Capture

Contents

Glossary	xi
1 Introduction	1
1.1 Reading instructions	1
1.2 Background	2
1.3 Purpose	2
1.4 Objectives	2
1.5 Goals	3
1.6 Scope	3
2 GPS	5
2.1 History	5
2.2 Principles	6
2.2.1 Trilateration	6
2.2.2 Pseudorange	7
2.2.3 Navigation message	9
2.2.4 Carrier Phase Ambiguity Resolution (CPAR)	9
2.2.5 Kalman filter	9
2.3 Errors	11
2.3.1 Ephemeris error	12
2.3.2 Satellite clock error	12
2.3.3 Atmospheric errors	13
2.3.4 Receiver Noise and Resolution	14
2.3.5 Multipath and Shadowing	14
2.3.6 Relativistic Effects	14
2.3.7 Dilution of Precision (DOP)	16
2.3.8 Constellation	16
2.4 Single Point Precision (SPP)	16
2.5 Real Time Kinematics (RTK)	17
2.6 Fixed Base Line (FBL)	17
2.7 Precise Point Positioning (PPP)	18
2.7.1 PPP with CPAR	18
2.7.2 Kalman filtering in PPP	18
2.7.3 International GNSS Service (IGS)	18
2.7.4 RINEX	19
2.8 GPS Velocity Measurements	19

3	Carabas	21
3.1	Synthetic Aperture Radar (SAR)	21
3.2	Flight path shape capture	22
3.3	Carabas GPS implementation	23
3.4	Errors in shape	23
3.4.1	Direction of the error	24
3.4.2	Absolute orientation error	24
3.4.3	GPS shape errors	24
3.4.4	Linear drift error	25
3.4.5	Steadfastness of solution	26
4	Method	27
4.1	Approach	27
4.2	Coordinate systems	29
4.2.1	WGS84	29
4.2.2	Scene Centre coordinates (SC)	29
4.2.3	SAR coordinates	30
4.3	Data collection	31
4.4	Data processing	31
4.4.1	RTKLIB	32
4.5	Data Analysis	33
4.5.1	Single Data Analysis	34
4.5.2	Comparable Data analysis	35
5	Results & Discussion	39
5.1	Full Flight Single Data Analysis	39
5.1.1	Flight path view	40
5.1.2	Position	40
5.1.3	Velocity	42
5.1.4	Acceleration	43
5.1.5	Baseline and Fixed Baseline	44
5.1.6	RTKLIB Quality Flag Standard Deviations	47
5.2	Full flight comparative analysis	47
5.2.1	Position deviation	48
5.2.2	Position dependence on positional deviation	50
5.2.3	Velocity dependence on change of deviation in position	50
5.3	SAR-run analysis	51
5.3.1	Deviation in shape	51
5.3.2	Power spectrum of deviation	55
5.3.3	Standard deviations of shape for all SAR-runs	56
5.4	Sub-run analysis	60
5.4.1	Duration impact on deviation of shape	60
5.4.2	Duration impact on change of bias	65
5.4.3	Duration impact on deviation of flight length	66
5.4.4	Duration impact on deviation of speed	67
5.5	Selected anomalous results from the approach	68
5.5.1	Failed SAR-runs	68

5.5.2 Forward navigation message error	69
6 Conclusion	73
7 Summary	75
Bibliography	77
A Extra Figures	I
A.1 All flights	I
A.2 All flight paths	I
A.2.1 Deviation over time	III
B Extra Tables	XXVII
B.1 Maximum and Standard Deviations for runs	XXVII
B.1.1 IGU	XXVII
B.1.2 IGS	XLI
C Example files	LV
C.1 RTKLIB PPP configuration files	LV
C.2 RTKLIB FBL configuration file	LVII
C.3 Rinex .obs file	LIX
C.4 RTKLIB .pos file	LX

Glossary

.nav	File extension of RINEX files containing navigation message data.
.obs	File extension of RINEX files containing observations e.g. pseudoranges.
.pos	File extension of RINEX files containing receiver positions.
AFT	Aft antenna of the Carabas.
AOD	Age Of Data. Age of navigation message data in satellites.
base	Reference GNSS receiver. For use in differential GNSS techniques together with a rover.
BeiDou	BeiDou Navigation Satellite System. A Chinese GNSS.
BKG	Bundesamt für Kartographie und Geodäsie. German Federal Agency for Cartography and Geodesy.
C/A	Coarse Acquisition. Public GPS ranging code.
CDMA	Code Division Multiple Access. Frequency sharing of several signals using near orthogonal codes.
control segment	GPS control segment. Ground network controlling GPS.
CPAR	Carrier Phase Ambiguity Resolution. GNSS accuracy enhancing techniques using the carrier signal.
CUI	Command-line User Interface. Program operated with text commands.
cycle slip	A jump in calculated position caused by incorrect integer resolution in CPAR.
DCB	Differential Code Bias. A SCP.
DLL	Delay Lock Loop. Method of syncing signal timings.
DOP	Dilution of Precision. Multiplicative GNSS error factor from satellite geometry.
EPE	Estimated Positional Error. Estimated positional error for the GNSS user.

ephemeris	Position of astronomical objects in the sky at a given time or times.
FBL	Fixed Base Line. Orientation processing technique.
FWD	Forward antenna of the Carabas.
Galileo	European GNSS under construction. 12 of 30 satellites in service May 2016.
GLONASS	Globalnaja Navigatsionnaja Sputnikovaja Sistema. Russian GNSS.
GNSS	Global Navigation Satellite System. Collection name for global navigation satellite systems. e.g. GPS, GLONASS and Galileo.
GPS	Global Positioning System. American GNSS.
GrafNav	Professional program package for GNSS processing. Used for computation of RTK and PPP.
IGR	IGS Rapid products. SCP by IGS.
IGS	International GNSS service. Provider of the SCPs IGU IGR and IGS.
IGS	IGS final products. SCP by IGS.
IGU	IGS Ultra-rapid products. SCP by IGS.
INS	Inertial Navigation System.
KPPP	Kinematic Precise Point Positioning. PPP processing for moving receivers.
LNAV	Legacy Navigation Message. GPS message with satellite information.
navigation message	GPS system information message. e.g. LNAV.
NAVSTAR-GPS	Navigation Signal Timing and Ranging Global Positioning System. Commonly referred to as GPS.
passfile	Carabas file containing information of SAR-runs.
PLL	Phase Lock Loop. Method of measuring carrier phase.
PPP	Precise Point Positioning.
PRN	Pseudo Random Noise. Satellite signal identifier.
pseudorange	Distance between transmitter and receiver, quotient of signal transition time and speed of light.
REF	Reference positional solution. GrafNav-RTK or RTKLIB-RTK.
RINEX	Receiver Independent Exchange Format. De facto standard for GNSS receiver data.
RMS	Root Mean Square. Arithmetic mean of the squares of a set of numbers.
rover	User GNSS receiver. Might be used with or without a reference base.

RTK	Real Time Kinematics. Differential GNSS processing.
RTKLIB	Open Source program package for GNSS processing. Used for computation of RTK and PPP.
RTS	Real-time Service. IGS Real time provided SCP for GPS.
SAR	Synthetic Aperture Radar. Technique for creating high resolution radar images through merging of multiple radar recordings.
SAR-run	The flight path during which the Carabas performs all recordings used for one complete SAR image.
SC	Target of a SAR-run.
SCP	Signal Correction Product. Corrections to the ephemeris and clocks of the satellites. e.g. IGS, IGR, IGU and RTS.
SD	Standard Deviation.
SNR	Signal Noise Ratio.
SPD	Slant Path Delay. Atmospheric signal delay from a satellite not in zenith.
SPP	Single Point Precision. Basic GPS processing.
sub-run	Part of SAR-run with predetermined length.
TDCP	Time Differencing Carrier Phase. Basis of method for accurate GNSS velocity estimation.
UERE	User Equivalent Range Error. Total average error in pseudorange.
VTEC	Vertical Total Electron Content. Charge electrons per unit area of atmosphere. Responsible for Ionospheric delay.
ZPD	Zenith Path Delay. Atmospheric signal delay from a satellite in zenith.

1

Introduction

The performance of a navigation solution is judged by an overall weighing of multiple attributes such as accuracy, precision, availability, coverage, reliability, durability, integrity and initialisation time quantifiable in metres, hours, rates and quotas. Different applications have different requirements, different weighting of attributes, resulting in application based performance. Here, the aim is to have high position precision, the accuracy of the position is irrelevant.

The Saab Carabas is a terrain imaging radar that uses Synthetic Aperture Radar (SAR). SAR is a technique where a high resolution radar image is created by the merging of multiple images recorded at different positions, effectively creating a large synthetic antenna. The SAR method requires detailed information of the shape of the flight as this correspond to the shape of the antenna.[11] Currently this shape is determined using Global Positioning System (GPS) and the Global Navigation Satellite System (GNSS) processing method Real Time Kinematics (RTK). RTK uses a ground receiver, base, as reference to eliminate errors and increase accuracy. The accuracy of RTK is high but the method requires the presence of a base in the area of operation. With the aim of removing this base the alternative GNSS processing method Precise Point Positioning (PPP), which uses corrected satellite information is tested.[10]

This thesis will study the PPP method with RTK as reference, in order to evaluate the performance of PPP, when used to capture the shape of a Carabas flight. Can the shape of a flight be reliably captured accurately with PPP? Under wish conditions can it be or not be captured? How much potential does PPP have? These are the questions answered.

1.1 Reading instructions

After the introduction the two theory chapters, GPS and Carabas follow. They contain the basic theories, concepts and data about GPS, PPP and the Carabas. Next is the method chapter, here the approach, the usage of the processing program RTKLIB, the analysed parameters and the analysis is explained. The results and discussions are in the same chapter, every result is preceded by an explanation of the test and followed by an interpretation and discussion. The results and discussions are then condensed in the conclusion. The complete thesis is finally recapitulation in the summary.

1.2 Background

This thesis is done in cooperation with Saab Surveillance. Saab is one of the world's premier suppliers of solutions for surveillance, threat detection and location, platform and force protection, as well as avionics.[10]

At Saab the Carabas is being developed, an airborne reconnaissance radar with foliage penetrating capabilities. The Carabas is a SAR, a radar that takes radar recordings of a target area from different directions and merging them into a single high resolution terrain image. In the creation of the image the phases of the recordings are preserved. An error in a position of the recorded shape of a flight can deteriorate the final image through negative interference. Therefore the error of the shape must be much smaller than the wavelength used by the Carabas.

A standard Single Point Precision (SPP) GPS receiver is not precise enough to determine the shape. Therefore the GPS flight path is improved through the differential technique RTK. It is an accurate and precise technique capable of determining the flight path and thus the shape of the flight. RTK requires a fixed GPS base station adjacent to the targeted area to serve as reference. The dependency on a local base station is undesired and alternative solutions are sought, PPP being one candidate.



(a) Photo of Carabas 3.



(b) Photo of a RTK base station.

Figure 1.1: Carabas 3 system separate units.

1.3 Purpose

Develop and evaluate a standalone high-performance GPS navigation solution for an airborne radar to remove unwanted work and risks associated with GPS base stations.

1.4 Objectives

- Implement the GPS processing solution PPP and test its performance.
- Evaluate the solution and compare with a solution based on RTK processing.
- Assess if the generated accuracy is sufficient for Carabas.

1.5 Goals

A standard deviation of 5 cm for the difference in shape between the RTK and the PPP solution using satellite Signal Correction Products (SCP) available at the end of a flight.

1.6 Scope

Expressions used in the scope are explained later in the main text.

Only the raw performance of the PPP solution as performed by RTKLIB is analysed. The solution has not been smoothed or filtered nor processed with any Inertial Navigation System (INS). Only GPS is analysed, no other GNSS are used. Only the L1 and L2 frequencies data are analysed, not the L5 frequency. Only SCP by the IGS final products (IGS) are used. The precision of the PPP solution is primarily analysed for the SAR-runs. The precision is only briefly analysed outside the SAR-runs such as in curves and for longer time spans.

2

GPS

The Global Positioning System (GPS), is an American Global Navigation Satellite System (GNSS) providing location and time globally. There are also the Russian Globalnaja navigatsionnaja sputnikovaja sistema (GLONASS), the European Galileo and the Chinese BeiDou Navigation Satellite System (BeiDou) which is under construction. All GNSS work principally in the same way. The methods and theory explained here are transferable to any other GNSS or can be done by combining of multiple systems. This thesis focuses on GPS, as only GPS Carabas flight data exist. Furthermore the PPP technique used requires special input in the form of SCPs that at this moment only are readily available for GPS.

The basic principle behind GNSS is trilateration. Through knowledge of the distance from one point to four other separate points with known position, the position of the first point is determined. In order for a GNSS to perform a trilateration these requirements of the basic principle must be solved. For GPS the known points are the satellites and the distances are called pseudoranges.

The satellites are tracked with a network of receivers on earth and their orbits are calculated. Together with the current time these orbits are sent to the satellites in the form of a message. This message is then redistributed from the satellites to the receivers so that they know the positions of the satellites for any given time. The pseudorange from the satellite to the receiver is calculated from the time it takes for a signal to transition from the satellite to the receiver multiplied with the speed of light.[8, 12]

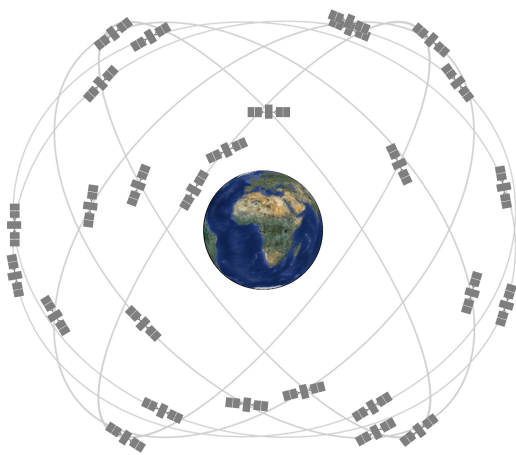
The calculations and predictions of the orbits as well as the calculations of the signal transition times have practical difficulties. In this chapter I will try to convey how these difficulties have been handled and how they still effect the resulting calculated position.

2.1 History

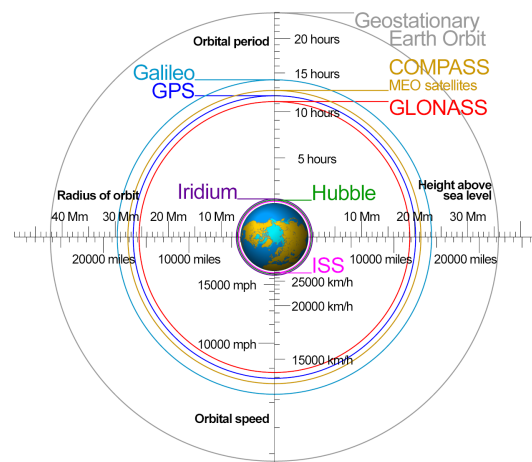
The Navigation Signal Timing and Ranging Global Positioning System (NAVSTAR-GPS) commonly referred to only as GPS, is a satellite-based radio-navigation system owned and operated by the United States Department of Defence. It was intended for use as a military branch spanning navigation and timings service. The first satellite was launched in 1978 and the system was fully operational in 1995 with 24 satellites providing global coverage. The satellites transmit signals on two IEEE

L-band¹ frequencies designated L1 and L2. These signals sent by the satellites used two separate codes for ranging, one open to anyone and one more precise, restricted to the military. The open code had an intentional error added to it to reduce the accuracy. The orbit height was chosen to give an orbit period of half a stellar day. Never satellites are continuously being added as the old ones expire providing more services and better performance. The intentional error added to the open code has since been deactivated.[6]

The GPS, is a huge, intricate, expensive and old system intended for use by military forces during war. All of these factors have contributed to and imposed limitations on the practical maximum precision of the system.[6]



(a) The GPS constellation of 24 satellites. GPS constellation and orbits. Six orbits with four satellites in each angled 55° from the equator. Original picture NASA.[15]



(b) Comparison of orbits for different systems. The GPS orbits are medium earth orbit with an orbit period of half a stellar day. Original picture Wikipedia.[21]

Figure 2.1: GPS constellation and orbit comparison.

2.2 Principles

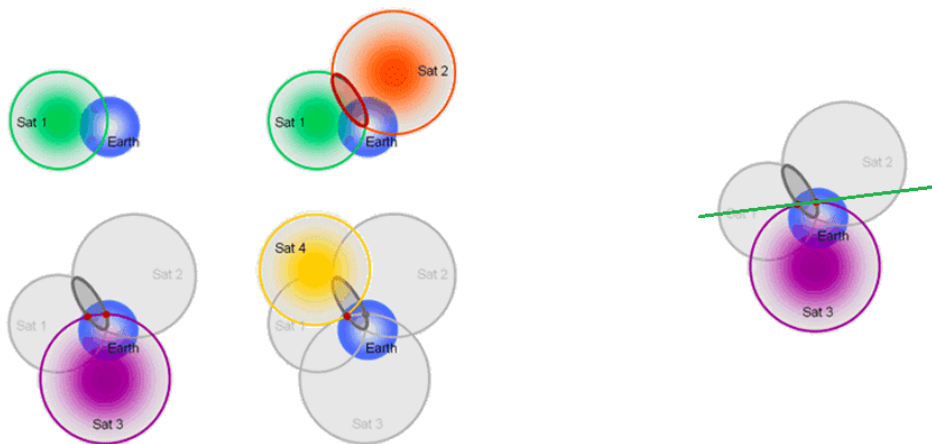
The basic default principle of current GNSSs is trilateration of pseudoranges generated from signal transition times. Instantaneous velocity can be determined from the Doppler shifts of the signals. The accuracy can further be improved by considering the carrier phase.[8, 12]

2.2.1 Trilateration

Trilateration is the technique of using distances to objects to determine a position as oppose to triangulation which uses angles. For a singly defined position four

¹Institute of Electrical and Electronics Engineers (IEEE) L-band, 1 - 2 GHz, not to be confused with NATO L-band 60 - 60 GHz or old NATO L-band 390 - 1 550 MHz

distances and therefore four satellites are needed. See figure 2.2a for illustrations of allowable positions for different numbers of satellites. With three satellites two possible solutions exists. Practically a fourth satellite is required to determine the transition time for the satellite signals. The fourth satellite also uniquely solve the position. Imagine that only three satellites exist. Unless the receiver has a clock perfectly synchronised to the satellites there is no way to know how long ago the signals were sent. The difference in time between the satellites and the receiver would add uniformly to the pseudoranges. There would then always be a line of possible solutions passing through the plane generated of the three satellites. See figure 2.2b.



(a) The distance to one satellite gives you a spherical surface of positions. Two satellites gives a ring where the two circles intersect. Three satellites gives two points. Four satellites give a definite position.

(b) With only three satellites and without a perfect clock any position on the green line is possible. As it is possible for the signals to have a common bias towards the receivers time.

Figure 2.2: 3D Trilateration. Original pictures by Michael Schmandt.[17]

2.2.2 Pseudorange

The distances used in the GPS implementation of trilateration are known as pseudoranges ρ . It is the recorded time difference between the satellite signal sending time T_s and the user receiving time T_u multiplied by the speed of light. The true range, r , is the pseudorange without its errors ϵ .

$$\rho = c(T_s - T_u) \quad (2.1)$$

$$r = \rho - \epsilon \quad (2.2)$$

Timings are found from the ranging codes of the different satellites carrier signals. The standard open code is Coarse Acquisition (C/A). It is a 1023 chips long code

transmitted at 1.023 Mbit/s with a period of 1 ms. The code is made in such a way that it will only auto correlate strongly with an aligned copy of itself. By delaying and mixing the incoming signal the middle of the code signal is found and tracked enabling accurate timings and therefore pseudoranges, this is known as the Delay Lock Loop (DLL). See figure 2.4 for details. All satellites use the same frequencies but different codes through Code Division Multiple Access (CDMA). The codes are all pseudo randomly generated gold codes with little correlation. The satellites are referred to by their Pseudo Random Noise (PRN), the seed of the code generation.[8, 12]

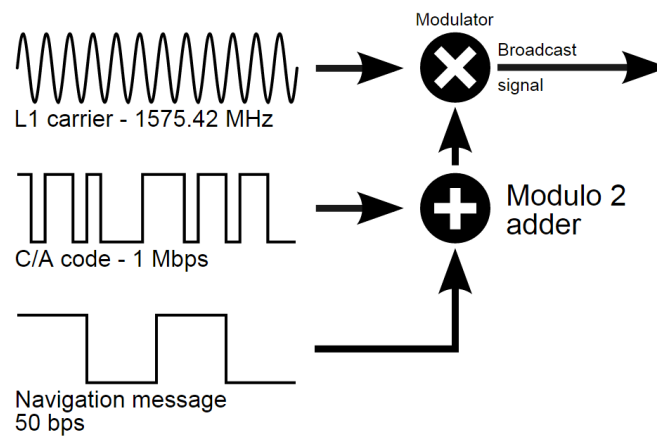


Figure 2.3: Signal composition. The L1 carrier is modulated by the C/A code for ranging and the navigation message containing the position of the satellites. Original image wikipedia.[23]

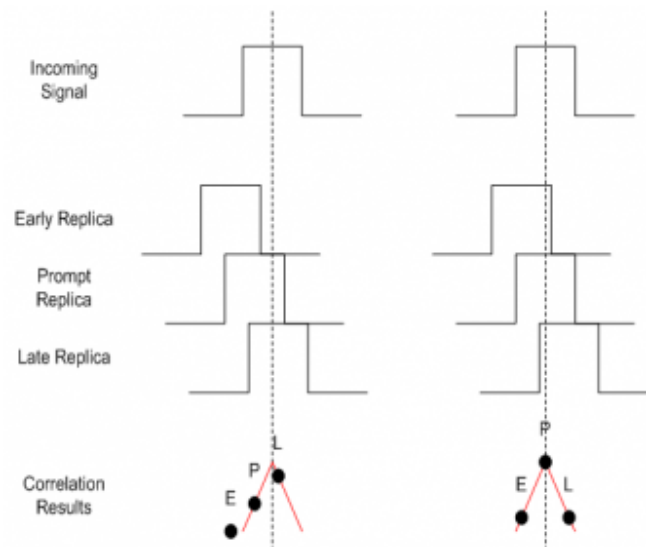


Figure 2.4: DLL early late correlation. On the left the signal is too early. The signal will therefore correlate well with the late replica. On the right the signal is correctly delayed, strongly correlating only at the centre and equally bad with the late and early replica creating a triangle. Original image Hofmann.[8]

2.2.3 Navigation message

The carrier signals are in addition to the range code also modulated by the navigation message. This message contains additional information required by the user receiver. The navigation message contains:

- Clock correction and satellite health.
- Satellite ephemerides.
- Atmospheric parameters and GPS time
- Almanac containing system common information.

The data in the navigation message is updated in the satellite by the GPS control segment. The clock and ephemeris will update at least once every 24 h. The age of data under normal operation is no more than 26 h. The data can be uploaded more often if the quality of the data fails to satisfy a number of criteria. The actual average maximum Age Of Data (AOD) is on the order of 10 hours. For full list of criteria see [7].

Without the information in the navigation message the position of the satellite is unknown making trilateration impossible. The current message, Legacy Navigation Message (LNAV) is comprised of 25 frames. The LNAV is transmitted at 50 bps and it takes 30 seconds to download one frame. Every frame is divided into five sub-frames each with a download time of 6 seconds and they can be downloaded separately. The first three sub-frames of every frame contain the satellite specific essential information while the two last sub-frames differ from frame to frame and contain the almanac and other system common information. The total send cycle from one satellite takes 12.5 minutes while only 18-36 seconds is required for the essential information. LNAV is sent on both L1 and L2 carriers of all satellites and can be downloaded out of order and in parallel, reducing the download time. The LNAV does not always need to be downloaded, the information can be saved by the receiver. The LNAV will not be completely outdated within 180 days.[7]

2.2.4 Carrier Phase Ambiguity Resolution (CPAR)

The phase of a GPS carrier can be accurately determined using a Phase Lock Loop (PLL). The wavelengths of the L1 and L2 carrier waves are only approximately 19 and 24 cm. Tracking of the carrier phase can therefore provide precision of GPS solutions. Compared to ranging codes the precision can be over two orders of magnitude better depending on technique. The downside or difficulty with Carrier Phase Ambiguity Resolution (CPAR) is that it is hard to deduce the number of full wavelengths between the satellite and the user. If one pseudorange changes abruptly with one wavelength a cycle slip has occurred. A cycle slip is the result of an incorrectly resolved integer in the CPAR measurement. In the receiver solution this is visible as a jump of ≈ 30 cm.[12]

2.2.5 Kalman filter

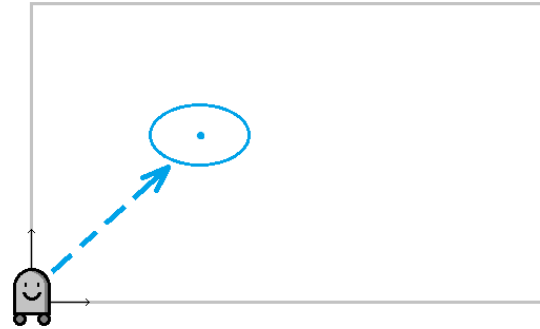
A Kalman filter is a technique for estimating the true property state out of a time series of measurements with Gaussian noise. A Kalman filter can be used to filter out the most likely position from several GNSS readings, to track pseudoranges or

signal delays.

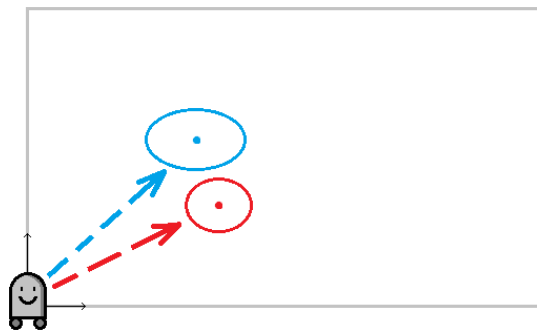
The Kalman filter starts from a position or state, visualised in 2.5a. It tracks the state and predicts how it will evolve over time 2.5b. By comparing the predicted and the measured state 2.5c it will determine the most likely true state 2.5d. This true state 2.5e then serves as a basis for the next prediction 2.5f.



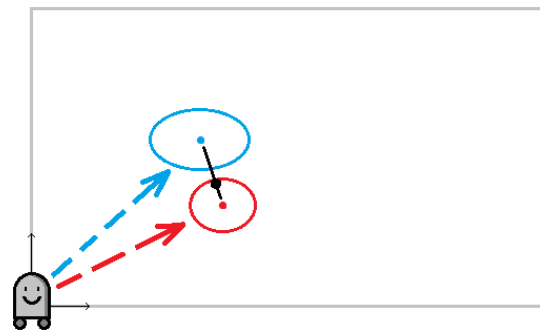
(a) Start and estimated new state



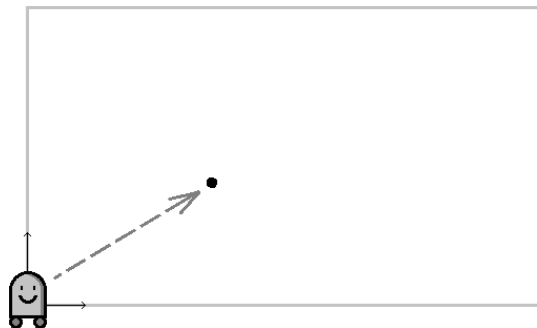
(b) Uncertainty of new state



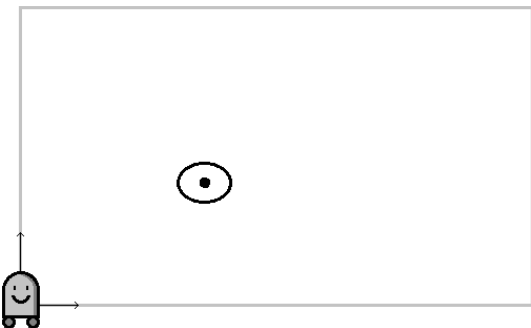
(c) Measuring of new state



(d) Covariance of new state



(e) Determining of new state



(f) Estimate uncertainty of state

Figure 2.5: Kalman loop. Original images mayitzin.com.[14]

2.3 Errors

The GPS is a very large and very accurate² system and has therefore numerous influencing factors. The nature of the errors might be physical limitations, instrumental, deliberate or legacy. Errors are reduced by continuous calibration, technological advances and compensation by estimation or measurement. One model for the error is Estimated Positional Error (EPE), it is the product of the combined pseudorange error factors, User Equivalent Range Error (UERE) and the Dilution of Precision (DOP) geometry factor.

$$\text{EPE} = \text{DOP} \cdot \text{UERE} \quad (2.3)$$

Where the UERE is the Root Mean Square (RMS) of the typical errors types, see Table 2.1 for typical sizes of errors for the basic GPS technique SPP.[8, 12]

Table 2.1: UERE for SPP with and without ionospheric correction 1σ [m].[8]

Error source	Bias	Random	Total
Broadcast ephemeris	2.1	0.0	2.1
Broadcast clock	2.0	0.7	2.1
Ionospheric delay	4.0	0.5	4.0
Residual Ionospheric delay	0.0	0.1	0.1
Tropospheric delay	0.5	0.5	0.7
Receiver noise and resolution	0.5	0.2	0.5
Multipath delay	1.0	1.0	1.4
UERE	5.1	1.4	5.3
UERE Ionospheric free	3.1	1.3	3.3

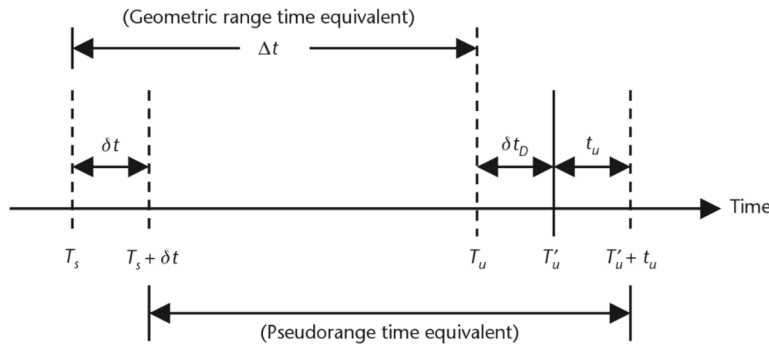


Figure 2.6: Range measurement timing relationship. [12]

Position is derived from known positions and pseudoranges which stems from timings. This is also the case for the errors, see figure 2.6 for the relationship between times, delays and there impact on the pseudorange. Errors in the ephemeris will not

²A position inside the constellation can be expressed with seven significant figures.

result in an error in the pseudorange but in the position. For a stand-alone GPS the total time offset is, [12]

$$\delta t_D = \delta t_{ion} + \delta t_{trp} + \delta t_{noise\&int} + \delta t_{mp} + \delta t_{hw} \quad (2.4)$$

where:

δt_{ion} = delay due to ionosphere

δt_{trp} = delay due to troposphere

$\delta t_{noise\&int}$ = errors due to receiver noise and interference.

δt_{mp} = multipath offset

δt_{hw} = receiver hardware offset.

With:

Δt = geometric range time equivalent

T_s = signal departure in system time

T_u = unobstructed signal arrival time in system time

T'_u = obstructed signal arrival in system time

δt = satellite clock offset from system time

t_u = receiver clock offset from system time

$T_s + t_u$ = signal departure in satellite clock time

$T'_u + t_u$ = obstructed signal arrival in receiver clock time

The pseudorange can from this be identified as

$$\begin{aligned} \rho &= c((T'_u + t_u) - (T_s + \delta t)) \\ &= c(T'_u - T_s + t_u - \delta t) \\ &= c(T_u + \delta t_D - T_s + t_u - \delta t) \\ &= r + c(t_u - \delta t + \delta t_D) \end{aligned}$$

where r is the true range $r = c(T_u - T_s)$. The nature of the errors determine how they can be handled.[12]

2.3.1 Ephemeris error

The ephemeris, the satellites positions in their orbits, drift from the predicted ones. The ephemeris error is tracked by the control segment and reported to the satellites at least every 24 hours. These errors are uncorrelated for all satellites. The drifts are typical 1-6 m per day this only results in a pseudorange error on the order of 1 m as most of the drift is tangential to the surface.[6, 12]

2.3.2 Satellite clock error

The satellites use atom clocks but they still need to be corrected as even they do drift. It does not help that they are exposed to relativistic effects compared to earth. The residual clock error δt varies from satellite to satellite depending on satellite block and the age of the latest correction. The corrections are added at least every 24 hours by the control segment. Typically these errors vary between 0.3-4 m.[6, 12]

2.3.3 Atmospheric errors

Light propagates through vacuum at 299 792 458 m/s but through the atmosphere the propagation speed will be lowered by the refractive index n .

$$v = \frac{c}{n} \quad (2.5)$$

If a mediums refractive index is frequency dependent it is dispersive.

Ionospheric model

The ionosphere is a region of the atmosphere. It contains dispersive ions which will delay the signal codes and advance the carrier phase frequency with an amount depending on the frequency. The delay depends on the total concentration of ions and fluctuates on a day night cycle with solar activity. The thin shell model is an approximation where all the dispersive ions are located in a thin shell at approximately 350 km above the surface. The thickness of this shell is directly proportional to the number of ions per unit area. It is often expressed as the Vertical Total Electron Content (VTEC) and measured in TEC units (TECU)s where $1 \text{ TECU} = 10^{16} e^-/\text{m}^2$. The signal delay α_f in metres for frequency f from the ionosphere is, [12, 18]

$$\alpha_f = \frac{40.3 \text{ TECU}}{f^2} \text{ m} \quad (2.6)$$

As the ionospheric effect is frequency dependent, it is possible to measure it by having signals of two different frequencies. Therefore receivers capable of using both L1 and L2 are capable of compensating for it. The VTEC vary with solar activity between 1 and 1000 TECU. Normally it produces an error on the order of 5 m in the pseudorange, producing an error for single frequency receivers of around 5 m. Dual frequency receivers can discount 99.9 % of the delay. It will however increase the noise in the signal.[12]

Tropospheric model

The troposphere is the lowest part of the atmosphere, it is approximately 20 km thick. It is by mass the largest part of the atmosphere and the place where all clouds exists. This quantity of air will delay signals propagating through it. The refractive index of air is low and refractivity N is used instead.

$$N = 10^6(n - 1) \quad (2.7)$$

The troposphere is mainly non dispersive and the delay of the signal ΔS_{Trop} from the satellite s to the receiver r is given by the refractivity as

$$\Delta S_{\text{Trop}} = 10^{-6} \int_s^r N ds \quad (2.8)$$

The refractivity depend on air pressure and tropospheric composition. Most of the tropospheric delay comes from the dry gases and is easily modelled. The largest compositional change comes from the concentration of water vapour. The delay of

the satellites signals through the troposphere, can be approximated by the Slant Path Delay (SPD) from the Zenith Path Delay (ZPD) and the angle θ from zenith

$$SPD = \frac{ZPD}{\cos \theta} \quad (2.9)$$

A typical tropospheric ZPD is 2.4 m. The troposphere is less uniform then the ionosphere but not as high up. A good model of the troposphere is the Saastamoinen model, using the standard atmosphere as a basis, a more accurate path mapping function through the troposphere can be made. The troposphere can also be estimated from Niell's mapping function which considers typical hydrostatic pressure distribution at different latitudes.[12, 18]

2.3.4 Receiver Noise and Resolution

The receivers DLL can not perfectly track the GPS C/A code. Depending on the quality of the receiver and antenna the error can be as low as a 0.5 m. The receivers PLL is better and can resolve ranges less than 1 cm.[12]

2.3.5 Multipath and Shadowing

When parts of the signal reach the receiver through indirect paths the signal is delayed making tracking more difficult. For an aircraft this error is not as prominent due to the lack of reflective objects e.g. buildings. Only the aircraft itself will create these effects. If the aircraft has a non uniformly shadow producing a bias in the position, then a rotation of the aircraft will change the bias.

2.3.6 Relativistic Effects

Unaccounted relativistic effects would create large errors in the GPS clocks. Special relativity (SR) makes the satellites clocks move slower and General Relativity (GR) makes the satellites clocks move faster compared to a clock on the earths surface. This error have been accounted for by letting the satellite clocks go slower and adjusting the frequencies of the codes.

From SR time goes slower for systems moving fast compared to an outside observer according to the Lorentz transform.[16]

$$\Delta t' = \gamma \Delta t \quad (2.10)$$

where Δt is the duration of an event in one frame and $\Delta t'$ is the duration of the same event when observed from a frame moving relative to the first frame. Their relation γ is the Lorentz factor

$$\gamma = \frac{1}{\sqrt{1 - \frac{v^2}{c^2}}} \quad (2.11)$$

Giving

$$\frac{\Delta t}{\Delta t'} = \frac{1}{\gamma} = \sqrt{1 - \frac{v^2}{c^2}} \quad (2.12)$$

For small v this is Taylor expanded to

$$\frac{\Delta t}{\Delta t'} \approx 1 - \frac{v^2}{2c^2} \approx 1 - 8.35 \times 10^{-11} \quad (2.13)$$

for $v = 3874 \text{ m/s}$ This means that from SR an observer on earth will experience that what is one second for the satellite is $8.35 \times 10^{-11} \text{ s}$ too short.

From (GR) time goes slower near heavy objects. This results in the satellite clocks going faster according to the gravitational time dilation equation.[16]

$$\frac{1}{\gamma} = \sqrt{1 - \frac{2GM}{rc^2}} \approx 1 - \frac{GM}{rc^2} \quad (2.14)$$

The time dilation between two points near the same mass is the fraction of their respective time dilation.

$$\frac{\Delta t'}{\Delta t''} = \frac{\frac{\Delta t}{\Delta t'}}{\frac{\Delta t}{\Delta t''}} = \frac{\frac{1}{\gamma_{\text{earth}}}}{\frac{1}{\gamma_{\text{satellite}}}} \approx 1 - \left(\frac{GM}{r_{\text{earth}}c^2} - \frac{GM}{r_{\text{satellite}}c^2} \right) \approx 1 + 5.3 \times 10^{-10} \quad (2.15)$$

using $r_{\text{satellite}} = 26\,541\,000 \text{ m}$, $r_{\text{earth}} = 6\,357\,000 \text{ m}$, $M = 5.974 \times 10^{24} \text{ kg}$ and $G = 6.674 \times 10^{-11} \text{ Nm}^2/\text{kg}^2$. The total time dilation is the ratio of the time dilation and the sum of the effects of special and the general dilation.

$$\frac{\Delta t_{\text{satellite}}}{\Delta t_{\text{earth}}} \approx 1 - 8.35 \times 10^{-11} + 5.3 \times 10^{-10} \approx 1 + 4.47 \times 10^{-10} \quad (2.16)$$

The time dilation from general relativity dominates over the dilation from the special relativity resulting in that from earths view the clocks in the satellites goes too fast by $0.447 \text{ ns/s} = 38 \text{ }\mu\text{s/day}$.³ This has been compensated for in the GPS by changing of the fundamental clock rate from 10.23 MHz to $10.229\,999\,995\,43 \text{ MHz}$.

In reality all orbits are slightly elliptical and no orbit is stable because effects such as solar pressure will push on the satellites. The elliptical orbits produce slightly separate relativistic effects for the respective satellites offsetting the timings and effecting the pseudoranges. For a typical eccentricity of 0.01 the clocks oscillate $21 \text{ ns} = 6.1 \text{ m}$ over one rotation. The maximum allowed eccentricity is 0.02.

During the signal transmission time the earth will rotate up to 21 m. This is know as the Sagnac effect and is easily compensated. General relativity also produce an advancement of the perihelion $\frac{\Delta\omega}{\omega} = 4.5 \times 10^{-10}$ [2]. This change is too small to be a problem in the time between the measured corrections. The drift of the rubidium atomic clocks and the uncorrected relativistic effects are two of the largest contributors to the need of measured SCPs.[8, 12, 16]

³Without correction for relativity for circular orbits all clocks would drift uniformly and therefore not introducing any accumulating errors in the pseudorange provided that all satellite clock correction from the master control segment would be simultaneous. Not $c \cdot 38 \text{ }\mu\text{s/day} = 11.4 \text{ km/day}$ The error would instead be in the ephemeris as the time offset would result in an additional drift in the position of the satellites by $v \cdot (\Delta t' - \Delta t) = 3874 \text{ m/s} \cdot 38 \text{ }\mu\text{s/day} = 0.133 \text{ m/day}$ and a Doppler shift in all directions of 4.47×10^{-10} .

2.3.7 Dilution of Precision (DOP)

The true error in the position as experienced by a user is as mentioned previously the UERE multiplied by the DOP. The DOP is a factor originating from the geometry of the available satellites. If all angles between all available satellites are large then the DOP is low. See figure 2.7.

A GPS receiver on the earth can not see the satellites under the horizon. This causes the vertical DOP (VDOP) to be larger than the horizontal DOP (HDOP). The vertical accuracy and precision is therefore worse than it is horizontally. If satellites are unavailable or unseen the DOP will increase.

For a receiver with elevation mask of 5° the HDOP will be between 0.7 and 2.5 while the VDOP will be between 1.2 and 5.[12]

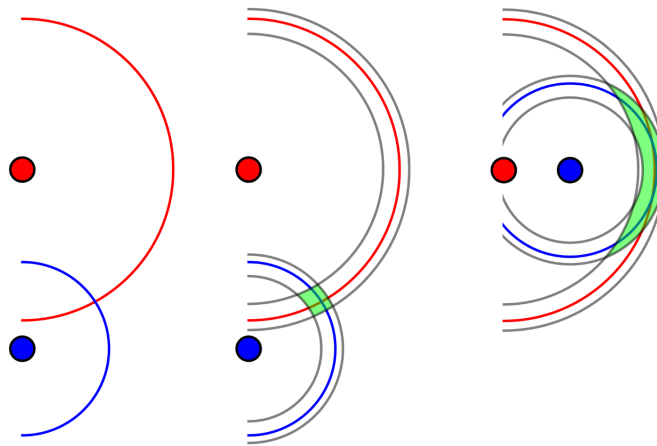


Figure 2.7: DOP. The geometry of the system produce different uncertainty's in position for the same pseudorange error, the green area is larger in the right picture. Original picture Wikipedia. [22]

2.3.8 Constellation

The GPS satellites are not uniformly distributed around the world. All satellites are in planes inclined 55° from the equator. This results in less coverage at the poles. The satellites are also of different generations with differences in clock accuracy's and signals. Not all satellites transmit the L2C signal, to find the ionospheric free correction, the military L2 signals must instead be tracked using the squaring technique this is less accurate than using the L2C. See table 2.2 for active open satellites and signals.[8]

2.4 Single Point Precision (SPP)

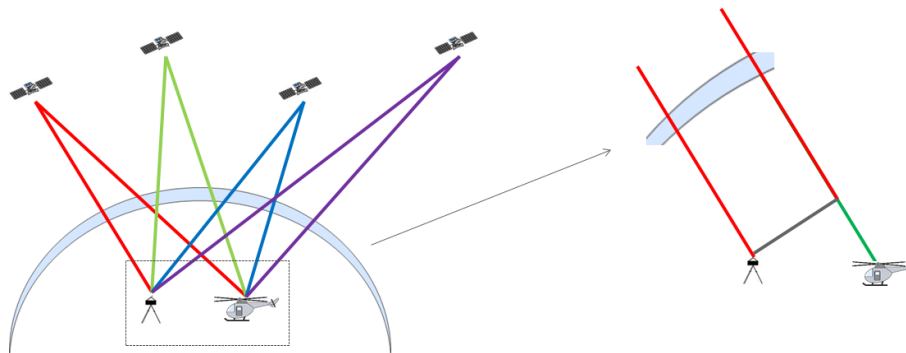
SPP is the default GPS positioning. It requires no additional information and finds the position through C/A pseudoranges. The UERE in Table 2.1 were achieved through SPP.

Table 2.2: Active Open GPS Satellite Signals.[4]

Frequency/Code	Satellites	Block
L1C/A	31	All
L2C	19	IIRM ->
L5	12	IIF ->
L1C	0	III ->

2.5 Real Time Kinematics (RTK)

In RTK the base, a reference GPS receiver is used to improve the accuracy and precision of the position of the rover, the movable receiver. With the base it is possible to reduce the clock, ephemeris, ionospheric and tropospheric errors as long as the receiver, rover, is not too far from the base. This is done by deducing the position of the rover relative the base from the differences in ranges between satellites \rightarrow rover and satellites \rightarrow base. See figure 2.8 CPAR and Kalman filtering further increases the accuracy and precision of RTK. The downside of RTK is the dependency on the base. The error reducing capabilities diminishes as the distance between the base and rover increases.[18]

**Figure 2.8:** RTK differentiation.

2.6 Fixed Base Line (FBL)

FBL is similar to RTK. It uses two receivers and calculates where they are relative to each other by comparing their difference in range. The difference from RTK is that here both of the receivers are moving but at a constant distance between each other. The FBL method gives no information of position only the receivers relative position. CPAR is often used for FBL processing This can for instance be used to calculate in which direction the Carabas helicopter is pointing.

2.7 Precise Point Positioning (PPP)

PPP uses downloaded SCPs to the broadcast clocks and ephemeris in order to reduce their error contribution and increase the accuracy. A PPP solution can however not remove the atmospheric delays by measurement. It uses instead models of the error factors and a Kalman filter to estimate the delays and compensate for them. The estimation requires time to collect enough data for an accurate system state, this time is the convergence time. For stationary receivers the convergence time can be around 60 min. For a moving receiver Kinematic Precise Point Positioning (KPPP) is used. The movements of the receiver complicates the estimations of the error factors, this increases the convergence time. The convergence time can be reduced by including more satellites such as from Galileo or GLONASS.[13] The advantage over RTK is that PPP performance is not limited by the closeness of a base, for PPP high quality SCP are instead essential.

2.7.1 PPP with CPAR

Carrier Phase Ambiguity Resolution (CPAR) is harder to implement for PPP than for RTK. For RTK only the part of the range which is the difference between the base and rover range need to be resolved. While for PPP the full range with delays from the atmosphere needs to be resolved making it harder to find the correct number of wavelengths. PPP also benefit less from the CPAR then RTK as the receiver error which CPAR reduces is the largest error source in RTK but only one of several for PPP. In some cases CPAR has proven to reduce the convergence time.[3]

2.7.2 Kalman filtering in PPP

In the PPP implementation of RTKLIB the Kalman filter will track and model the receiver position, the atmospheric effects and the pseudoranges. No dynamic model regulating the possible changes of the position state of the receiver platform has been implemented for PPP in RTKLIB. The atmospheric effects for the different satellite signals is treated as a few separate unknowns, namely the VTEC and the East and North Tropospheric delay gradients. More measurements will make it possible to better model these errors sources. The satellite clock and ephemeris errors have no common component and are all modelled. More satellites will also increase the number of unknown pseudoranges. This is one reason as to why the quality of the SCP have such an impact on the accuracy and precision of the position.[18]


2.7.3 International GNSS Service (IGS)

The International GNSS service (IGS) is an organisation providing open access to high-quality SCP. IGS is a voluntary federation of over 200 self-funding agencies, universities, and research institutions in more than 100 countries.⁴ It is functioning as a component of the Global Geodetic Observing System (GGOS) and member of the World Data System (WDS). The SCPs are available through several FTPs. See

⁴As a comparison the control segment has 16 stations.

figure 2.9 for a list of products. The GPS SCPs come in three qualities are referred to as IGS, IGS Rapid products (IGR) and IGS Ultra-rapid products (IGU). The IGS also supplies real time SCPs through IGS Real-time Service (RTS) the quality of which has been shown to exceed IGU.[1] The IGS also supply SCPs for other GNSS but currently only in final product quality.

Products



GPS Satellite Ephemerides / Satellite & Station Clocks

Type		Accuracy	Latency	Updates	Sample Interval
Broadcast	orbits	~100 cm	real time	--	daily
	Sat. clocks	~5 ns RMS ~2.5 ns SDev			
Ultra-Rapid (predicted half)	orbits	~5 cm	real time	at 03, 09, 15, 21 UTC	15 min
	Sat. clocks	~3 ns RMS ~1.5 ns SDev			
Ultra-Rapid (observed half)	orbits	~3 cm	3 - 9 hours	at 03, 09, 15, 21 UTC	15 min
	Sat. clocks	~150 ps RMS ~50 ps SDev			
Rapid	orbits	~2.5 cm	17 - 41 hours	at 17 UTC daily	15 min
	Sat. & Stn. clocks	~75 ps RMS ~25 ps SDev			5 min
Final	orbits	~2.5 cm	12 - 18 days	every Thursday	15 min
	Sat. & Stn. clocks	~75 ps RMS ~20 ps SDev			Sat.: 30s Stn.: 5 min

Figure 2.9: SCPs from the IGS homepage <http://www.igs.org>

2.7.4 RINEX

Receiver Independent Exchange Format (RINEX) is a data format for GNSS signal data. Standardised data recording allows for post processing and combination of data from different systems.

The data is split into three types of files containing observations data, navigation message and meteorological data. Observational data is the receiver recorded observations, the code pseudoranges phase measurements and Doppler shift for all frequencies for all visibly satellites. The RINEX files produced by RTKLIB have file extensions .obs .nav for observation and navigation data.

2.8 GPS Velocity Measurements

An alternative to capturing the shape of a flight path using calculated positions is to deduce the shape from integration of velocity. The simplest measurement of velocity is to differentiate two consecutive positions. The accuracy of this type of measurement is however proportional to the precision of the position and inversely proportional to the duration between the measurements. For a GPS solution with

a precision of 1 m the average velocity accuracy over 1 minute will be in the order of 1 cm while the average velocity accuracy over 0.01 s will be 100 m. One basis for accurate high frequency velocity measurements is instead the signal Doppler shifts. When the receiver tracks the code using the early-late correlation it can directly record the Doppler shift in the signal code. Resulting in velocity measurements with accuracy of a few cm/s. With Time Differencing Carrier Phase (TDCP) Graas [5] has shown that velocity measurements can reach mm/s accuracy for 1 s sampling for a stand-alone GPS receiver. High accuracy in velocity can also be reached through PPP methods. The PPPVE method proposed by Tu [19] can track a displacement with a precision of 2 cm. Xincun [24] demonstrates a velocity error of 0.2 mm/s for an air plane performing gravity measurements.

3

Carabas

The Carabas is a Synthetic Aperture Radar (SAR) mounted on an airborne platform, in this case a helicopter. The Carabas radar uses frequencies in the bands VHF and UHF with wavelength 1-15 meters. The long wavelengths enables the signal to pass through smaller objects giving the Carabas foliage penetrative capabilities. The azimuth resolution ρ_a for a real aperture radar is

$$\rho_a = \frac{R\lambda}{l} \quad (3.1)$$

Where R is the distance to the target, λ is the wavelength and l is the length of the aperture. High resolution imaging with a large wavelength from a long distance requires a long aperture. A classical antenna spanning kilometres is an engineering challenge and impractical on an airborne platform. Carabas instead uses a synthetic aperture created through the combining of multiple images taken throughout a flight. The maximum resolution of a SAR is

$$\rho_a = \frac{R\lambda}{2L \sin \theta_0} \quad (3.2)$$

Where L is the length of the synthetic aperture and θ_0 is the side looking angle from the vertical. Instead of having a real aperture kilometres long, the Carabas will fly the length of the aperture and create the image through post processing.

3.1 Synthetic Aperture Radar (SAR)

In SAR the antenna used for imaging is synthetic. A smaller antenna is moved while performing radar recordings of range and phase, creating multiple radar readings of the same area from different directions. The radar image is created, through post process combining of the radar recordings. In order for the recordings to be correctly combined, the relative positions of the recording sites must be known. The relative positions of the recording sites are analogous to the shape of the antenna. The phases of the recordings are considered in the combining. The image is created through positive interference. If the shape of the flight path is incorrect with distances one quarter of the wavelength, two images will cancel out through negative interference. In order not to degrade the quality of the image, an error in the position should not result in an error in the distance travelled by the signal of more then approximately one tenth of the wavelength.

3.2 Flight path shape capture

The purpose of the flight path recording is to deduce the shape of the flight path, more accurately the shape of the flight path of the antenna. This can be made in several ways. It is possible to determine the shape using exact absolute position, precise position, accurate velocity or accurate acceleration. RTK gives exact position. PPP or autofocus¹ gives precise position. Doppler measurements gives accurate velocity. Inertial Navigation System (INS) gives accurate acceleration. The shape determining technique of this thesis uses precise position.

Independent of how the shape of the flight path was determined its use is the same. The purpose of it is to provide information to the SAR processing so that the readings can be combined into a radar image. In the 2D case, the raw data recordings of a SAR-run from an object, will in flight direction and radial coordinates X, R be a hyperbole with its lowest point at the true position and a curvature dependent on the distance. A illustration of the 2D case can be found in figures 3.1 - 3.3. In the 3D case the shape of the hyperbolas also depend on the height difference between the SAR and the object.

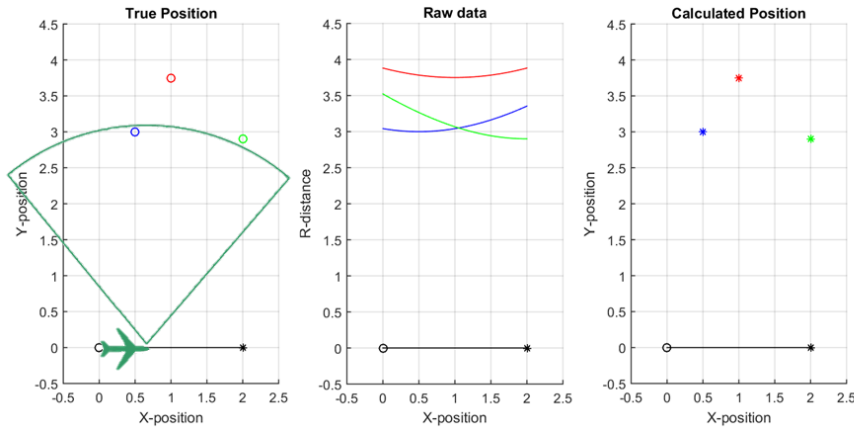


Figure 3.1: Ideal 2D recording. The Carabas is flying on the X axis looking left. The distances to the three objects is recorded as a function of the X position creating hyperbolas in the raw data. The hyperbolas are then processed yielding the calculated positions.

¹Determination of aperture shape from SAR image. Not explained here. Read Jakowatz [11] for details.

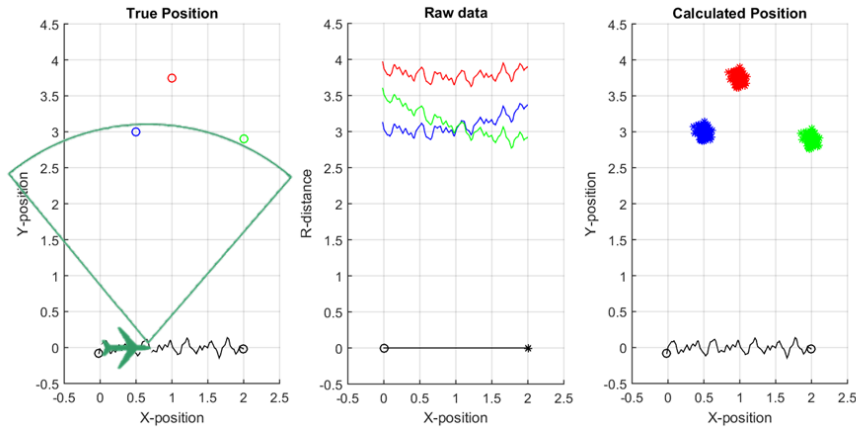


Figure 3.2: Incorrect 2D recording. The SAR is oscillating in its path but and this is not compensated for, smudging the calculated positions.

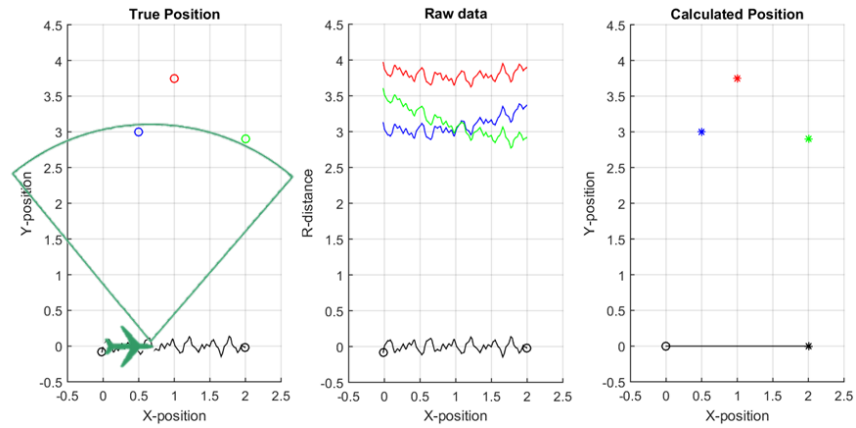


Figure 3.3: Compensated 2D recording. The SAR is oscillating but the motion is captured and corrected for in the summation.

3.3 Carabas GPS implementation

To track the flight path of the Carabas antenna, the relative positing throughout the SAR-run most be known, but also the orientation. This is mainly because it is impractical to mount a GPS antenna on the SAR antenna underneath the helicopter. The Carabas helicopter has therefore two GPS antennas mounted on the tail boom deducing the position of the SAR antenna from the relative positioning of the GPS antennas. From their relative position the pitch and yaw of the helicopter is computed. The roll can however not be calculated from only two antennas instead a MEMS-gyroscope is used in a consecutive processing.

3.4 Errors in shape

The purpose of the GPS on the Carabas is to find the shape of the synthetic antenna so that a SAR image can be made. The precision of the shape will be better then the precision of the position. If the flight path is rotated or translated the shape of

the flight path, the synthetic antenna is preserved. A translation of the flight path will not reduce the resolution of the SAR image only move it. Similarly a rotation in the horizontal plane will only rotate the image.² Two flight paths of the same shape are said to be congruent and the rotation and translation are said to be isometric, shape preserving transforms. This means that when using a GNSS such as GPS for the flight path capture it is the precision and not the accuracy of the position that is important. It is the standard deviation of the error not the root mean square. As most applications of GPS value accuracy over precision a study of the short term precision of the Carabas GPS solution is needed to verify possible precision.

3.4.1 Direction of the error

Errors in the recorded shape will produce different errors in the travelled signal distance depending on the direction of the error. If the error is in the direction directly towards the target then this will result in an error in the distance travelled by the signal twice as large as the error in position. If the error is in a direction perpendicular to the direction of the target, the error in the signal distance travelled will be minimal. The requirements on the precision of the shape can therefore be said to be most important in the target direction, second in the flight direction and third in their cross product.

3.4.2 Absolute orientation error

The quality of the flight path shape capture is determined by the error in the shape, the error in congruence. The size of this error is the standard deviation of the difference between the true flight path and the captured flight path after it has been rotated and translated in the way which gives the error. The problem of finding the best rotation matrix R and translation vector t which minimises the least squares error E between two sets of coordinates is known as the absolute orientation problem.

$$\arg \min_{R,t} E(A, B, R, t) = \arg \min_{R,t} \left(\sum_i \|RA_i + t - B_i\|^2 \right) \quad (3.3)$$

Where A and B are the true and measured positions. R and t can be calculated through Horns unit quaternions method.[9]

3.4.3 GPS shape errors

GPS solution errors which will remain after rotation and translation are among others large amplitude noise, trapezoids as generated by cycle slip in CPAR GNSS techniques and drift of the solution bias. For PPP typical drifts can be changes in the DOP or changes in the error factor parameters during convergence.

²Transforms of the synthetic aperture have effects analogous to those of a camera. If the aperture moves the image moves. If the apertures form changes the image is distorted.

3.4.4 Linear drift error

A fixed bias in the position solution will not effect the shape of the flight path. If the bias is changing in size or direction the shape will be distorted. For the solution bias drift the speed, the direction and their derivatives are important for the accuracy of the shape. The duration of a SAR-run is short compared with the changes of weather or satellite geometry, around 1 minute. The drift in bias can possibly be seen as linear for these durations. A linearly drift of the bias in the flight direction of ΔX during one SAR-run will result in a sd of the error in the flight direction corresponding to the standard deviation of uniform distribution

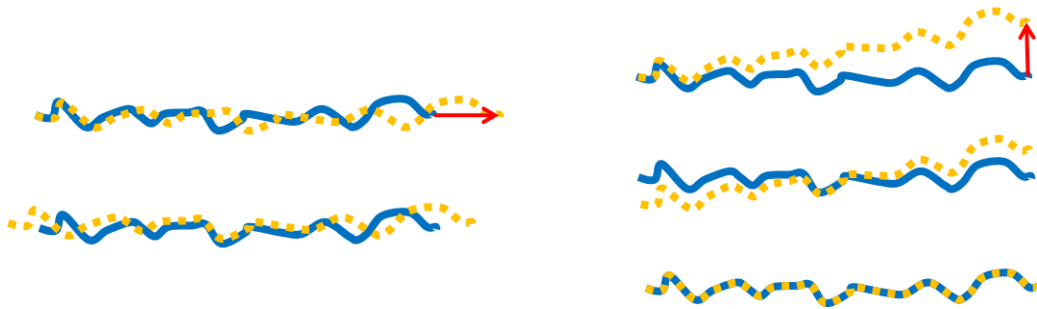
$$\sigma_X = \sqrt{E(\Delta X^2) - E(\Delta X)^2} = \Delta X \sqrt{\int_0^1 x^2 dx - \left(\int_0^1 x dx\right)^2} = \frac{\Delta X}{\sqrt{12}} \approx \frac{\Delta X}{3.5} \quad (3.4)$$

The sd of the error is reduced because the error in part can be explained by a translation $\frac{\Delta X}{2}$ in the flight direction. See figure 3.4a A linearly drift Δr in the angle ϕ from the flight direction will for a long straight flight increase the flight length by

$$\Delta X = \sqrt{(\Delta r \sin \phi)^2 + (L_{\text{Flight}} + \Delta r \cos \phi)^2} - L_{\text{Flight}} \approx \Delta r \cos \phi \quad (3.5)$$

The drift perpendicular to the flightpath rotates the flight and the only remaining error is the increase in flight length. The average sd of the shape error for a linearly changing bias in unknown direction is then

$$\sigma_X = \frac{\Delta r}{\sqrt{12}} \frac{2}{\pi} = \frac{\Delta r}{\pi\sqrt{3}} \approx \frac{\Delta r}{5.4} \quad (3.6)$$



(a) Linear drift in flight direction. The standard deviation of the error is reduced by translating the recorded shape

(b) Linear drift perpendicular to flight direction. The error is removed through a rotation and translation

Figure 3.4: Linear drifts effect on the standard deviation of the shape of a SAR-run. The blue line is the true position, the yellow line is the recorded position and the red arrow is the total size and direction of the drift during the SAR-run.

For a straight flight a linear drift can be rotated to only affect the sd of the error of the shape in the flight direction X . This error is a scaling of the shape. Linear drift in a direction perpendicular to the flight direction has little or no effect on the shape. See figure 3.4b

3.4.5 Steadfastness of solution

The quality of the shape capture is now dependent not only on the precision of the GNSS solution but also on the angle between the flight direction and the direction of the drift in bias. To estimate how reliably the PPP method can capture the shape it is possible to take the standard deviation of the standard deviations of shape, this value is the steadfastness standard deviation. It is defined as:

$$S = \sigma(\sigma_i) = \sqrt{\frac{1}{N-1} \sum_{i=1}^N (\sigma_i - \bar{\sigma}_i)^2} \quad (3.7)$$

Where N is the number of SAR-runs, σ_i is the standard deviation of shape and $\bar{\sigma}_i$ is the mean of the standard deviations of shape.

$$\bar{\sigma}_i = \frac{1}{N} \sum_{i=1}^N \sigma_i \quad (3.8)$$

The steadfastness indicates how reliable the standard deviation of the shapes are.

4

Method

Standard SPP GPS does not satisfy the the required precision criteria of 5 cm. The quality of the solution is therefore improved using the GNSS post processing method PPP. This chapter describes how the measurements were conducted, how RTKLIB was used to process the GPS observations, how the resulting GPS position solutions were analysed and how all these processes were chosen.

A total of 12 measured flights with 182 SAR-runs have been processed and analysed. The processing was done in RTKLIB using PPP with three qualities of SCPs, IGU, IGR and IGS. The analysis was made by comparing the shape of the PPP solution with the one from the professional RTK solution GrafNav. The process with the smallest standard deviation of the shape between the RTK and PPP solution was chosen.

4.1 Approach

Initially I tried to familiarise myself with GPS. Trying to understand how a solution is reached and the error sources. With this basic knowledge I went on to generating PPP solutions through the RTKLIB GUI. In order to analyse and compare different solutions, I created a MATLAB script taking one reference solution and several PPP solutions generated with different GUI settings and compared them to each other. The quality of the solutions was determined from the standard deviations of the deviation in position. To speed up the process and minimise confusion I wrote a MATLAB script controlling the RTKLIB Command-line User Interface (CUI), generating PPP solutions from different GPS data files and RTKLIB CUI configuration files.

With these scripts I tested my way through different settings in RTKLIB. Trying to find the best solutions using the most accurate corrections of IGS ephemerides, clock and Differential Code Bias (DCB)s in combination with the most accurate PPP techniques using CPAR and a dynamic model. The results did however seem strange. The reason was that CPAR for PPP had not been implemented. When selected RTKLIB would instead default to other settings. Turning off all CPAR settings improved the precision. Changes made in the dynamic models parameters, such as maximum acceleration did not effect the resulting solution. The reason for this was that the dynamic model had not been implemented for PPP. I tried to add one by copying the dynamic model from the RTK code into the PPP code and hard code acceleration limits in the RTKLIB source code. This did not result in any improvement of the precision. However as the KPPP method was able to achieve

high precision during short time spans using the best IGS SCP I was content with the results and moved on.

The precision using IGS was good but IGS is not a good solution for Carabas as it is not available until several days after a flight. I went on to try to reduce the quality of the corrections to those available during a flight. Tests with broadcast were dismissed for being too noisy. Leaving the IGU, IGR and RTS. I registered for a RTS account at Bundesamt für Kartographie und Geodäsie (BKG) but could not use them for analysis, as I could not find any saved real time streams from the time of the flights. A recording and subsequent analysis of RTS during the next flight would be interesting. The choice of SCP therefore fell on IGU for clock and ephemeris correction. Other types of corrections were discarded as the potential gain in precision was not apparent. This includes the DCB corrections which are more important for a CPAR based method.

Tests with the IGU SCP gave worse results than with IGS. The standard deviations of the deviation of position were not good enough. In order to better evaluate the quality of the solutions I wrote a new MATLAB script. The script instead of comparing the position of the PPP and the RTK solution compared their shapes, by calculating the standard deviation between their positions after rotation and translation. The new results showed that PPP using IGU sometimes had the precision required to capture the shape. The largest problem was that the forward antenna (FWD) for some flights suffered from bad satellite reception, having low Signal Noise Ratio (SNR) according to the RTKLIB log files. This reduced the number of usable satellites. At times the number of usable satellites went down to values where the PPP technique apparently no longer could resolve a position. Some FWD files would not produce any output for any technique.

As the aft antenna (AFT) solution was not suffering from bad SNR in the same extent as the FWD solution I saw the possibility of using only the AFT antenna for position and getting the heading of the Carabas with FBL processing. FBL had been shown to work for only a few satellites by Videkull [20]. When tested, this did not work as planned, large parts of some flights were still missing. A reduction of elevation mask allowing for more satellites gave me a FBL solution, but with lower quality factor than achieved by Videkull. The FBL made it possible to calculate the FWD antenna from the AFT antenna.

While trying to understand why FBL processing worked where PPP did not, I discovered a more complete reason as to why some FWD position solution files fail. The RINEX navigation, .nav file created for the FWD antenna was sometimes incomplete. It seemed like the problem with the reception of the FWD antenna prevented the navigation message from being downloaded and therefore prevented the processing of the PPP solution. By using the .nav file of AFT the FWD .pos files could be created.

In total I tested approximately 200 combinations of settings for PPP and 100 for FBL before settling. I do not claim to have exhausted the settings and a better configuration for this application surely exist.

4.2 Coordinate systems

Table 4.1: Coordinate system comparison

Name	Type	Axis name	Axis designation
WGS 84	Elliptical Geodetic	Latitude Longitude Height	lat lon h
Scene Centre	Local tangent plane	East North Up	x y z
SAR	Cartesian	Flight Target Z	X R Z

4.2.1 WGS84

World Geodetic System 1984 (WGS 84) is the standard coordinate system of GPS. A position is expressed as the geodetic latitude, longitude and height on the WGS 84 reference ellipsoid.

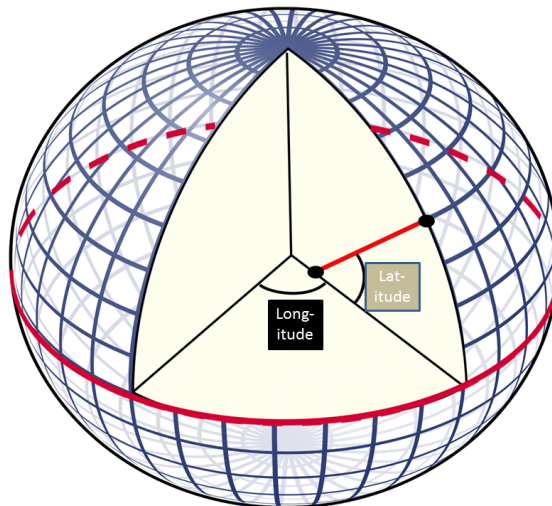


Figure 4.1: WGS 84 in exaggerated geodetic view.

4.2.2 Scene Centre coordinates (SC)

The Scene Centre (SC) coordinate system is a Cartesian system where a position is expressed in distance in east, north and up (ENU) from the datum which is the scene centre. The coordinates are designated x, y and z.

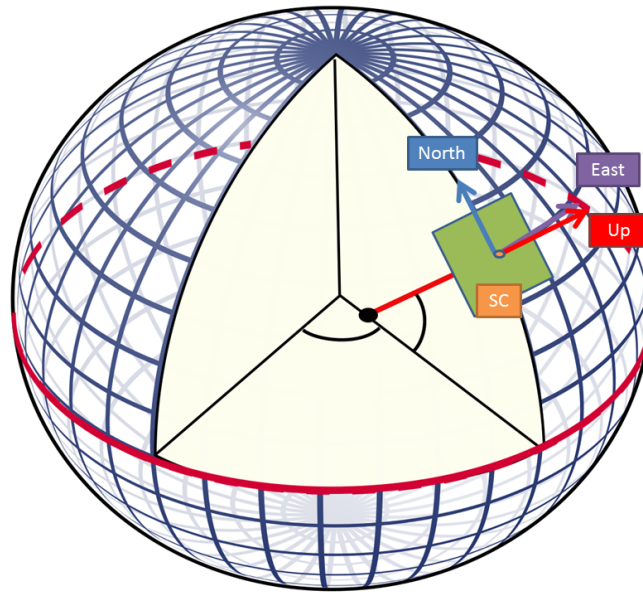


Figure 4.2: Scene Centre ENU coordinates.

4.2.3 SAR coordinates

The requirements on the precision of the position is strictest in the direction towards the centre of the area being imaged.

The SAR image precision requirements depend on the direction. To accurately measure the most critical distances the SAR coordinate system was created. It is a Cartesian system rotated so that the X-direction is the flight direction, the Y or R direction is the direction towards the scene centre and Z is the cross product of X and R. Depending on if the Carabas is recording an image on its left or right side the Z direction will be up or down.

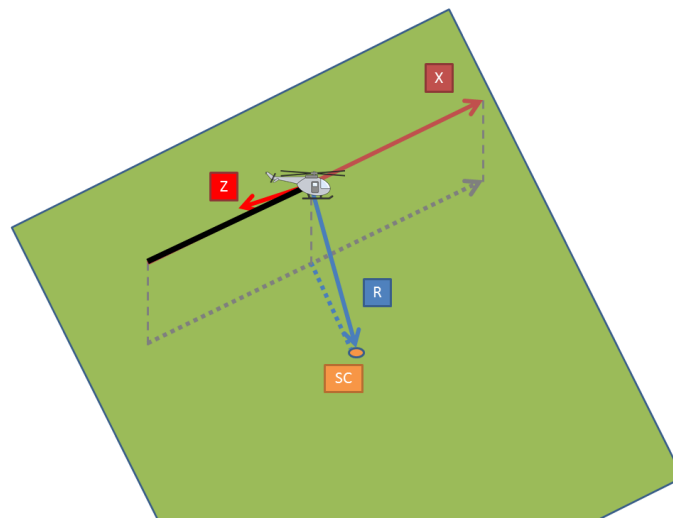


Figure 4.3: SAR coordinates XRZ

4.3 Data collection

All analysed flight data were recordings from previous flights of the Carabas manoeuvring and performing SAR-runs. During the SAR-runs the Carabas aimed to fly with constant speed and bearing. This Carabas, Carabas3 is mounted on a Schweizer 300C helicopter. The GPS data was recorded with a Javad Delta Duo G2D-4 GNSS receiver using dual Antcom 53G1215A-XT1 antennas at 10 Hz. This data is stored in raw data javad.jps files. The start and stop times of the SAR-runs are recorded in the passfile and timeLut.mat. The selections of flights were to take all flights with a previously made GrafNav solution and a corresponding passfile. All SAR-runs except the ones marked calibration (CAL) were included in the results.

During future flights the RTS SCPs can be recorded from the RTKLIB program RTKNAVI.

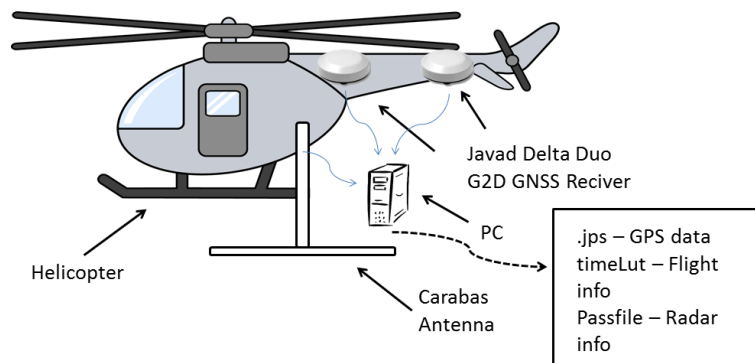


Figure 4.4: Data Collection

4.4 Data processing

The processing of the GPS data is done by RTKLIB. In order for the processing to be uniformly and quickly done the processing is controlled from a MATLAB script. The script takes the javad.jps files and converts them using RTKLIB RTKCONV (convbin.exe) into RINEX navigation.nav and observation.obs files. The script downloads the SCPs as ephemerides.sp3 and clocks.clk files with RTKLIB RTKGET or directly from the IGS ftp. Finally the script calls the RTKLIBs post processing program RTKPOSTs executable rnx2rtkp.exe and tells it to process the data of the observation.obs and navigation.nav file with the downloaded SCPs using the settings defined in the RTKPOST config.conf file. The final data processing is made three times for every flight once for the PPP processing of the AFT and FWD antenna respectively and once for the FBL processing. The processed position solutions are then stored in the three files AFT.pos, FWD.pos and FBL.pos. The

used configuration files can be seen in the appendix C.1 for PPP and C.2 for FBL processing. The appendix also contains cutouts from a .obs file C.3 and a .pos file C.4

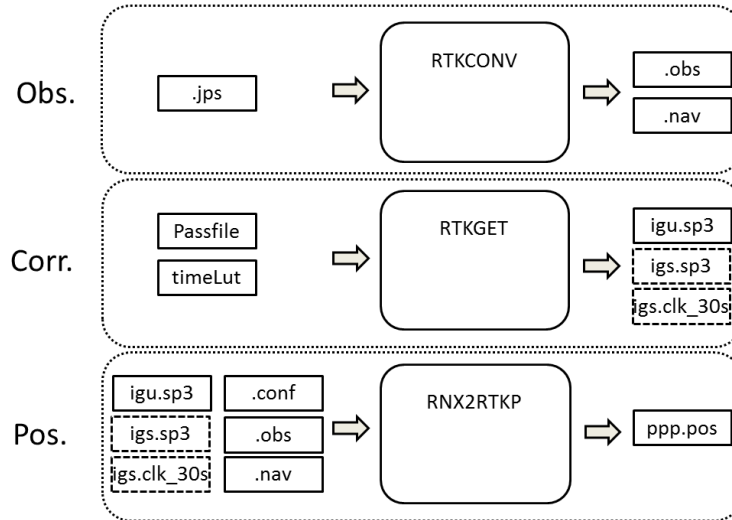


Figure 4.5: Data Processing

4.4.1 RTKLIB

The open-source GNSS processing software RTKLIB written by Tomoji Takasu has previously been tested with the Carabas using the differential GPS processing technique RTK and performed on level with the professional software GrafNav.[20]

RTKLIB Settings

In order for RTKLIB to generate position solution it needs to be configured. This is done through choices in the GUI or by specifying a previously constructed config.conf file. RTKLIB can be configured in numerous ways, allowing the selection of different processing types, models techniques and parameters for several steps of the GNSS processing.

The RTKLIBs RTKPOST is the main program for post processing. RTKPOST can process the GNSS observation using multiple processing method. These methods include SPP, RTK, PPP and FBL. The processes can use different models such as atmospheric models. They can also use extra techniques and corrections such as SCPs or CPAR. The models and techniques all have parameters which can be set. There are also settings regarding how the data should be presented. Not all combinations of settings have been implemented. For a more detailed explanation of the settings of RTKLIB see the RTKLIB manual [18]. The configuration files used have been included in appendix B.

4.5 Data Analysis

RTKLIB contains tools for comparing solutions, but for this evaluation the major part of the analysis was made by MATLAB scripts. The analysis can be divided into two types, single and comparative analysis. Single analysis refers to all analysis which are possible to do without the use of a reference RTK solution. The acceleration is an example of a single analysis. The reasoning behind the distinction between single and comparative analysis is that the single analysis always can be performed even without a reference solution. The single analysis can therefore serve as a quality indicator of future flights. The comparative analysis is the evaluation of the PPP performance when compared with the RTK solution for instance the comparison of the recorded flight path shapes. Both parts of the analysis have been run through the same script.

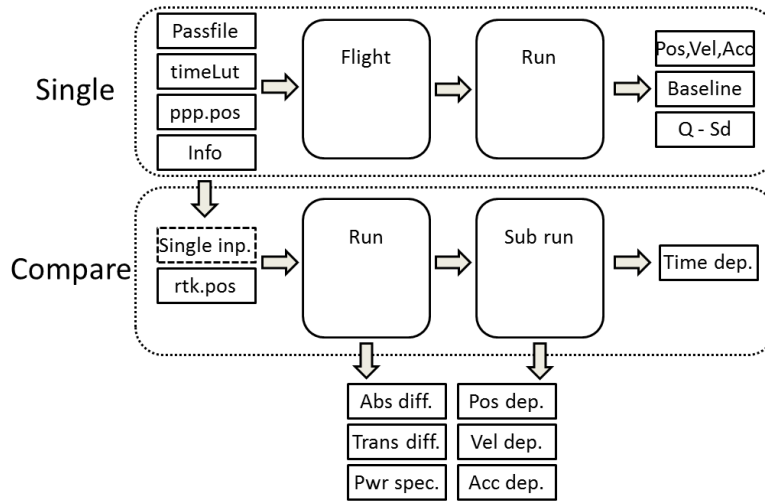


Figure 4.6: Data Analysis

The MATLAB script loads the AFT.pos, FWD.pos and FBL.pos files generated with PPP processing and the corresponding reference solutions (REF). The REF can be any other set of AFT.pos, FWD.pos and FBL.pos files but all the results were made using the GrafNav position solution as reference. The files are all synced in time, if the REF has a lower sample frequency then the PPP the non-existing REF data point are set as NaN, if the PPP solution lacks points they are interpolated.

The position solutions are transformed from WGS 84 coordinates into scene centre ENU coordinates. If selected the FWD solution could here be replaced by a combination of AFT and the FBL. In the presented results this was not done, instead the FWD solution generated with the AFT navigation file was used. The scene centre and the times of the SAR-runs are found in the passfiles with time look up in the timeLut.mat.

The SAR-runs are cut out and rotated into the SAR-XRZ coordinate system. The rotation is done by finding the rotation matrices that rotates every one of the REF SAR-runs into SAR-XRZ coordinates. These matrices then rotate the PPP solutions into SAR-XRZ. Next all PPP SAR-runs are isometrically transformed to

minimise the least square error with the reference solutions using Horn's method.[9] The difference in shape is then calculated as the standard deviation of the difference between the transformed PPP solutions and the REF solutions for the SAR-runs.

In order to increase the number of measurements of the same length the SAR-runs are cut up into overlapping sub-runs of predetermined lengths. The standard deviation of the difference in shape of the sub-runs are calculated in the same way as with the SAR-runs

4.5.1 Single Data Analysis

In the single analysis it is possible to identify and estimate some errors with the generated position without comparison with a high quality reference solution. The flight is analysed as a whole and for SAR-runs. Everything possible to do without a REF solution falls into this analysis.

Flight path view By looking at the flight path or bird eye view it is possible to analyse the overall shape of the flight. Determining if the SAR-runs are made in the correct places. It is hard to make any statements on the precision of the position solution in the flight path view because of the scales involved.

Position Time evolution of the east, north and up components gives information of how the Carabas flew. It is hard to make any statements on the precision of the position solution in the position view because of the scales involved.

Velocity Differentiation of the time evolution of the east, north and up position components gives the east, north and up component of the velocity. The norm of the velocities gives the absolute velocity or speed. The velocities apart from telling the velocities during the flights will show high frequency changes in position.

Acceleration Differentiation of the time evolution of the east, north, up and absolute velocity gives the east, north, up and total acceleration. Depending on the sampling interval and the smoothness of the position solution, the noise might contribute greatly to the acceleration. If the acceleration exceeds what is physically possible for the Carabas, then the high frequency changes in position must be noise in the recording limiting the precision of the recorded shape.

As the GPS receiver on the Carabas is capable of recording the GPS observations at 10 Hz, even small high frequency errors in the position results in large accelerations.

$$s = \frac{at^2}{2} \Rightarrow a = \frac{2s}{t^2} \quad (4.1)$$

Where s is the displacement, a is the acceleration and t is the sampling time.

Baseline The baseline is the relative position of the AFT and FWD antennas. In the FBL processing, the observations of the AFT and FWD antennas are processed together with the additional constraint that the distance between the two points is fixed. This makes it possible to determine in which direction the front of the Carabas

is pointing. The PPP processing of the AFT and FWD antennas is however parallel. By considering the relative position of the AFT and FWD antennas PPP positions, information about errors that differ between the AFT and FWD antennas solutions can be seen. If the baseline length, the distance between AFT and FWD is incorrect, at least one of the antennas position must be incorrect. If the baseline length depends on the heading of the Carabas one of the antennas will have a bias compared with the other one. If the noise in the position of the antennas are independent and random then the sum of these noises will be seen in the baseline length.

RTKLIB Q-value and Standard Deviation RTKLIB will output a Q-value and estimated standard deviations. The Q-value tells which kind of method was used to generate an epoch. The standard deviations are RTKLIBs estimates of the positional uncertainty.[18] This is mainly an estimate of the noise level and the corrections age, the true error can differ by orders of magnitude but it serves as an indicator for when something goes wrong with the solution.

4.5.2 Comparable Data analysis

The comparable data analysis is the main part in determining if it is possible to use a PPP solution to capture the flight motions. The analysis is done in MATLAB and compares the PPP solutions and the reference solutions of either RTKLIB-RTK or the professional Novatel GrafNav. The comparative analysis compares the position solutions in four ways.

- Full flight comparison of position in scene centre ENU coordinates.
- SAR-run Comparison of shape in SAR XRZ coordinates.
- Combined SAR-run comparison of shape in SAR XRZ coordinates.
- Combined sub-run comparison of shape in SAR XRZ coordinates.

The purpose of the comparable analysis is to estimate how the PPP solution differs from the REF in ways effecting the quality of the SAR image. The deviation is analysed as a function of duration, position, velocity and acceleration.

Full flight comparison

Full flight comparison of position in scene centre ENU coordinates gives an indication of the long term stability of the solution. In the full flight comparison the entire flight is analysed, that includes a potential start or landing.

Position deviation in scene centred coordinates The deviation of position between PPP and REF. Illustrate the long term stability of the deviation in position.

Position dependency of position deviation The deviation of position as a function of position to determine if the error is dependent of the position. The PPP solution has no local preference. Therefore a large dependency here might indicate that the quality of the reference solution is decreases as the receiver moves from the reference receiver.

Velocity dependency of change in position deviation The deviation of position as a function of velocity. If the deviation in position changes independent of velocity then the change of the deviation is more likely related to the duration of a flight and not the length of it. The velocity used here is calculated from the REF solution.

Acceleration dependency of change in positional deviation The deviation of position as a function of acceleration. During a SAR run the aircraft strive to fly straight. This correspond to a very small acceleration. If there was a well implemented dynamic model the Kalman filter should be able to more accurately track the position during periods of low acceleration. Acceleration is also caused by change of direction. If the change of deviation is dependent of the acceleration this might indicate a bias from the antennas.

SAR-run comparison

In the SAR-run comparison only the performance during the actual SAR-runs are considered. SAR image quality is primarily effect by the precision in the SAR-R direction, second in the SAR-X direction but not very much by the precision in the SAR-Z direction. Every SAR-run is therefore rotated into this system. The SAR-XRZ directions are found by first taking all points of the REF solution between the start time and the end time of a SAR-run and linearly fitting a line through them, this is the X direction. Second the direction perpendicular to X and towards the scene centre is found, this is the R direction. Finally the third direction is giving by the cross product of X and R this is the Z-direction. The inverse of these vectors gives the rotation matrix with which both the REF run and the PPP run is rotated.

To find the best, in least square sense, allowed transformation between the PPP and the REF solution Horn's Quaternion Method[9] is used. This gives the best translation and rotation matrix for aligning the PPP with the REF solution. The differences between the REF position solution and the transformed PPP SAR-run represented in the SAR-XRZ coordinates is the difference in shape.

Deviation of shape The deviations in shape between the PPP and the REF solution of the SAR-runs in the X, R, Z direction and the norm of the deviation A.

Maximum deviation of shape The maximum deviation of the shape during a SAR-run.

Standard deviation of deviation of shape The standard deviation of the deviation of the shape. It is the main value used for determining if the PPP solution can capture the flight motions during a SAR run.

Power spectrum of deviation of shape The power spectrum reveals if the deviations in shape change with a high or low frequency. Identifying whether the majority of the deviation is high frequency noise or low frequency drift.

Sub-run comparison

The SAR-runs are all of different duration. To determine how the duration effects the deviation of shape, all SAR-runs have been cut into overlapping sub-runs. The advantage of overlapping sub runs is more data points. The disadvantage is that outliers will turn into outlier clouds which might look like trends. The sub-runs have been made using 5 s increments in duration and 5 s between the start of every sub-run. A SAR-run with a total duration of 30 s would be analysed as six 5 s, five 10 s, four 15 s, three 20 s, two 25 s and one 30 s long sub-runs.

Duration impact on standard deviation of shape To determine if the standard deviation of the shape is dependent on flight duration, the sub-runs standard deviations of shape are plotted in a 2D-histogram normalised per duration.

Duration impact on change of bias To determine if the difference in deviation of sub-runs between PPP and REF change with duration, the sub-runs difference in deviations are plotted in a 2D histogram normalised per duration.

If the start and end time of a sub-run is t_1 and t_2 , then the starting and ending point is \vec{A}_{t_1} and \vec{A}_{t_2} for the reference solution and \vec{B}_{t_1} and \vec{B}_{t_2} for the PPP solution. The difference in bias at t_1 is then $\vec{r}_{t_1} = \vec{A}_{t_1} - \vec{B}_{t_1}$ and $\vec{r}_{t_2} = \vec{A}_{t_2} - \vec{B}_{t_2}$ at t_2 . The absolute change in bias is then:

$$\Delta r = |\vec{r}_{t_2} - \vec{r}_{t_1}| \quad (4.2)$$

Duration impact on deviation in length To determine if the difference in length of sub-runs between PPP and REF change with duration the sub-runs difference in lengths are plotted in a 2D histogram normalised per duration.

The deviation in length is:

$$\Delta L = \left| |\vec{B}_{t_2} - \vec{B}_{t_1}| - |\vec{A}_{t_2} - \vec{A}_{t_1}| \right| \quad (4.3)$$

Duration impact on deviation of speed To determine if the error in average speed is dependent on the duration of the sub-runs the difference in deviation is divided by duration giving the difference in speed. The difference in speed is plotted in 2D histogram normalised per duration.

The deviation of speed is:

$$\Delta v = \frac{|\vec{r}_{t_2} - \vec{r}_{t_1}|}{t_2 - t_1} \quad (4.4)$$

5

Results & Discussion

The results are presented in the order described in the method: full flight single, full flight-, SAR-run- and sub-run comparison. Of the full flight results only a representative single flight analysed with the IGS and IGU SCPs is presented. The results of the SAR-run and sub-run analysis are presented for all flights using all qualities of SCPs. A selection of results from the approach are also included.

Every result section is followed by a discussion.

A total of 12 flight with 182 SAR-runs generated with PPP using the IGS, IGR and IGU SCPs are analysed and compared using GrafNav as reference. Results are designated by processing methods (RTK PPP FBL), antennas (AFT FWD) and SCP (IGS IGR IGU). Single SAR-run results can also be referred to by their SAR-run IDs. The full flight results are in ENU position coordinates and the SAR-, sub-run results are in SAR XRZ coordinates.

Table 5.1: Analysed flights

Name	Runs	Passfile
130213b	10	D0208
130213c	10	D0209
130222a	12	D0210
141001a	21	E0904
141003a	22	E0910
141003b	18	E0911
141006a	21	E0912
141006b	18	E0913
141006c	10	E0914
141006d	12	E0915
141007a	16	E0916
141007b	12	E0917

5.1 Full Flight Single Data Analysis

The single flight analysis, not compared with the reference GrafNav solution, for the complete flight, not only the SAR-runs. These results are all from flight 141007b using the IGU and IGS corrections for the AFT and FWD antenna. Appendix A contain results from other flights. Time 0 correspond to the start of the first

SAR-run. The single flight analysis represent all information available after a flight without a comparative solution and might serve as a quality control for future flights.



Figure 5.1: Legend of full flight data analysis

5.1.1 Flight path view

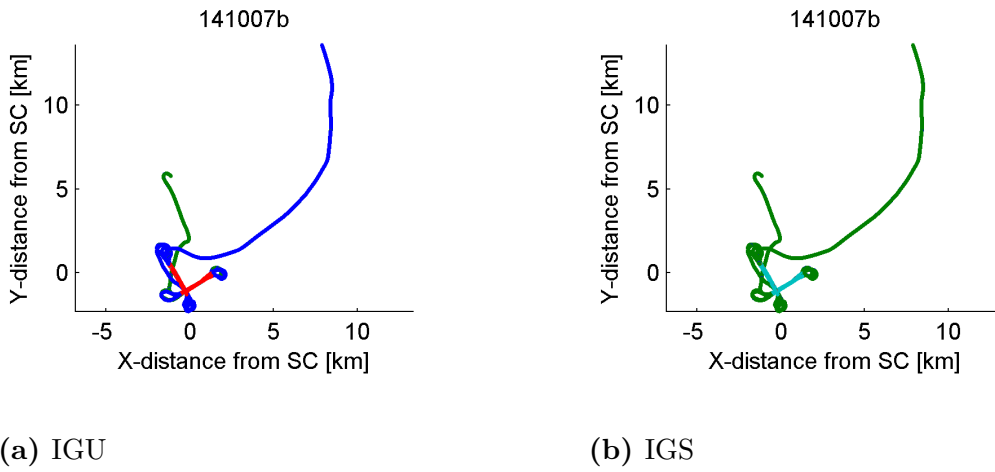
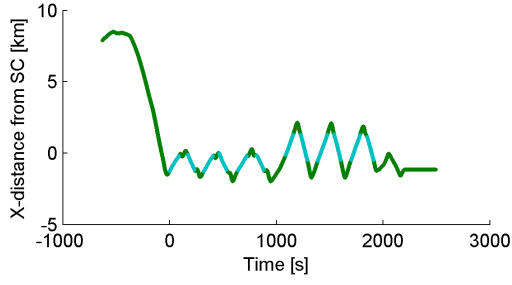


Figure 5.2: Flight141007b Flight path in scene centred coordinates for AFT and FWD. The SAR-runs have been highlighted. On this scale no difference can be seen between the AFT and FWD antenna.

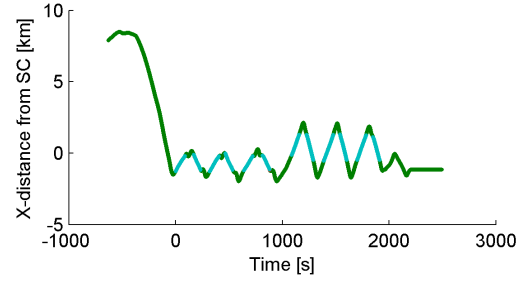
The analysed flights have similar compositions even if they look different in the flight path view. The GPS positions starts in flight on the way towards the scene centre area. While in the area it will fly back and forth on different heights while performing straight SAR-runs. Between each SAR-run the Carabas will turn sharply. In the end the Carabas flies away and lands. In some flights it is sometimes possible to see highlighted SAR-runs outside the normal straight parts. See figure A.4b. The reason as to why the passfiles contain SAR-runs like this is unknown to me but I expect that they are failed or incorrectly marked calibration SAR-runs. These SAR-runs have not been removed but kept and analysed together with the rest of the SAR-runs. As these SAR-runs contains curves they are made under less favourable circumstances, and will therefore not falsely improve the performance.

5.1.2 Position

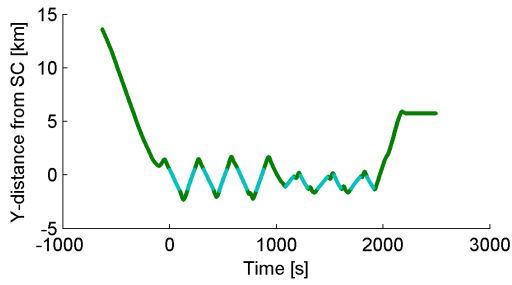
The position analysis in Figures 5.3a - 5.3f shows the flight path in the scene centred ENU coordinates xyz. All figures contain the overlapping AFT and FWD solution for PPP and REF.



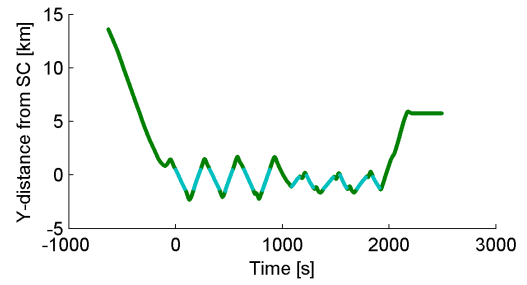
(a) IGU x



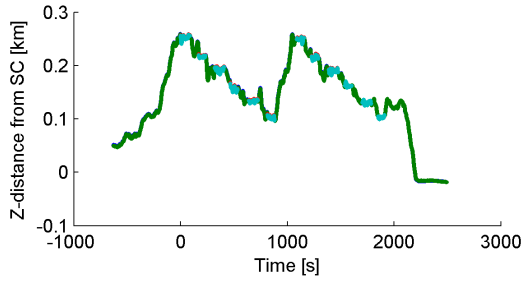
(b) IGS x



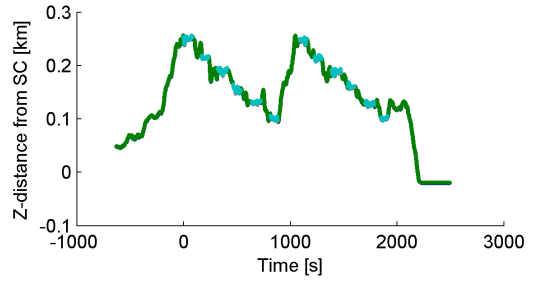
(c) IGU y



(d) IGS y



(e) IGU z



(f) IGS z

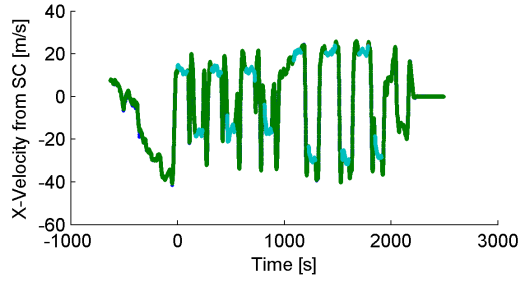
Figure 5.3: Flight141007b, Flight path in scene centred coordinates by time in for AFT and FWD. The SAR-runs have been highlighted.

No difference is seen between the AFT and FWD antenna or between IGU and the better IGS SCP. The colour of the flights and SAR-runs are therefore not important.

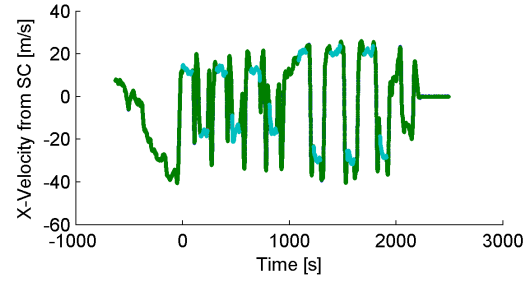
It can sometimes be seen that the flight have SAR-runs very close to the start or end of the GPS registration. See figure A.1a. As the PPP technique requires a start up time for convergence the precision of these SAR-runs might be worsened. The last SAR-run is affected the same way as the Kalman filter also process the observations in reverse.

5.1.3 Velocity

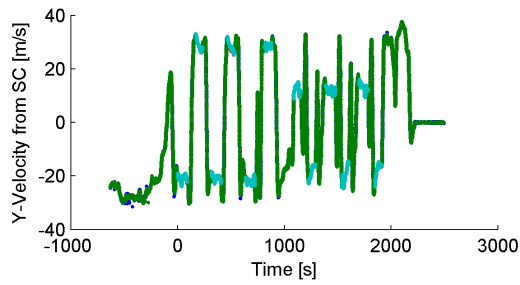
The velocities are computed as the derivatives of the positions in ENU coordinates. The total velocity is the RMS of the velocities.



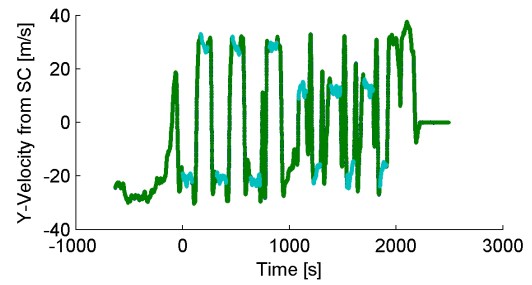
(a) IGU x



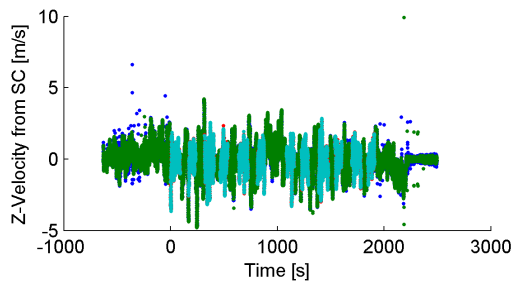
(b) IGS x



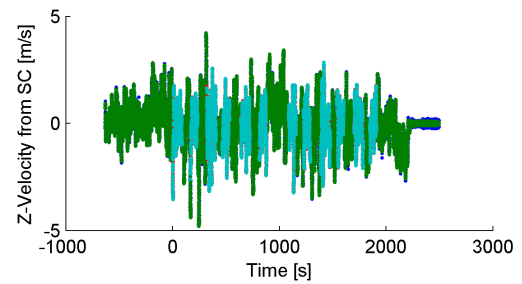
(c) IGU y



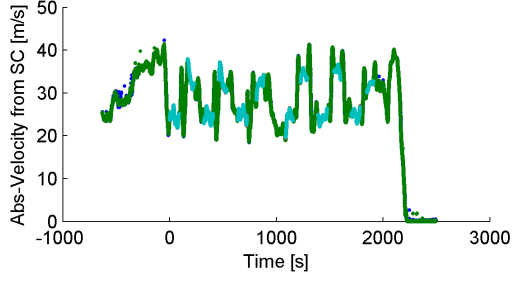
(d) IGS y



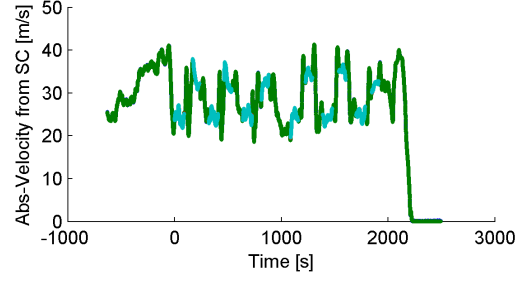
(e) IGU z



(f) IGS z



(g) IGU tot



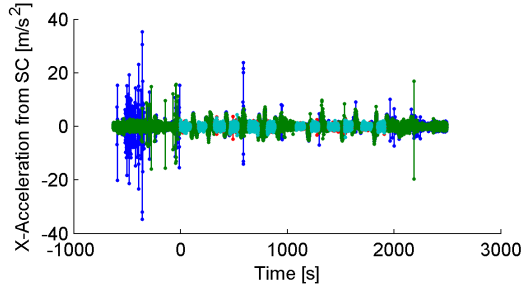
(h) IGS tot

Figure 5.4: Flight 141007b Velocity by time in for AFT and FWD. The SAR-runs have been highlighted.

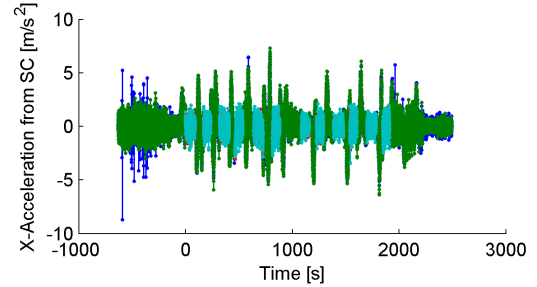
The velocity analysis show that the Carabas flies between 20 and 40 m/s during the SAR-runs. The recording is started in flight and stopped when stationary. Only slight differences between AFT and FWD can be seen.

5.1.4 Acceleration

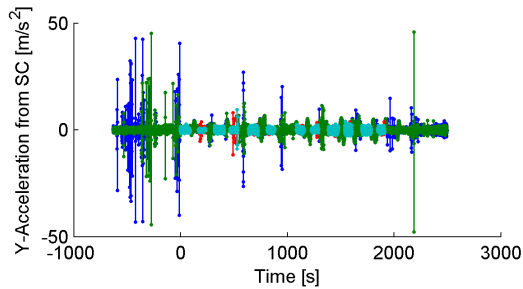
The accelerations are computed as the derivatives of the velocities in ENU coordinates. The total acceleration is the RMS of the accelerations.



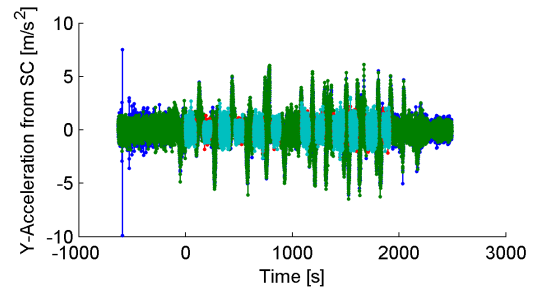
(a) IGU x



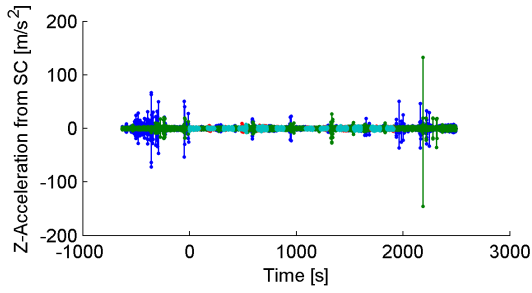
(b) IGS x



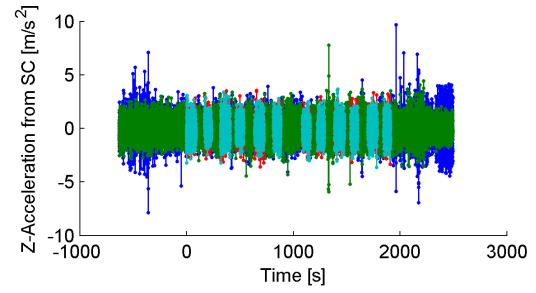
(c) IGU y



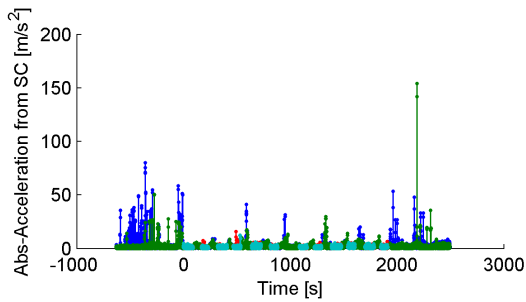
(d) IGS y



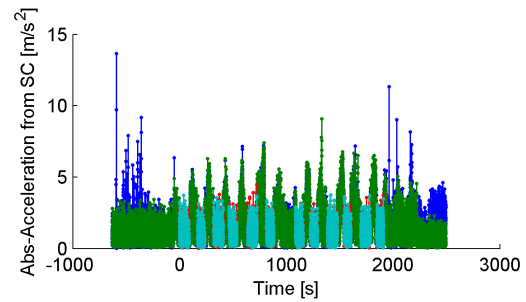
(e) IGU z



(f) IGS z



(g) IGU tot



(h) IGS

Figure 5.5: Flight 141007b Acceleration by time. For AFT (blue) and FWD (turquoise).

The accelerations from the noise peaks in the IGU solution drowns out the true accelerations created by the sharp turns. The noise in the acceleration is lower during the SAR-runs suggesting a more stable solution. In the IGS figures the turns can be seen. The acceleration noise is worst in the up, z-direction. The recorded acceleration is less than 10 m/s^2 in the curves and it has a median of 1 m/s^2 on the SAR-runs. 0.5 % of the accelerations are above 10 m/s^2 . The acceleration peaks are often mirrored in the time axis. A five point travelling mean smooth filter reduces the median acceleration by half.

5.1.5 Baseline and Fixed Baseline

The baseline is the relative position of the AFT and FWD antenna when processed separately. Fixed baseline is the relative position between the AFT and FWD antenna when processed together and with a fixed distance between them.

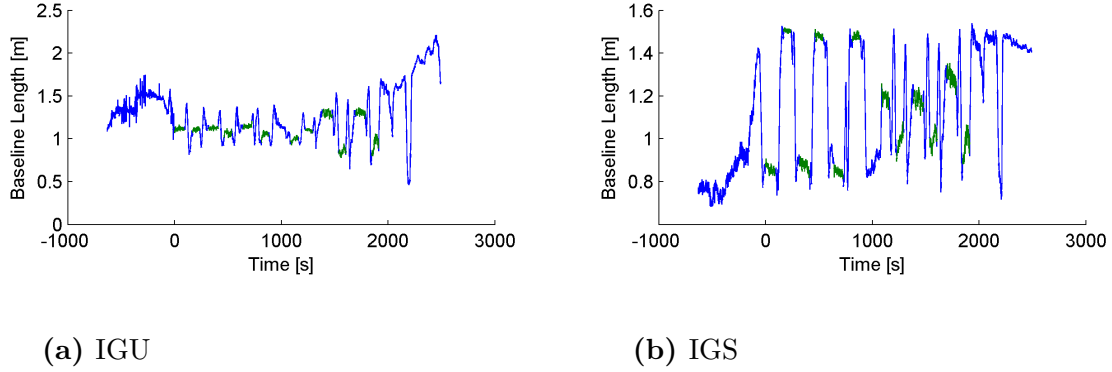


Figure 5.6: Baseline length by time. SAR-runs highlighted.

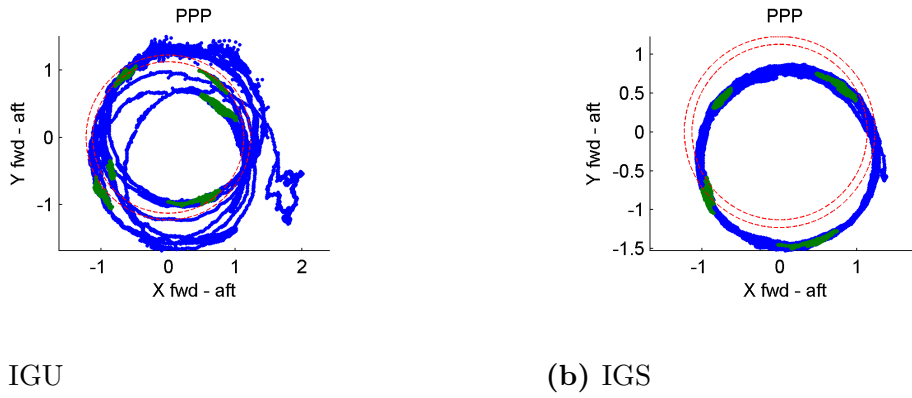


Figure 5.7: 141007b 2D baseline. The red dotted circles indicate the span where the baseline would move if the position solutions were accurate.

The baseline length changes with time. During the SAR-runs when the Carabas is flying in constant direction the baseline length is however uniform. The baseline length changes greatly between the SAR-runs when the Carabas changes direction. The baseline length is dependent of the heading of the Carabas. This indicating that the AFT and FWD solutions positions have different biases.

When the baseline is seen from above in a 2D figure the baseline creates a circle which is offset from the origin. For the IGS solution the offset for this flight is constantly 25 cm in the y direction. This is the result of the FWD position having a bias in the negative y, south direction larger then the one of the AFT antenna. That the difference in bias does not change suggests that the biases are constant, the alternative would be that they changed uniformly. For the IGU solutions the difference in bias change over time.

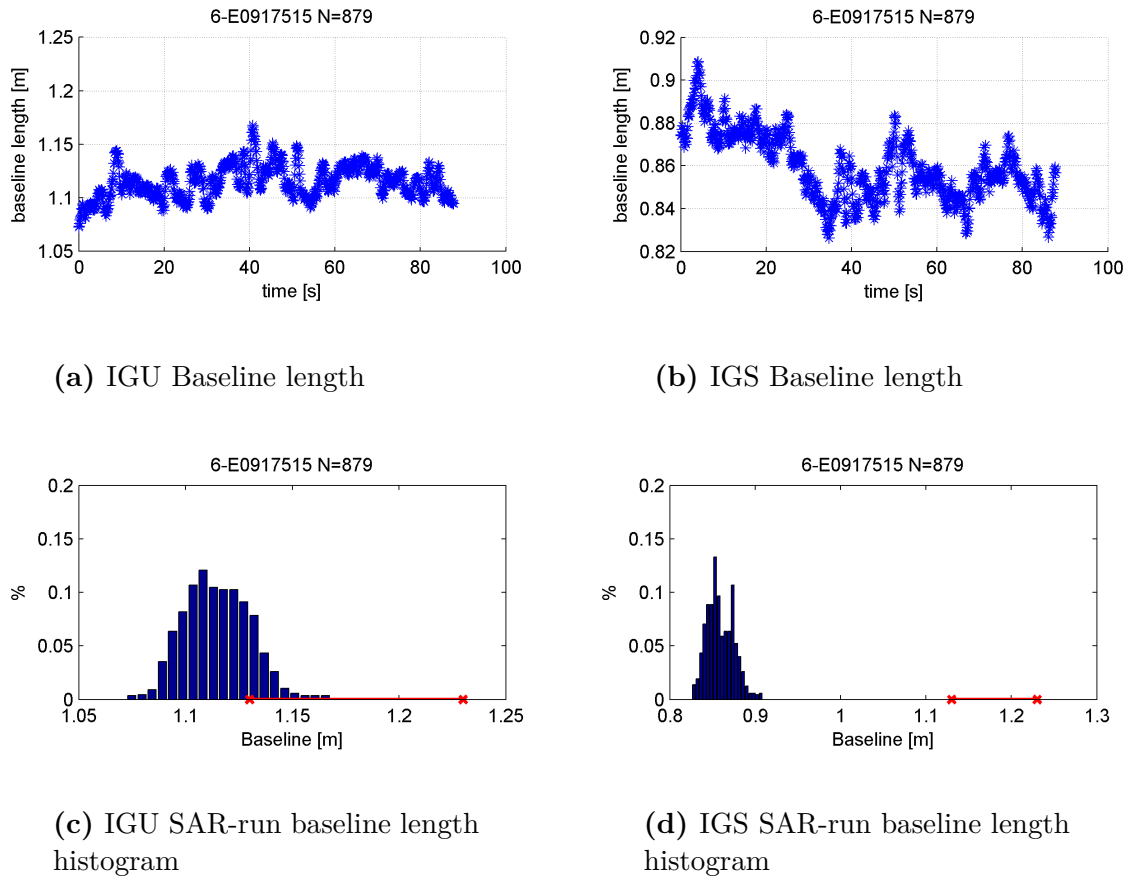


Figure 5.8: 141007b baseline of SAR-run E091715. The red line indicate the span where the baseline would move if the position solutions were accurate.

Analysis of the baseline during a SAR-run, 5.8a-5.8d show that the baseline length does not drift¹. The noise in the baseline length is the sum of the noise of the AFT and FWD solution position in the flight direction. The noise in the baseline length can therefore be used to estimate the precision of the position in the flight direction.

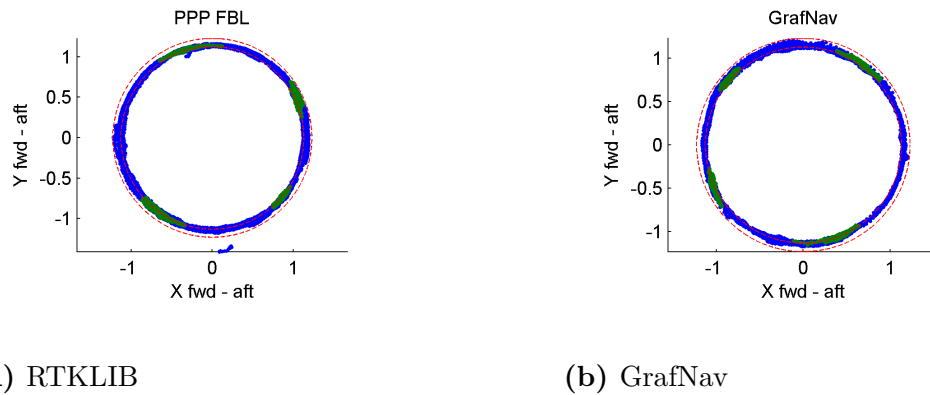


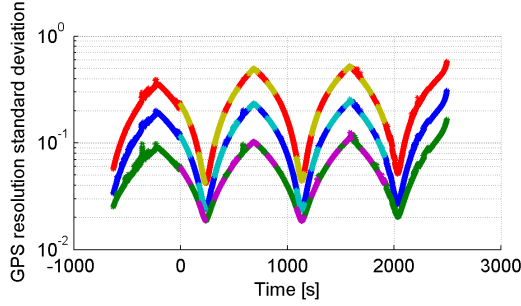
Figure 5.9: 141007b Fixed baseline

¹This is only from a single SAR-run but the other ones are similar. Most are in fact a bit better as this run is the first one of a flight.

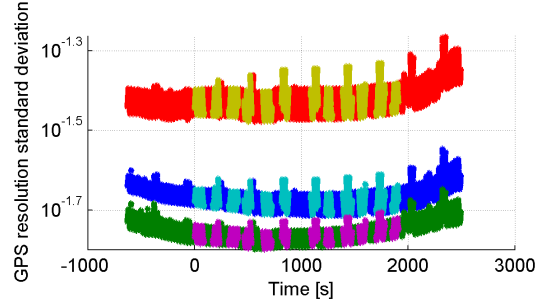
The fixed baseline processing of RTKLIB is most of the time able to resolve the CPAR. GrafNav losses the ambiguities less often.

5.1.6 RTKLIB Quality Flag Standard Deviations

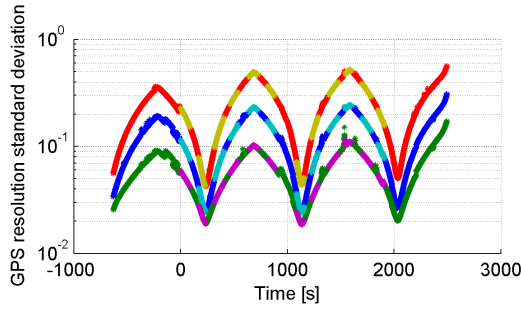
Standard deviations of the error in position as reported by RTKLIB.



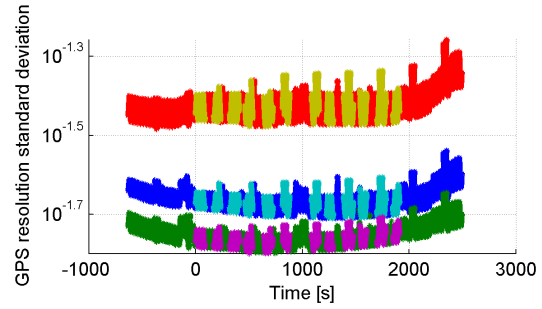
(a) IGU AFT



(b) IGS AFT



(c) IGU FWD



(d) IGS FWD

Figure 5.10: RTKLIB reported standard deviations. Blue is x-direction, Green is y-direction and Red is z-direction.

The RTKLIB reported standard deviations mostly shows the resolution of the SCPs. For the IGS data processing it is possible to see that the standard deviations are worse in the beginning and end of a flight. Two possibilities for this can be the PPP solutions convergence time and that the Carabas is on the ground where the low elevation mask might pose a problem. The standard deviation oscillates for IGU by 900 s and for IGS with 30 s this is the same as the update intervals of the SCP.

5.2 Full flight comparative analysis

The full flight comparison results come from the analysis of a complete single flight, including all runs and turns. The results here are all from flight 141007b using configuration conf095, for details see Appendix C.1.

5.2.1 Position deviation

The deviation of position between the PPP solution and the REF solution.

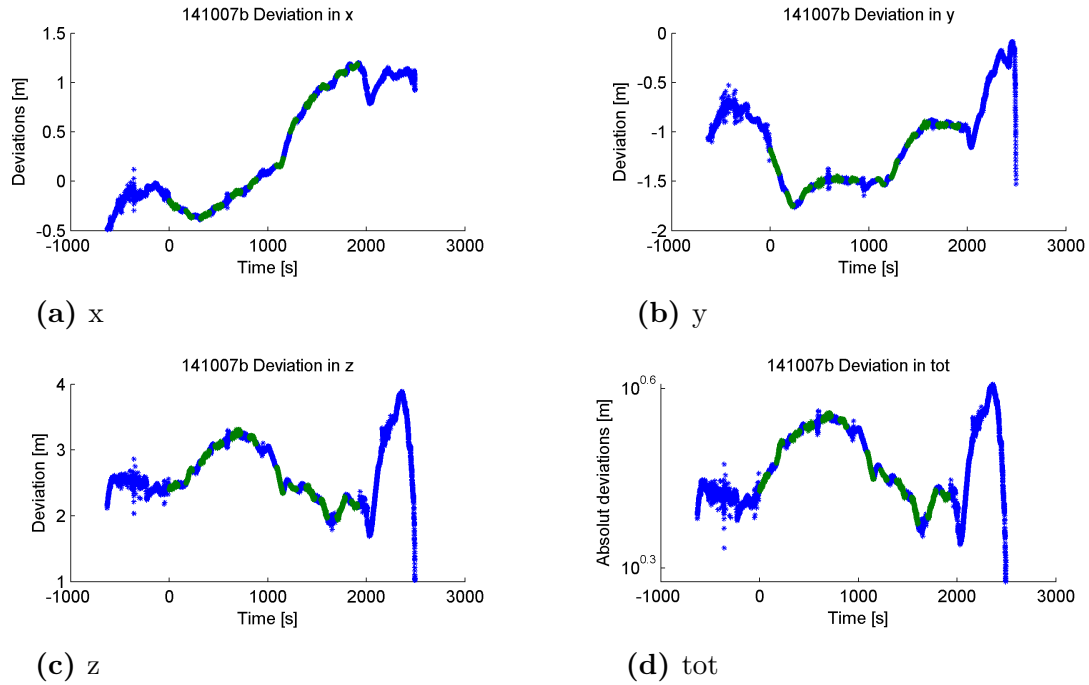


Figure 5.11: Flight 141007b IGU. Deviation between the REF and the PPP solutions for the AFT antenna in blue the green sections are the runs.

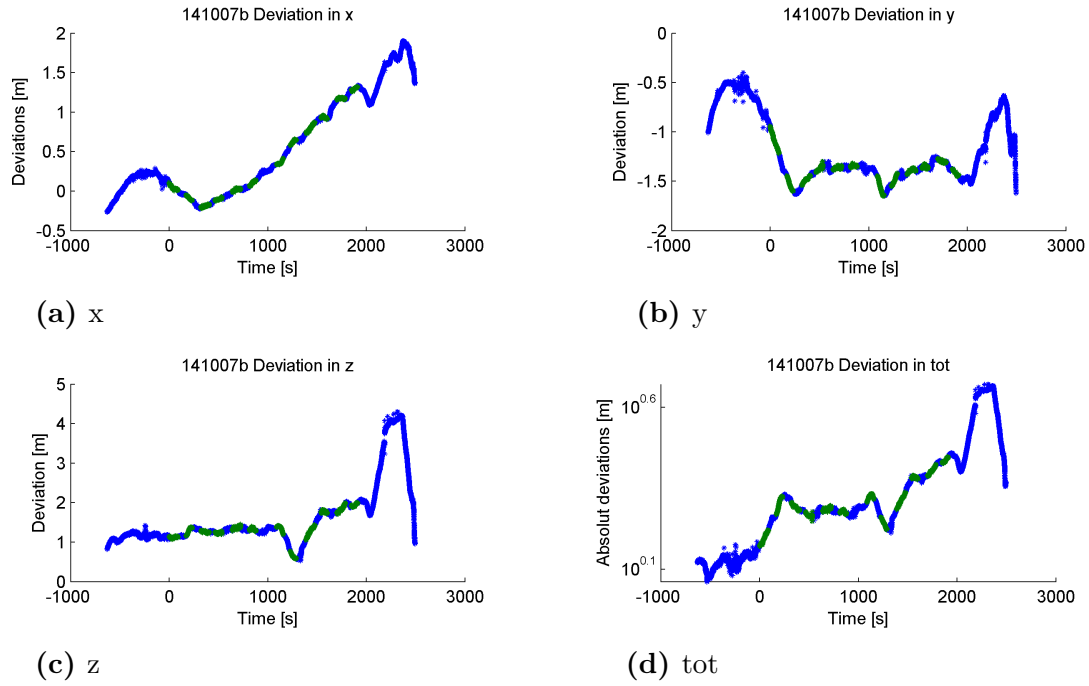


Figure 5.12: Flight 141007b IGU. Deviation between the REF and the PPP solutions for the FWD antenna in blue the green sections are the runs.

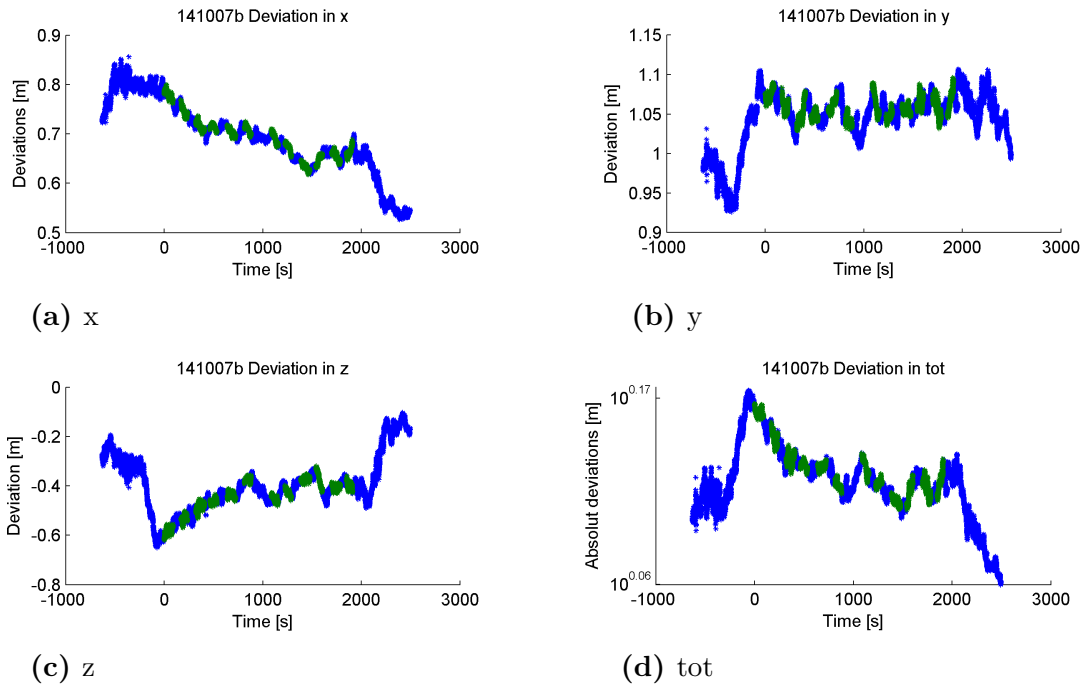


Figure 5.13: Flight 141007b IGS. Deviation between the REF and the PPP solutions for the AFT antenna in blue the green sections are the runs.

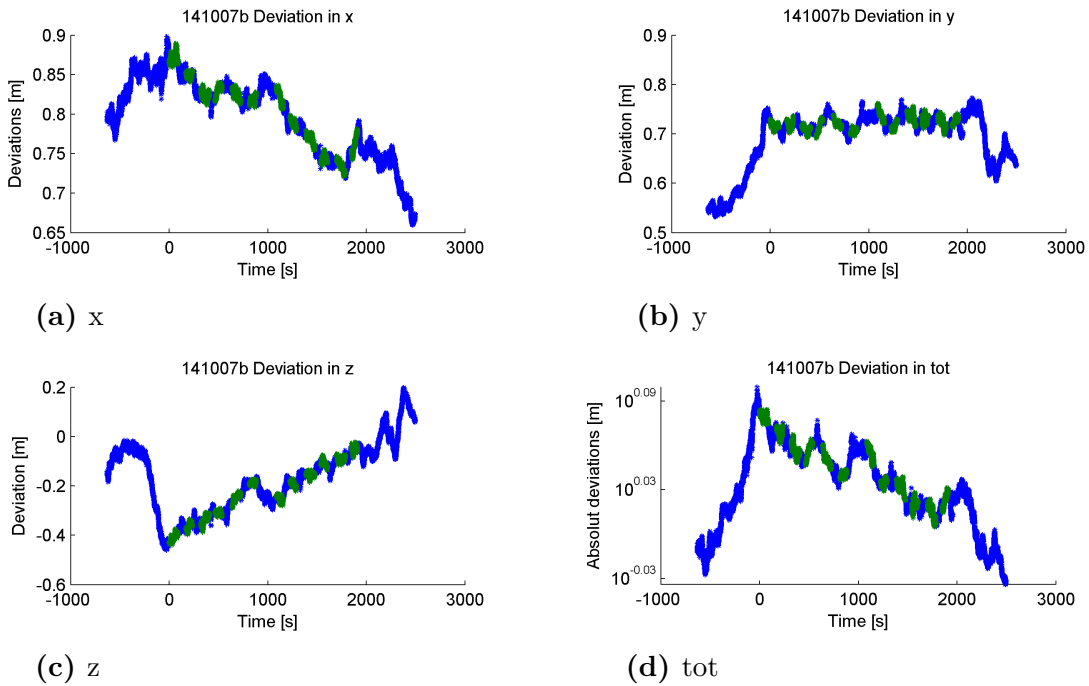


Figure 5.14: Flight 141007b IGS. Deviation between the REF and the PPP solutions for the FWD antenna in blue the green sections are the runs.

The deviation between PPP and REF can often be several meters for IGU. For IGS the deviation is less than a meter. The deviation is mostly continuous but drifts with time. The deviation is slightly different for AFT and FWD.

5.2.2 Position dependence on positional deviation

The deviation in position by the Carabas position from the scene centre. If the deviation would be constant for all instances of the same position and rapidly changing with changes in position there would be a large positional dependency.

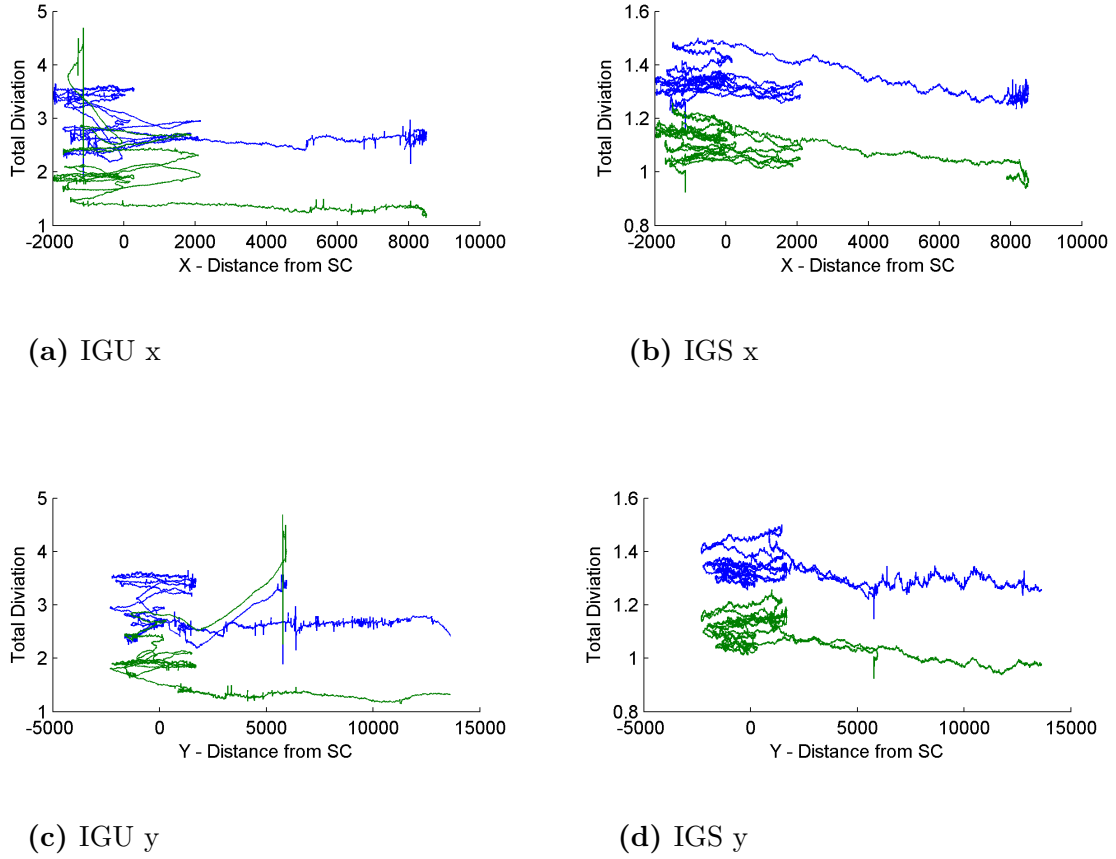


Figure 5.15: Deviation dependence on position.

As it is now the long flight in towards the SC give no large contribution compared with the one given by time.

5.2.3 Velocity dependence on change of deviation in position

How the deviation of position changes depending on the velocity, will clarify if the deviation of the position is dependent on the duration or the length of the SAR-run.

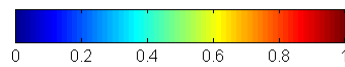


Figure 5.16: Jet legend used for coming Figure.

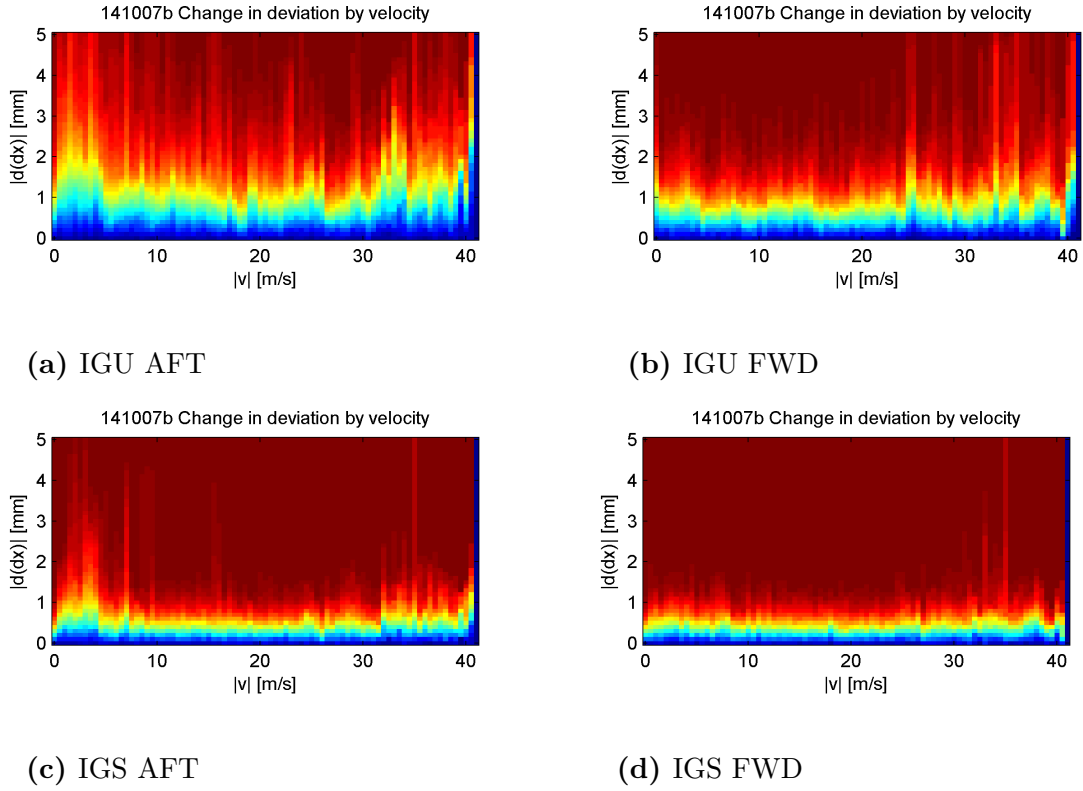


Figure 5.17: Change in deviation by velocity.

From the 2D histograms of absolute velocity and absolute deviation normalised by velocity no velocity dependant deviation changing tendency is seen.

5.3 SAR-run analysis

The separate analysis of the SAR-runs. These results are only based on the performance during the straight SAR-runs. It is the shape of the SAR-runs which is analysed, meaning the deviations in position after the rotation and translation from Horn's method have been made. The results are expressed in the SAR-XRZ coordinate system of the respective run.

5.3.1 Deviation in shape

Comparison of shape between the PPP and RTK solution. Flight 14007b and its first SAR-run is presented here. The deviations are shown for IGS and IGU SCPs. For deviation in shape of additional flights and SAR-runs see Appendix A.2.1 and B. A total 183 runs were analysed.

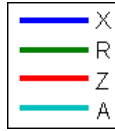


Figure 5.18: Legend for coming Figure.

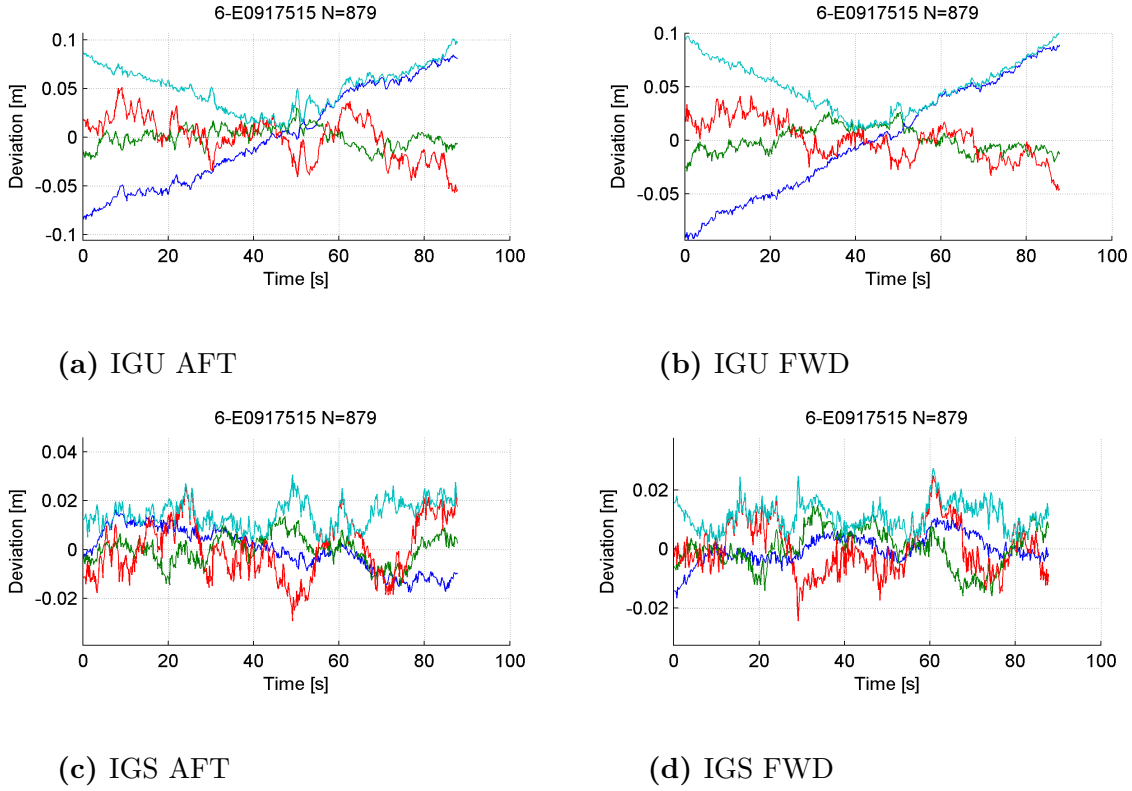


Figure 5.19: Run E0917515

The deviations are smaller when IGS is used compared to when IGU is used. Most of the deviations have the shape of noise. In this specific SAR-run the X-component of the deviation has a large linearly dependency of time. This can be explained by a drift in the bias of the position, scaling the shape in the flight direction. See Section 3.4.4 for clarification.

A Comparison of the IGU and IGS solutions for all SAR-runs show that the IGS solutions is consistently better then the IGU. It is especially the SAR-runs with large deviations for the IGU solution that improve when instead using IGS.

Table 5.2: Flight 141007b AFT IGU: Maximum and Standard deviation of the deviation of shape from the reference for the SAR-runs in mm.

Run	N	max(X)	max(R)	max(Z)	max(A)	Sd(X)	Sd(R)	Sd(Z)	Sd(A)
6-E0917515	879	84	30	51	101	50	10	22	56
7-E0917516	636	36	21	23	59	24	12	12	29
8-E0917517	879	43	18	43	51	18	9	19	28
9-E0917518	709	38	44	36	65	11	9	11	18
10-E0917519	841	22	28	67	73	9	13	21	26
11-E0917520	674	24	27	44	53	11	10	20	25
12-E0917521	697	38	26	28	53	14	10	11	21
13-E0917522	620	96	15	26	108	62	9	10	63
14-E0917523	888	69	26	57	86	44	9	24	51
15-E0917524	624	28	24	39	56	12	9	17	23
16-E0917525	837	18	17	52	64	10	8	18	23
17-E0917526	614	39	13	33	51	11	5	15	19

Table 5.3: Flight 141007b AFT IGS: Maximum and Standard deviation of the deviation of shape from the reference for the SAR-runs in mm.

Run	N	max(X)	max(R)	max(Z)	max(A)	Sd(X)	Sd(R)	Sd(Z)	Sd(A)
6-E0917515	879	16	14	26	31	9	6	11	15
7-E0917516	636	9	16	23	31	5	8	12	15
8-E0917517	879	22	19	32	46	14	8	13	21
9-E0917518	709	9	12	26	27	4	5	9	11
10-E0917519	841	13	10	21	28	9	4	10	14
11-E0917520	674	11	13	22	23	5	5	7	10
12-E0917521	697	28	10	18	36	17	3	8	19
13-E0917522	620	11	10	18	22	5	4	6	10
14-E0917523	888	15	12	18	22	7	4	8	12
15-E0917524	624	19	10	16	23	10	6	7	13
16-E0917525	837	27	16	19	31	14	6	9	18
17-E0917526	614	38	9	26	46	14	4	10	18

Table 5.4: Flight 141007b FWD IGU: Maximum and Standard deviation of the deviation of shape from the reference for the SAR-runs in mm.

Run	N	max(X)	max(R)	max(Z)	max(A)	Sd(X)	Sd(R)	Sd(Z)	Sd(A)
6-E0917515	879	89	27	42	101	53	11	18	57
7-E0917516	636	39	15	33	68	30	8	11	33
8-E0917517	879	39	15	32	42	17	7	15	24
9-E0917518	709	34	39	35	72	17	7	11	22
10-E0917519	841	17	24	54	60	7	11	21	24
11-E0917520	674	25	22	49	56	13	9	25	29
12-E0917521	697	62	29	32	81	27	16	18	36
13-E0917522	620	56	20	30	76	42	9	9	44
14-E0917523	888	65	34	42	83	44	9	22	50
15-E0917524	624	30	12	53	53	15	6	16	22
16-E0917525	837	14	13	55	56	7	6	16	19
17-E0917526	614	18	15	28	38	7	5	10	14

Table 5.5: Flight 141007b FWD IGS: Maximum and Standard deviation of the deviation of shape from the reference for the SAR-runs in mm.

Run	N	max(X)	max(R)	max(Z)	max(A)	Sd(X)	Sd(R)	Sd(Z)	Sd(A)
6-E0917515	879	11	15	25	27	5	7	9	12
7-E0917516	636	11	13	22	25	5	6	9	12
8-E0917517	879	15	15	21	38	5	7	10	13
9-E0917518	709	13	10	23	24	8	4	8	12
10-E0917519	841	8	10	25	27	5	5	9	11
11-E0917520	674	10	11	21	21	4	4	6	9
12-E0917521	697	22	14	20	30	13	5	9	17
13-E0917522	620	10	13	18	21	4	5	7	10
14-E0917523	888	17	14	20	31	9	7	9	14
15-E0917524	624	19	11	20	32	8	7	8	13
16-E0917525	837	18	17	19	28	10	7	8	15
17-E0917526	614	21	11	28	33	12	4	12	17

5.3.2 Power spectrum of deviation

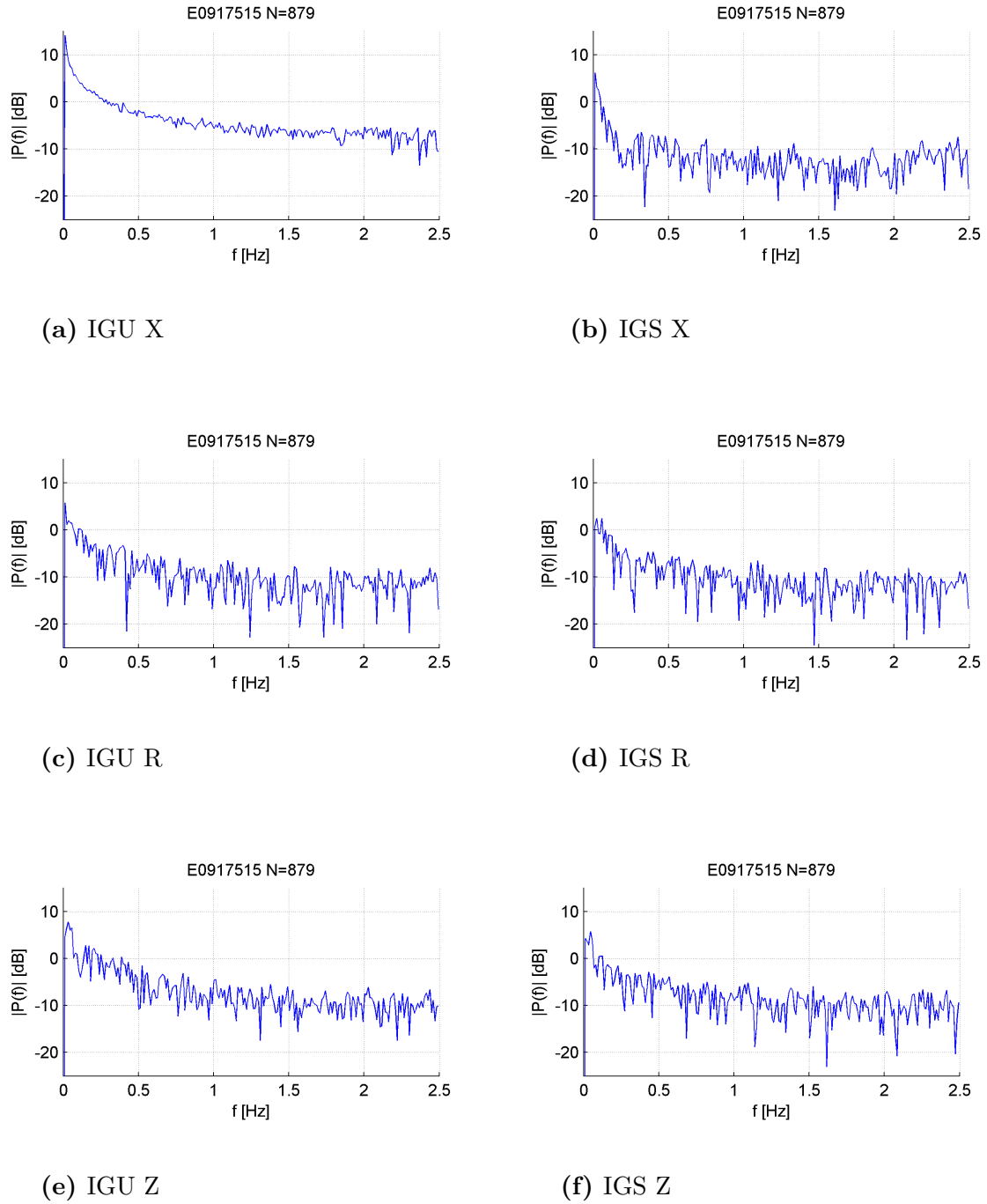


Figure 5.20: Power spectrum for run E0917515.

The power spectrum on the deviation of shape show that the deviation has a large low frequency component compared.²

²This is only the power spectrum of a single SAR-run but the others are similar. This SAR-run has a larger deviation in the X-direction for IGU then the norm.

5.3.3 Standard deviations of shape for all SAR-runs

The standard deviation of the shape, the standard deviation of the transformed SAR-runs PPP solution compared with the RTK-solution, is the most accurate estimate of the quality of the positioning techniques in respect to SAR image processing, presented here. The standard deviation of the shape is therefore presented for all SAR-runs of all flight using all available qualities of SCPs. For each combination of correction, antenna and direction the mean standard deviation of shape and steadfastness standard deviation S is also calculated. The steadfastness standard deviation is the standard deviation of the standard deviations of shape.

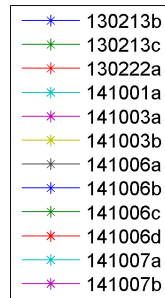
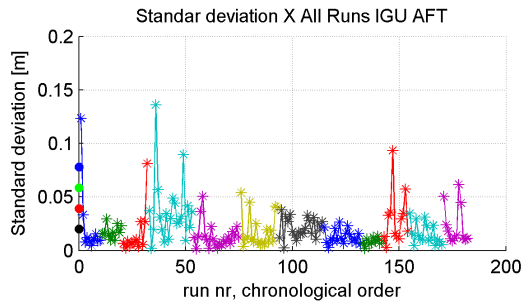
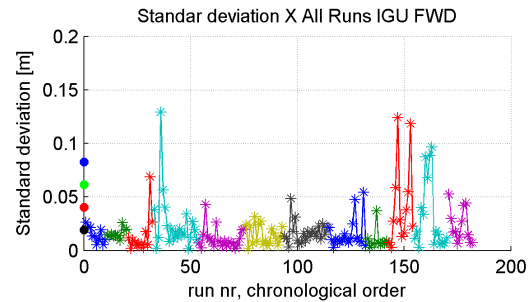


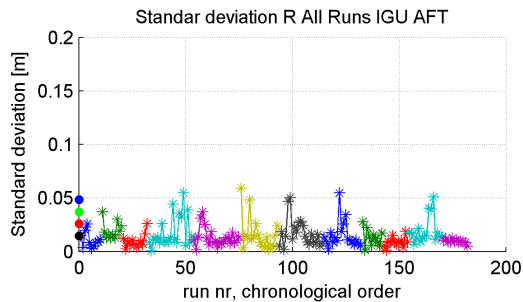
Figure 5.21: Legend with the different flights for the standard deviations of shape for all SAR-runs.



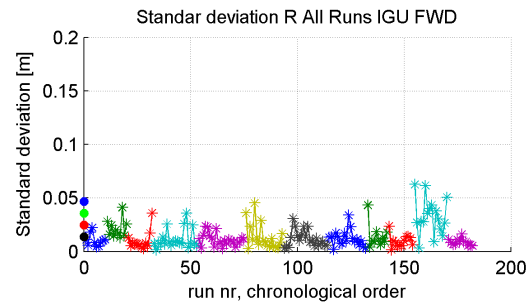
(a) X AFT



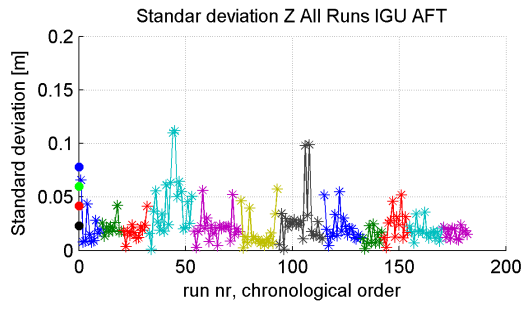
(b) X FWD



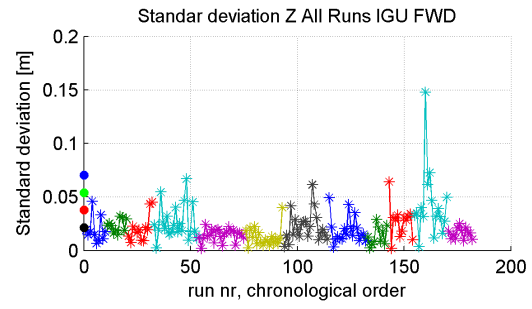
(c) R AFT



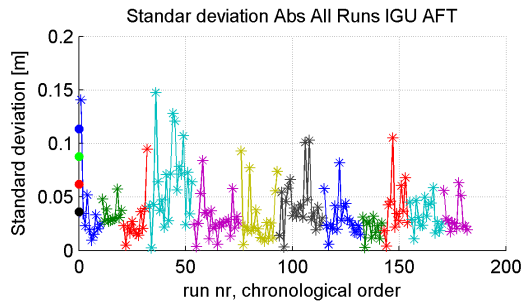
(d) R FWD



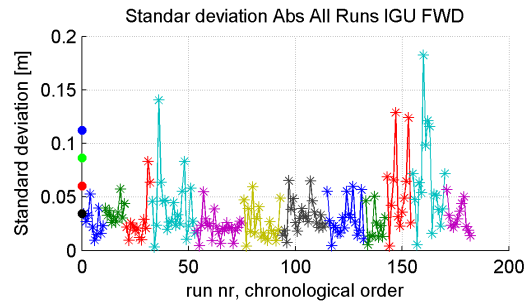
(e) Z AFT



(f) Z FWD

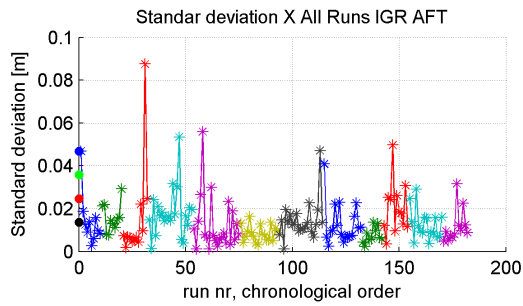


(g) A AFT

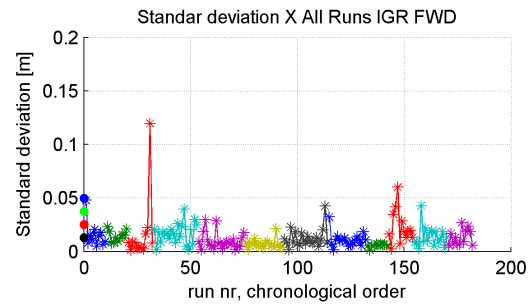


(h) A FWD

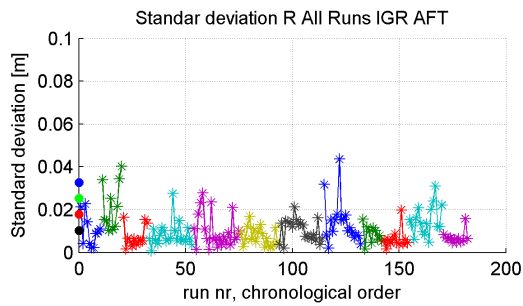
Figure 5.22: IGU Standard deviations of shape.



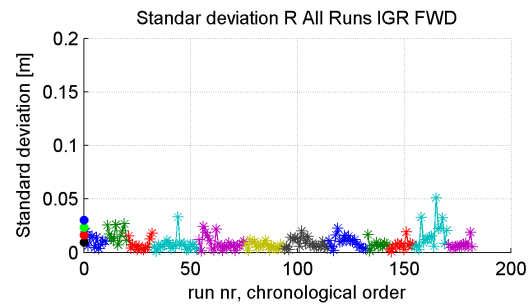
(a) X AFT



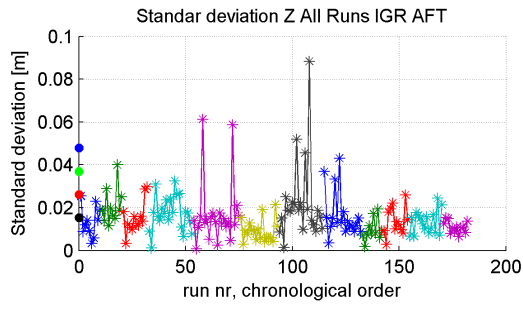
(b) X FWD



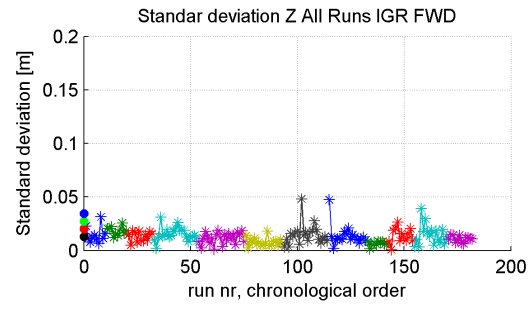
(c) R AFT



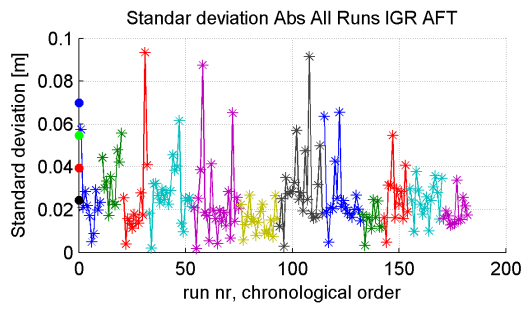
(d) R FWD



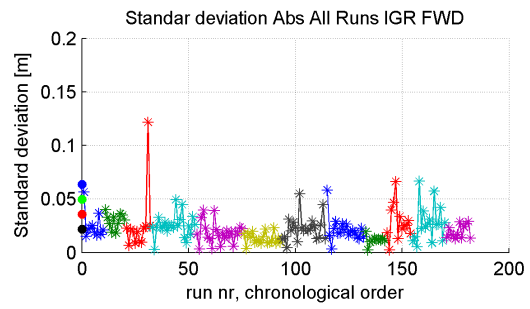
(e) Z AFT



(f) Z FWD

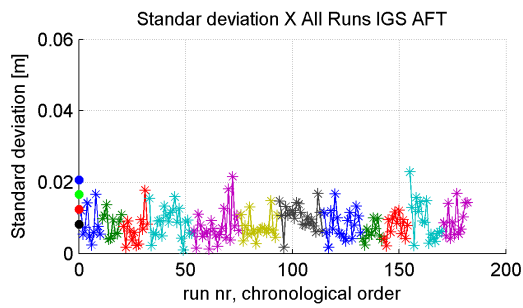


(g) A Aft

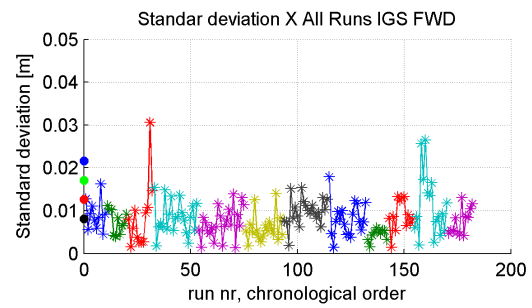


(h) A FWD

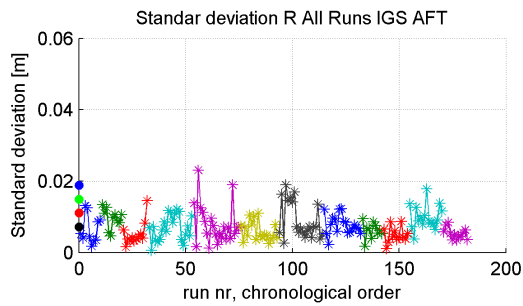
Figure 5.23: IGR Standard deviations of shape.



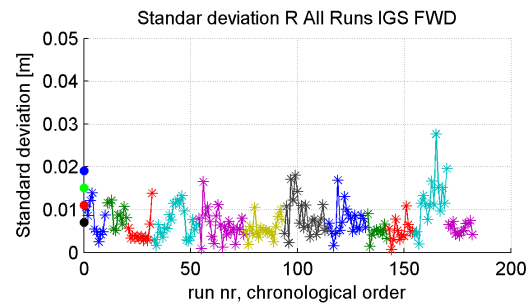
(a) X AFT



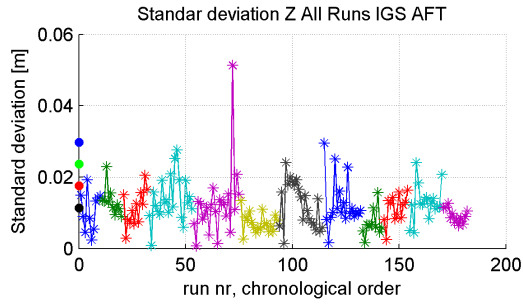
(b) X FWD



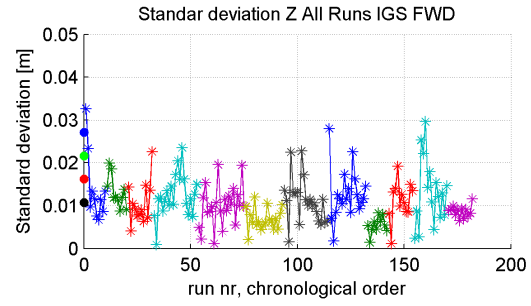
(c) R AFT



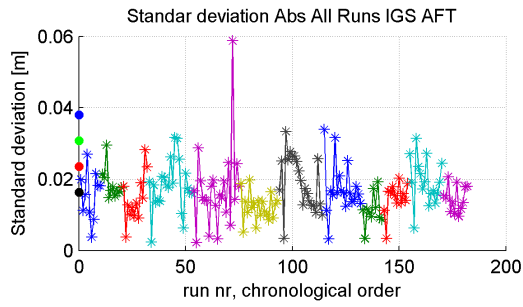
(d) R FWD



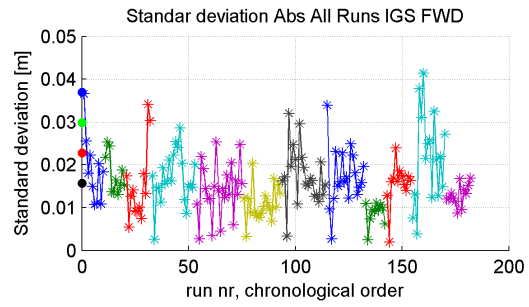
(e) Z AFT



(f) Z FWD



(g) A Aft



(h) A FWD

Figure 5.24: IGS Standard deviations of shape.

The shape capturing capabilities are best when using the IGS SCP and worst for the IGU. The IGU will pass the 5 cm over 90 % in in a single direction and 80 % in the absolute. If a SAR-run fail for one antenna or direction there is an increased risk that it will fail in the other directions too. The average standard deviation of shape is under 5 cm in all direction. The steadfastness standard deviations are of the same order as the standard deviation of shape. This is caused by large difference between SAR-runs of the same type. In total this means that the PPP technique is capable of capturing the shape, but that the technique is not completely reliable. See tables 5.6 and 5.7 for more detailed statistics.

Table 5.6: Number of SAR-runs with a standard deviation of shape larger then 5 cm and the success ratio.

		X		R		Z		A	
		N	%	N	%	N	%	N	%
IGU	AFT	11	94.4	5	97.3	17	90.7	37	79.7
	FWD	13	92.9	3	98.4	7	96.2	35	80.8
IGR	AFT	3	98.4	0	100	4	97.8	11	94.0
	FWD	2	98.9	1	99.5	0	100	7	96.2
IGS	AFT	0	100	0	100	1	99.5	1	99.5
	FWD	0	100	0	100	0	100	0	100

Table 5.7: Average standard deviation of shape and steadfastness standard deviation of the SAR-runs in mm.

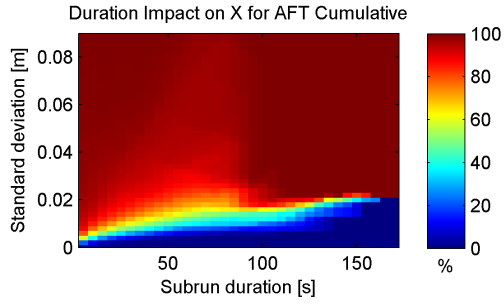
		X		R		Z		A	
		$\bar{\sigma}$	S	$\bar{\sigma}$	S	$\bar{\sigma}$	S	$\bar{\sigma}$	S
IGU	AFT	19.9	19.4	14.6	11.3	23.2	18.4	36.3	25.8
	FWD	19.4	21.1	13.8	11.0	21.3	16.4	34.3	26.0
IGR	AFT	13.6	11.1	10.4	7.5	15.3	10.8	24.3	15.2
	FWD	12.9	12.3	9.4	7.0	12.9	7.2	21.9	13.8
IGS	AFT	8.2	4.2	7.2	3.9	11.4	6.1	16.3	7.2
	FWD	8.1	4.5	7.1	4.0	10.8	5.4	15.7	7.1

5.4 Sub-run analysis

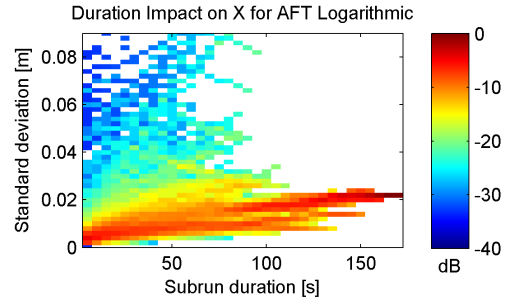
Sub-runs are parts of SAR-runs cut to specific durations. This enables analysis of the performance of the PPP method by duration. The duration impact on change in bias, change in length and the standard deviation of shape has been analysed.

5.4.1 Duration impact on deviation of shape

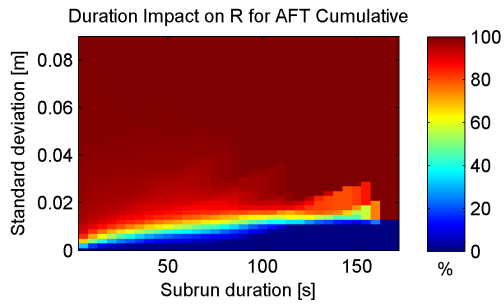
The standard deviations for all sub-runs according to their length for AFT and FWD with IGU, IGR and IGS SCPs.



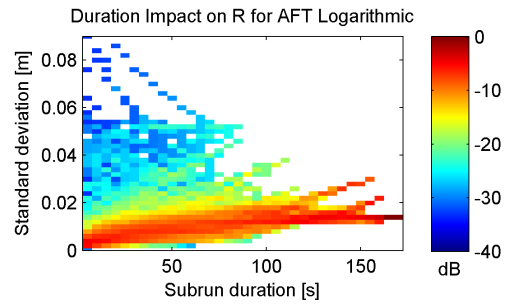
(a) X direction cumulative fraction.



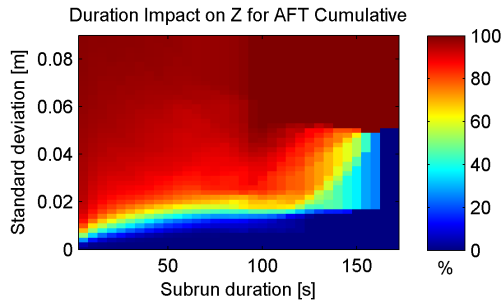
(b) X direction distribution logarithmic.



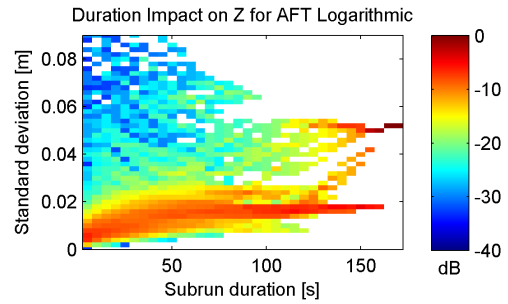
(c) R direction cumulative fraction.



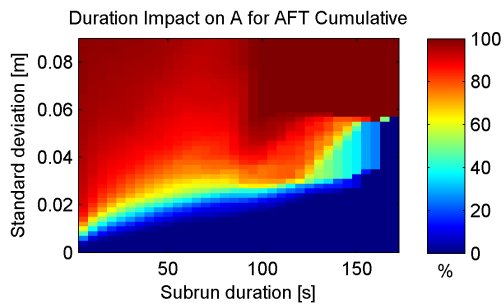
(d) R direction distribution logarithmic.



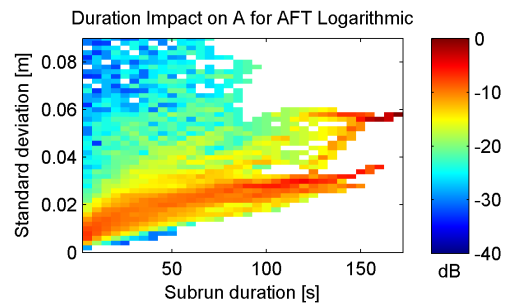
(e) Z direction cumulative fraction.



(f) Z direction distribution logarithmic.

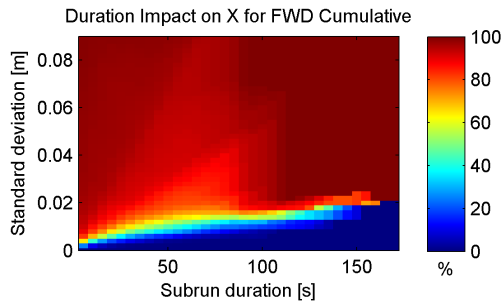


(g) A direction cumulative fraction.

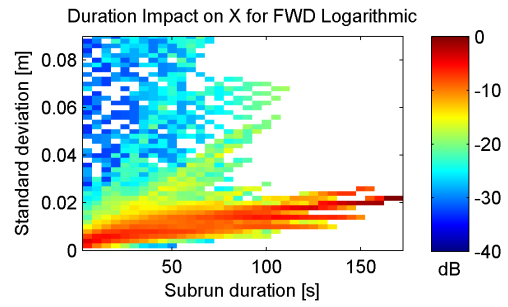


(h) A direction distribution logarithmic.

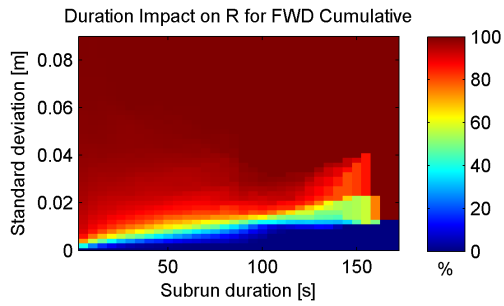
Figure 5.25: IGU All flights, Flight duration impact on standard deviation of deviation for AFT antenna.



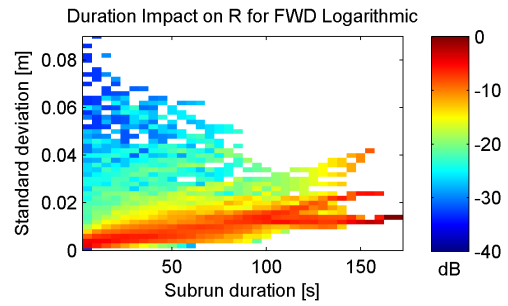
(a) X direction cumulative fraction.



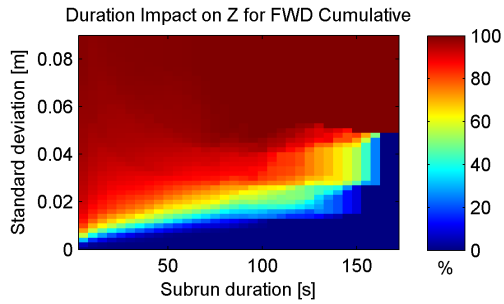
(b) X direction distribution logarithmic.



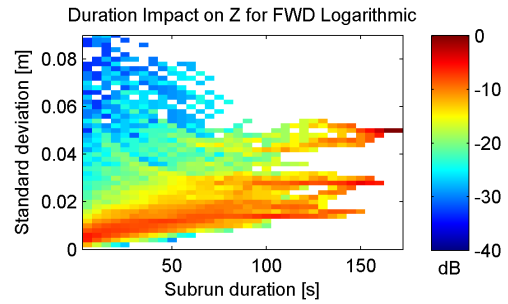
(c) R direction cumulative fraction.



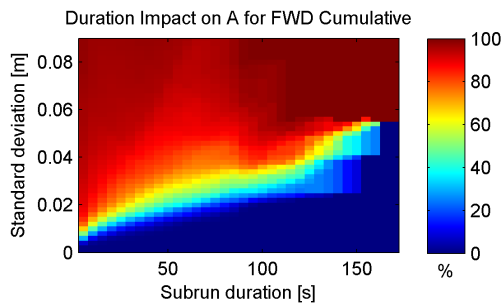
(d) R direction distribution logarithmic.



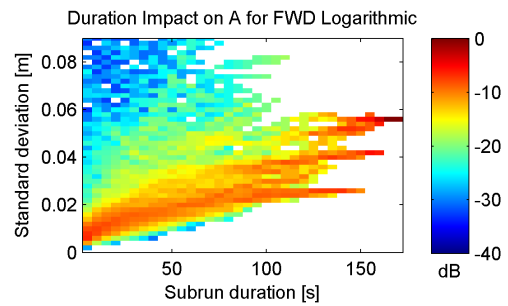
(e) Z direction cumulative fraction.



(f) Z direction distribution logarithmic.

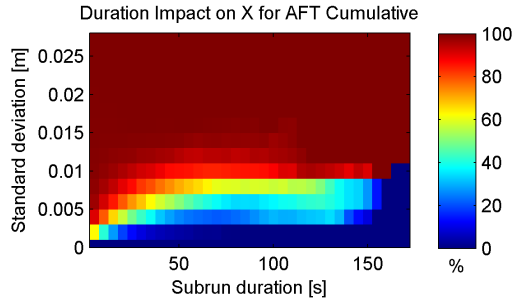


(g) Z direction cumulative fraction.

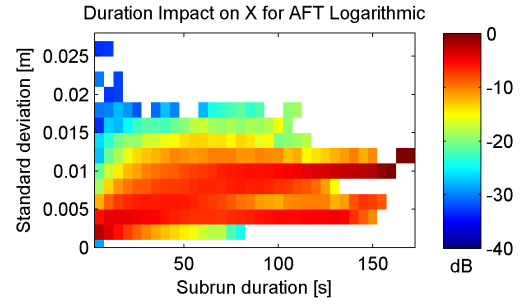


(h) Z direction distribution logarithmic.

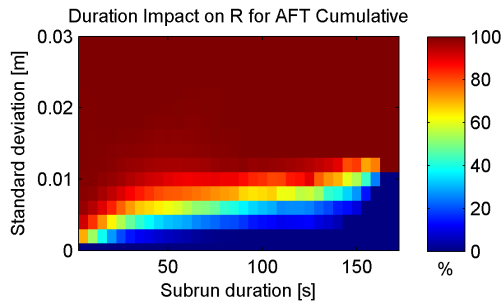
Figure 5.26: IGU All flights, Flight duration impact on standard deviation of deviation for FWD antenna.



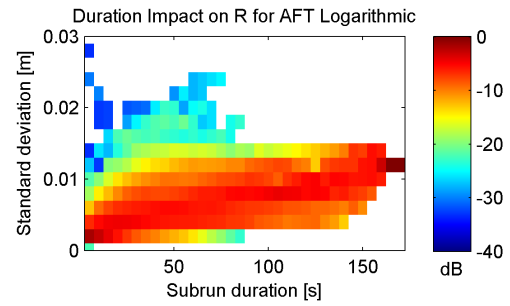
(a) Z direction cumulative fraction.



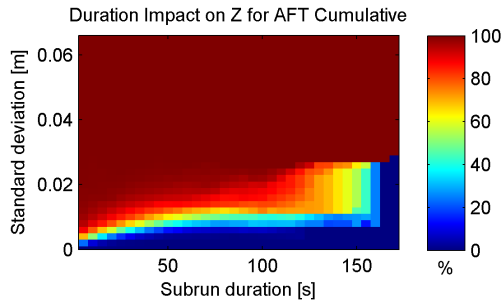
(b) Z direction distribution logarithmic.



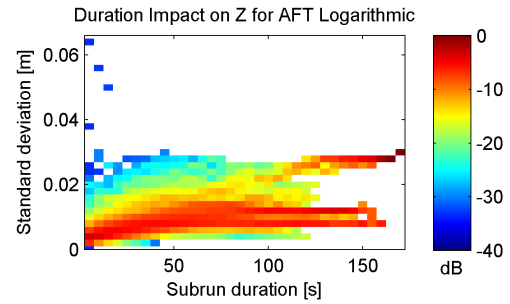
(c) X direction cumulative fraction.



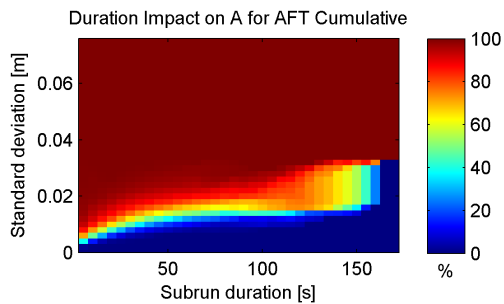
(d) X direction distribution logarithmic.



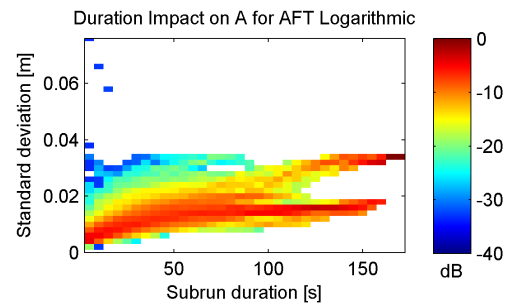
(e) R direction cumulative fraction.



(f) R direction distribution logarithmic.

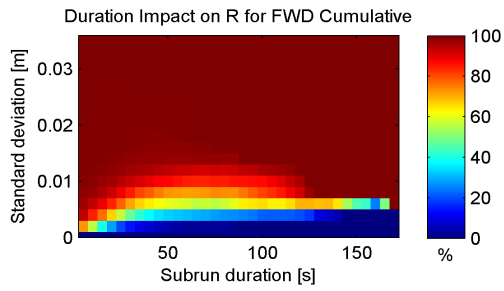


(g) Z direction cumulative fraction.

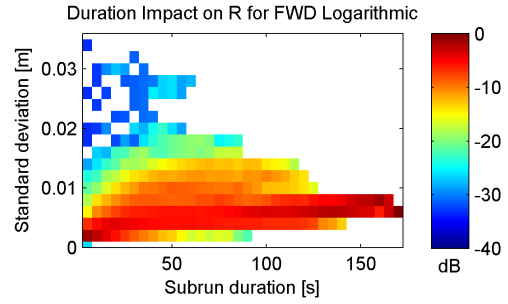


(h) Z direction distribution logarithmic.

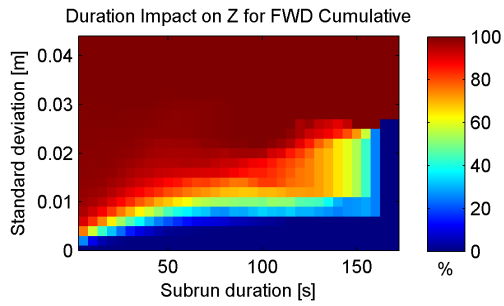
Figure 5.27: IGS All flights, Flight duration impact on standard deviation of deviation for AFT antenna.



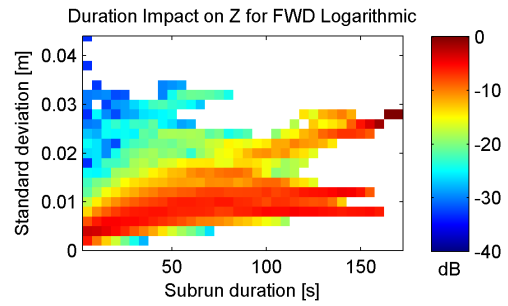
(a) X direction cumulative fraction.



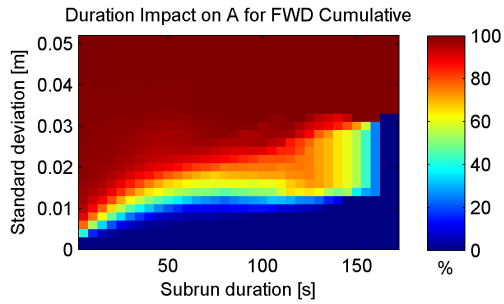
(b) X direction distribution logarithmic.



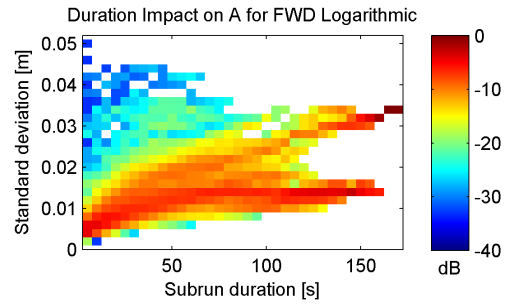
(c) R direction cumulative fraction.



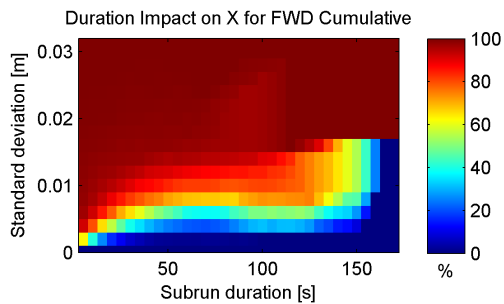
(d) R direction distribution logarithmic.



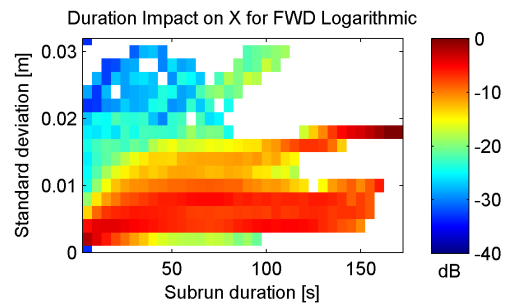
(e) Z direction cumulative fraction.



(f) Z direction distribution logarithmic.



(g) Z direction cumulative fraction.



(h) Z direction distribution logarithmic.

Figure 5.28: IGS All flights, Flight duration impact on standard deviation of deviation for FWD antenna.

The standard deviation of shape increases with duration in all directions and for all SCPs. For IGU the average standard deviation of a sub-run 100 s long is less than 2 cm in any of the direction and less than 4 cm in total. 90 % of the registered standard deviations of shape differ less than 1.5 cm from the mean. The figures are all obscured for longer durations as the number of SAR-runs over 100 s long are few.

5.4.2 Duration impact on change of bias

Difference in deviation between ends of sub-runs.

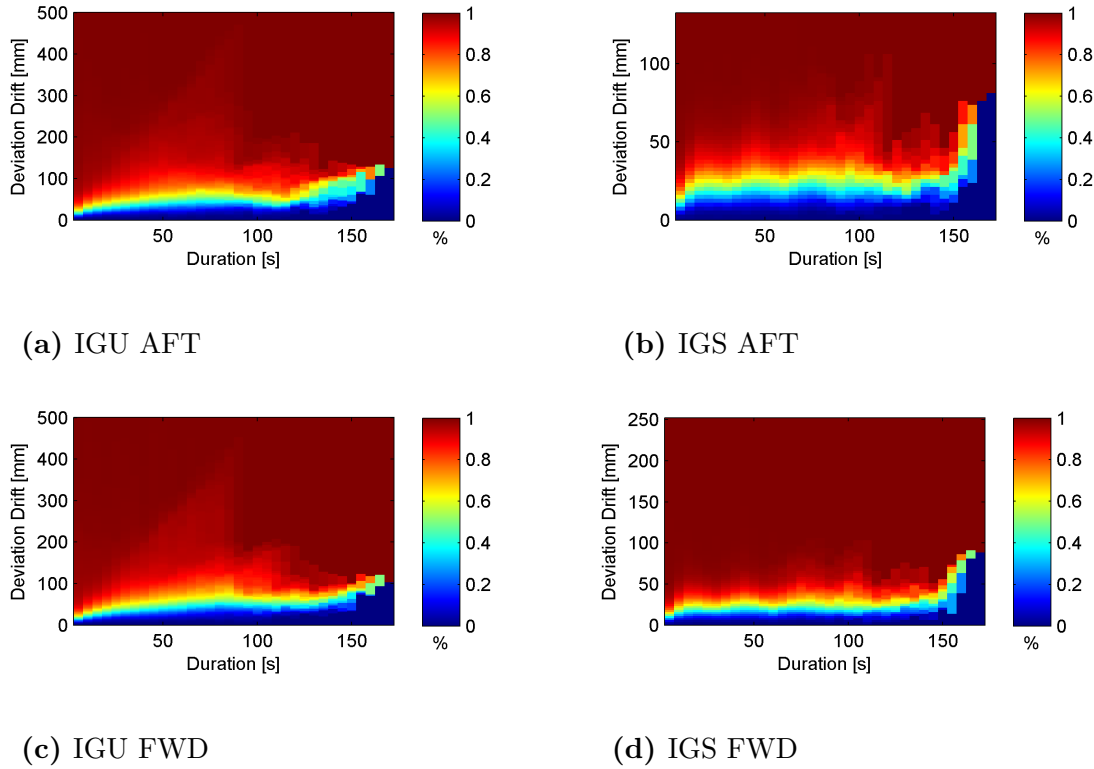


Figure 5.29: Difference in deviation between ends of sub-run

The change in bias is larger for sub-runs with longer duration. For IGU the change of bias of a 100 s long sub-run is 60 mm.

5.4.3 Duration impact on deviation of flight length

The difference in length of all sub-runs.

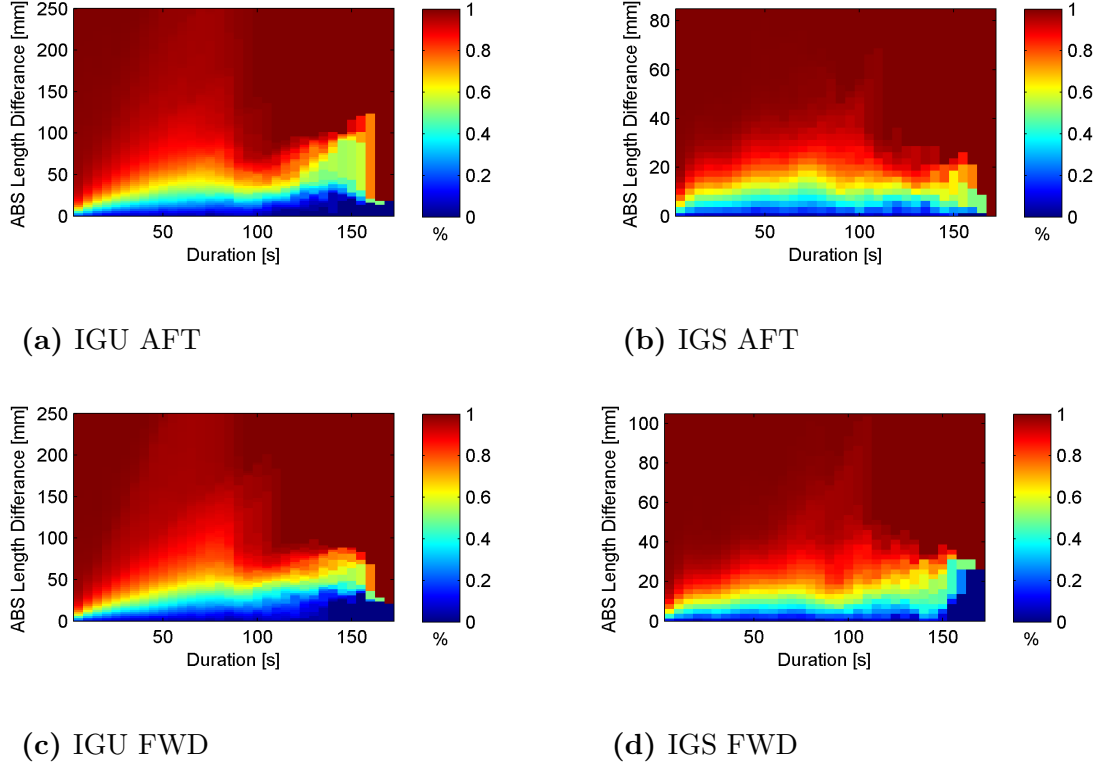


Figure 5.30: Difference in length of sub-run.

The deviation in length is larger for sub-runs with longer duration. For IGU the deviation of bias of a 100 s long sub-run is 40 mm.

5.4.4 Duration impact on deviation of speed

The deviation of speed is the change in deviation divided by duration.

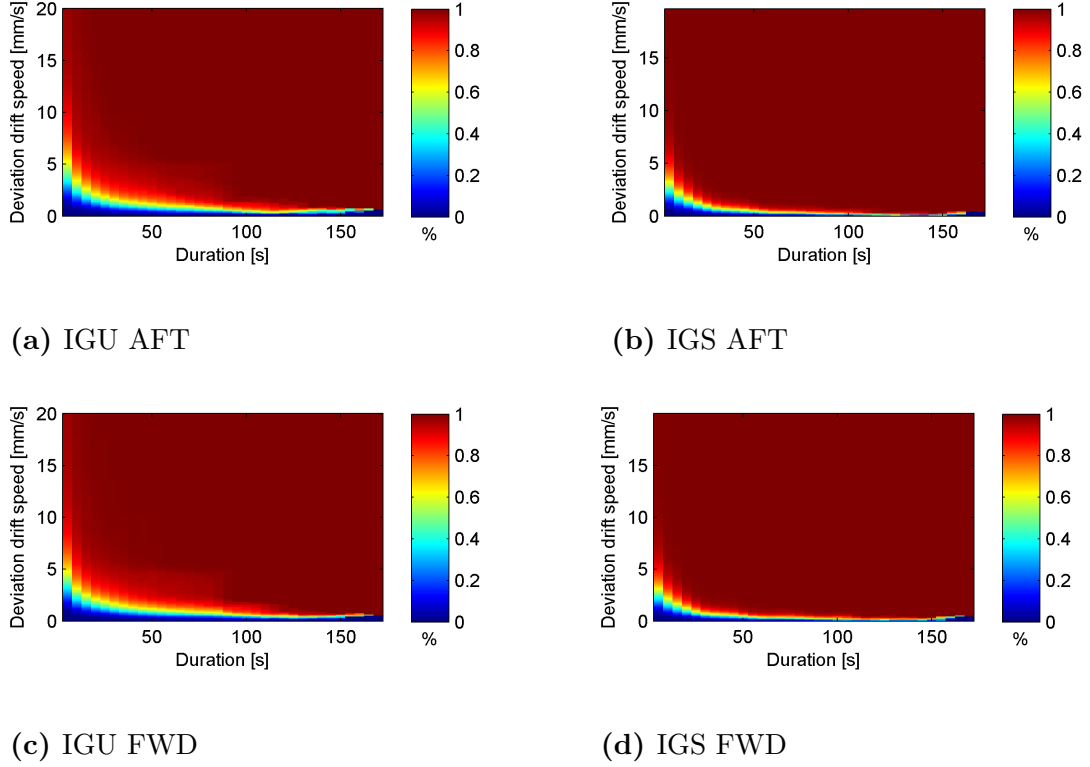
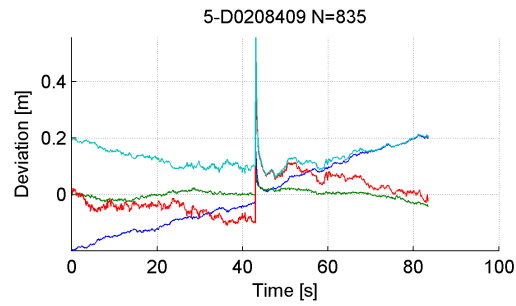


Figure 5.31: Duration impact of velocity error

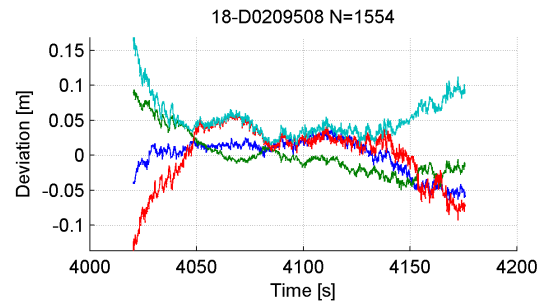
For longer SAR-runs the deviation of speed is decreasing as noise influences less. For IGU the deviation of speed of a 100 s long sub-run is 0.6 mm/s.

5.5 Selected anomalous results from the approach

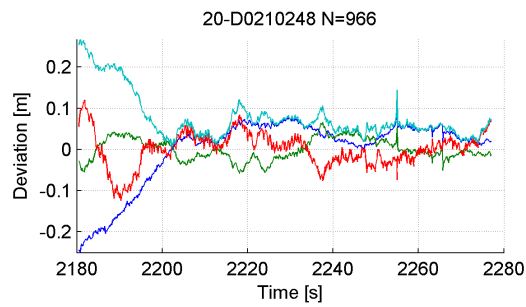
5.5.1 Failed SAR-runs



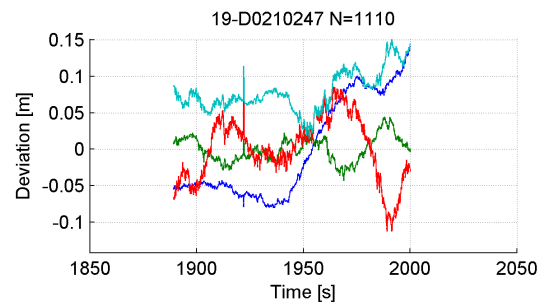
(a) D0208409



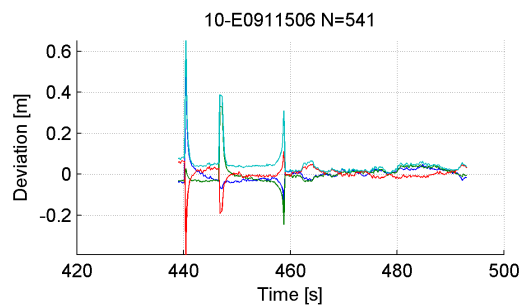
(b) D0209508



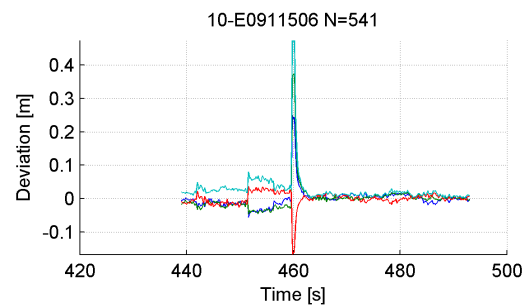
(c) D0210248



(d) D0210247



(e) E0911506 AFT



(f) E0911506 FWD

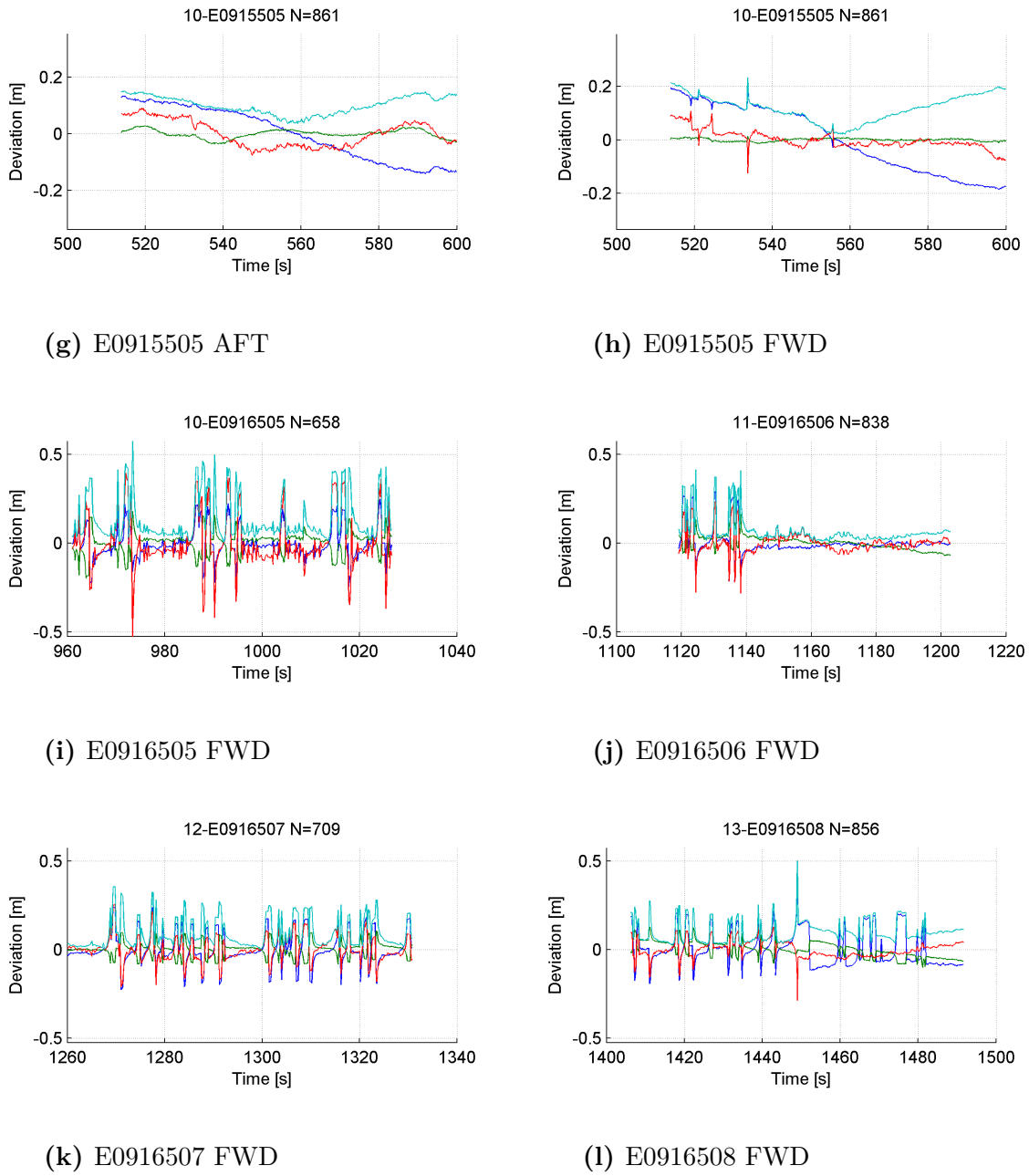


Figure 5.32: Selected anomalous SAR-runs

The errors can be divided in two types, spikes and drifts. The drifts can possibly be explained by the filter not being able to find the correct pseudorange error coefficients. The spikes can possibly be explained from including a satellite with bad reception which drifting in and out.

5.5.2 Forward navigation message error

During the approach, the FWD antenna sometimes gave errors of over 100 m and would sometimes not present any position at all. This problem was solved by using the AFT antennas navigation message for processing of the FWD antenna as this

enabled the FWD antenna solution to be generated. Even if this problem seems solved, the underlying cause has not been decided. Information and examples of this problem are therefore presented here from the RTKLIBs built in analysis.

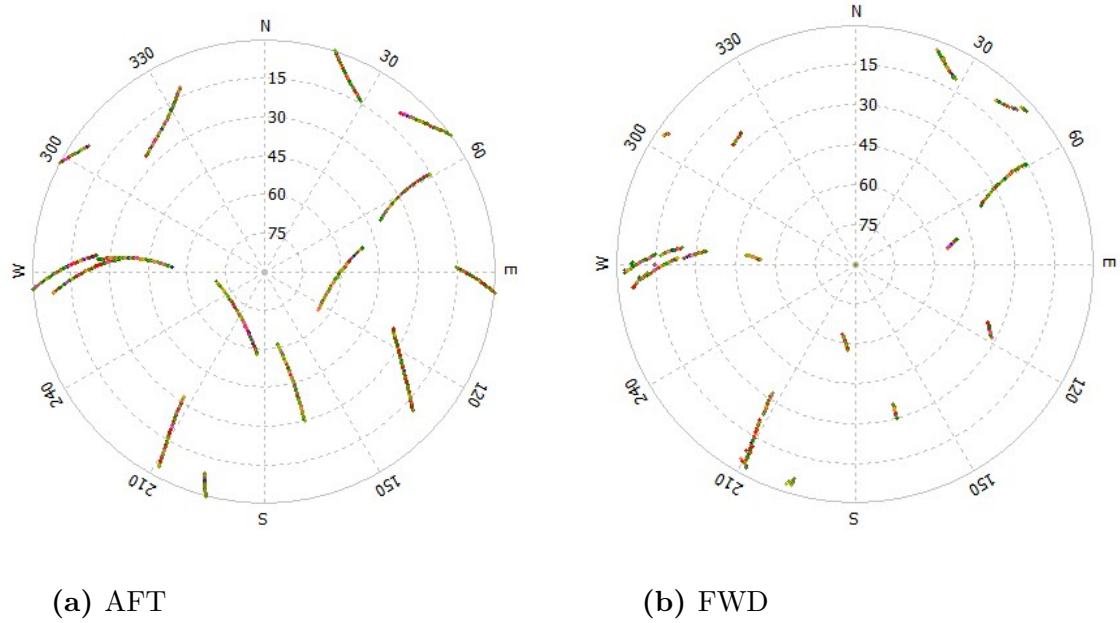


Figure 5.33: 141003b RTKLIB Skymap. Colour indicates SNR where green is good and red is bad.

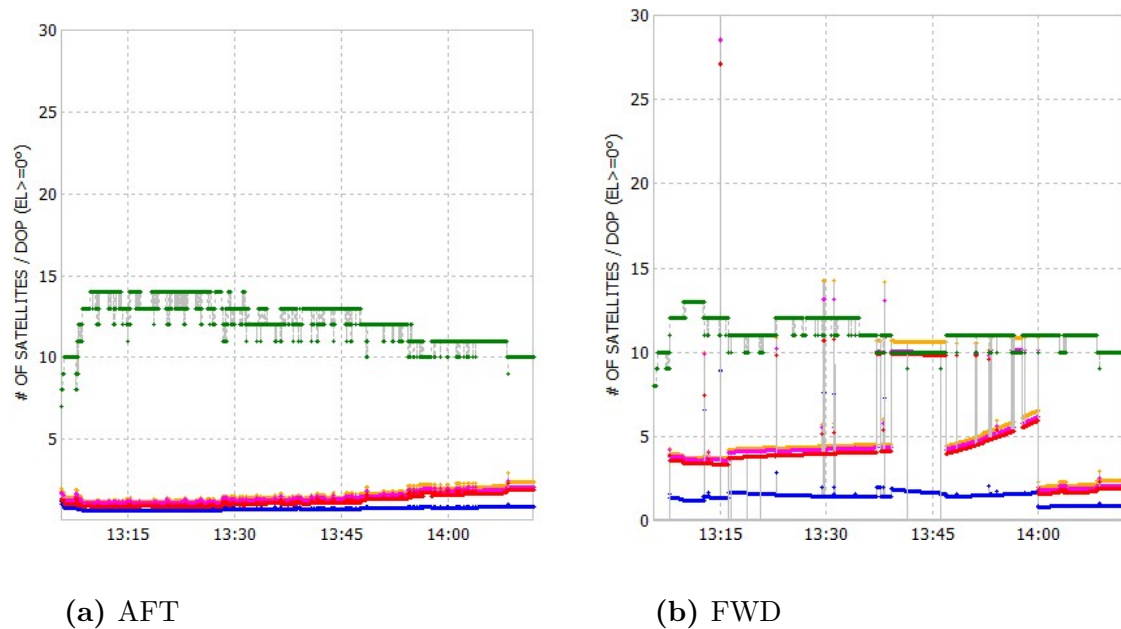


Figure 5.34: 141003b RTKLIB DOP. Green is number of satellites visible, the other colours are the DOP in different directions.

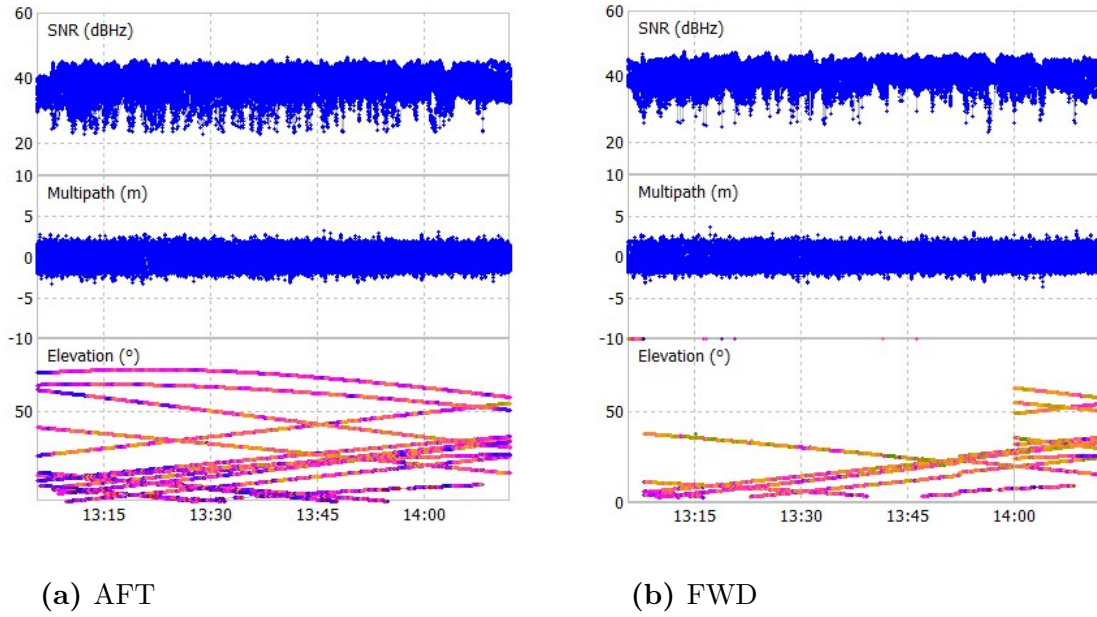


Figure 5.35: 141003b RTKLIB SNR Multipath Elevation. The top and middle blue plot are the SNR and multipath readings. The lowest third of the figures are the elevation of the recorded satellites

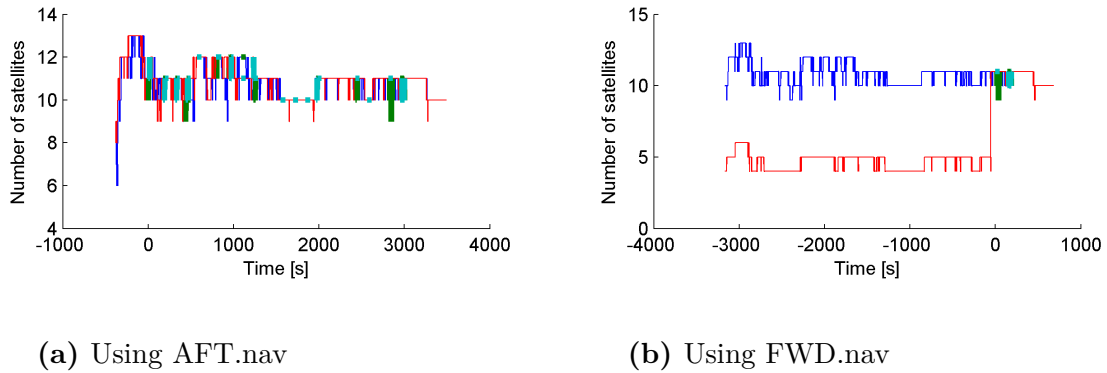


Figure 5.36: Number of usable satellites for AFT and FWD using different .nav files for the FWD antenna. Red is FWD and blue is AFT.

The skymaps in Figures 5.33a and 5.33b are the recorded positions of the satellites seen by the AFT and FWD antenna. When compared it is apparent that the FWD antenna often is unable to determine the position of the satellites. The RTKLIB DOP chart in Figures 5.34a and 5.34b show that the number of satellites visible for the FWD and AFT antenna is approximately the same. The DOP is however much larger for the FWD antenna. The periods of high DOP corresponds well with the period when in Figure 5.36b no satellites have registered elevations over 40° . From 14:00 satellites of high elevations appear and at the same time the number of usable satellites jump in Figure 5.36b. If instead the navigation message file of the AFT antenna is used for the processing of the FWD antenna the number of usable satellites increase, see figure 5.36a.

Apparently there is a problem with the navigation message of the FWD antenna.

The reason why it fails to download the FWD navigation message is unknown. It can possibly be explained by signal scrambling from the propeller preventing the 6s continuous download time required for a navigation message sub frames download.

6

Conclusion

The precision of the SAR-runs at the beginning and end of the GPS registration is worse than average. This can be caused by the longer convergence time of the PPP technique compared with RTK. Increasing the GPS recording time before and after the first and last SAR-run could therefore improve the average precision. CPAR has not been tested but if it can potentially reduce the convergence time.

For the SAR-runs the recorded median acceleration was 1 m/s^2 . Depending on the true 10 Hz acceleration of the Carabas, a dynamic filter might improve the precision. A simple filter should be able to remove single bad points with impossible acceleration.

Between the PPP and RTK solution the deviation was often several meters. During the interval of a SAR-run the deviation changed with a few cm. The power spectrum shows a large low frequency component in noise. From this the deviation can be explained as consisting of a cm noise and a bias of several metres that drifts a few cm per minute.

The performance of PPP changes with the quality of the SCPs. The PPP position solution generated with the high quality SCP IGS, deviates less from the reference, has lower noise, and has a slower change of bias than the IGU solution. The resulting flight path shape capture is also better for IGS. The usage of IGS RTS which is a calculated correction might therefore give better performance than the partially projected correction IGU.

A flight path shape is isometric. Rotation and translation of the recorded flight path does not deteriorate the quality of the SAR image. Linear drift in a direction perpendicular to the flight direction, X , can be discounted. This is verified by the results where the change in length is smaller than the change in bias and the standard deviation of shape is better in the looking direction R than in the X direction. The

80 % of the SAR-runs generated with PPP using the IGU SCPs passed the precision requirement of 5 cm standard deviation of shape for the SAR-runs. The average precision of the SAR-runs was 3.5 cm. The precision in the Z-direction will only marginally influence SAR-image. The success rate in the XR-plane was 90 % and the average precision was 2.5 cm.

The conclusion of the results is that PPP has the capabilities to capture the shape of a flight path with the precision required to generate a high resolution SAR-image. The reliability of the method to successfully record the shape of the SAR-run with sufficient precision for the generation of a high resolution SAR image is 90 %.

7

Summary

PPP a GNSS position processing method, has been evaluated in order to determine if it can be used in the creation of high resolution metre-wave SAR images, by the Carabas3. The position solution has been evaluated by comparison with a RTK position solution.

High resolution SAR image requires exact information of the shape of the SAR-run, the flight path during the recording of a SAR image. The exactness of the shape of the flight path is governed by the precision of the positioning technique and the shape of the flight path. Translations and rotations of the flight path will preserve the shape of the SAR-run and therefore not affect the resolution of the SAR image. For straight flight paths, linear changes in bias perpendicular to the flight direction will not degrade the exactness of the shape. The requirement on the method is that PPP should be able to capture the shape of the flight path of the Carabas with a precision of 5 cm during a SAR-run.

The data analysed were GPS observations from test flights with the Carabas. 12 flights with a total of 182 SAR-runs approximately 1 minute long recorded at 10 Hz were analysed. The PPP processing was made in RTKLIB. The RTKLIB implementation of PPP does not use CPAR. The SCPs IGU, IGR and IGS were used.

MATLAB scripts were used to analyse the generated position solutions. The deviation between the PPP and RTK solution was often several meters. During the interval of a SAR-run the deviation changed with a few cm. The deviation can be seen as consisting of a cm noise and a bias of several metres that drifts a few cm per minute. The bias changes with time, no dependence on velocity or position were observed. The quality of the SCPs influenced the quality of the PPP solution. The higher quality IGS SCP resulted in a position solution with a smaller deviation, less noise and slower drift of bias then in the IGU position solution.

The precision was passed by 80 % of the SAR-runs generated with PPP using the IGU SCPs. The average precision of the SAR-runs was 3.5 cm. The precision in the Z-direction will only marginally influence SAR-image. The success rate in the XR-plane was 90 % and the average precision was 2.5 cm.

PPP is a method which has the capabilities to capture the shape of a flight path with the precision required to generate a high resolution SAR-image. The reliability of the method to successfully record the shape of the SAR-run with sufficient precision for the generation of a high resolution SAR image is 90 %.

Bibliography

- [1] Mohamed Elsobeiey and Salim Al-Harbi. Performance of real-time precise point positioning using igs real-time service. *GPS Solutions*, pages 1–7, 2015.
- [2] Takehisa Fujita and Naohiro Kanda. Novel solution of mercury perihelion shift. *arXiv preprint arXiv:0911.2086*, 2009.
- [3] Jianghui Geng, Xiaolin Meng, Alan H Dodson, and Felix N Teferle. Integer ambiguity resolution in precise point positioning: method comparison. *Journal of Geodesy*, 84(9):569–581, 2010.
- [4] GPS.gov. Current and future satellite generations. <http://www.gps.gov/systems/gps/space/>, 2016. [Online; accessed 19-June-2016].
- [5] Frank Graas and Andrey Soloviev. Precise velocity estimation using a stand-alone gps receiver. *Navigation*, 51(4):283–292, 2004.
- [6] John G. Grimes. Global positioning system standard positioning service signal specification. *United States Coast Guard Navigation Center*, 2008.
- [7] John G. Grimes. Global positioning systems standard positioning service performance standard. *United States Coast Guard Navigation Center*, 2008.
- [8] Bernhard Hofmann-Wellenhof, Herbert Lichtenegger, and Elmar Wasle. *GNSS—global navigation satellite systems: GPS, GLONASS, Galileo, and more*. Springer Science & Business Media, 2007.
- [9] Berthold KP Horn. Closed-form solution of absolute orientation using unit quaternions. *JOSA A*, 4(4):629–642, 1987.
- [10] Hanna Isaksson. Carabas airborne reconnaissance system. <http://saab.com/air/sensor-systems/ground-imaging-sensors/carabas>, 2014. [Online; accessed 19-June-2016].
- [11] Charles VJ Jakowatz, Daniel E Wahl, Paul H Eichel, Dennis C Ghiglia, and Paul A Thompson. *Spotlight-Mode Synthetic Aperture Radar: A Signal Processing Approach: A Signal Processing Approach*. Springer Science & Business Media, 2012.
- [12] Elliott Kaplan and Christopher Hegarty. *Understanding GPS: principles and applications*. Artech house, 2005.
- [13] Ian Martin. Gnss precise point positioning: The enhancement with glonass. *Newcastle University*, 2013.

- [14] Mayitzin. Kalman-filter-a-painless-approach. <https://mayitzin.com/2015/06/04/kalman-filter-a-painless-approach/#more-1168>, 2015. [Online; accessed 19-June-2016].
- [15] Nasa. Gps constellation. http://www.nasa.gov/sites/default/files/gps_constellation_0.jpg, 2016. [Online; accessed 19-June-2016].
- [16] Wolfgang Rindler. *Relativity: special, general, and cosmological*. Oxford University Press on Demand, 2006.
- [17] Michael Schmandt. Trilateration. <http://giscommons.org/files/2010/01/2.141.gif>, 2010. [Online; accessed 19-June-2016].
- [18] Tomoji Takasu. Rtklib ver. 2.4.2 manual. 2013.
- [19] Rui Tu. Fast determination of displacement by ppp velocity estimation. *Geophysical Journal International*, 196(3):1397–1401, 2014.
- [20] Ronny Videkull. Evaluate and develop high-performance gps navigation using free gps software. *Chalmers University of Technology*, 2015.
- [21] Wikimedia. File:comparison satellite navigation orbits.svg. https://commons.wikimedia.org/wiki/File:Comparison_satellite_navigation_orbits.svg, 2016. [Online; accessed 19-June-2016].
- [22] Wikimedia. File:geometric dilution of precision.svg. https://commons.wikimedia.org/wiki/File:Geometric_Dilution_Of_Precision.svg, 2016. [Online; accessed 19-June-2016].
- [23] Wikimedia. File:gps signal modulation scheme.svg. https://commons.wikimedia.org/wiki/File:GPS_signal_modulation_scheme.svg, 2016. [Online; accessed 19-June-2016].
- [24] Yan Xincun, Ouyang Yongzhong, Sun Yi, and Deng Kailiang. Application of precise point positioning technology in airborne gravity measurement. *Geodesy and Geodynamics*, 5(4):68–72, 2014.

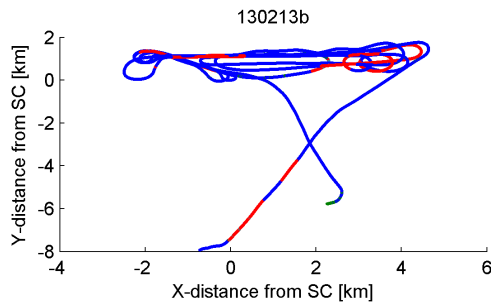
A

Extra Figures

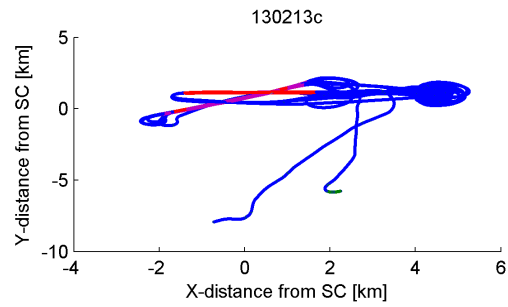
A.1 All flights

A.2 All flight paths

Birds eye view of all analysed flights in SC coordinates. The AFT and FWD of PPP and RTK with all sub-runs are plotted in all figures.

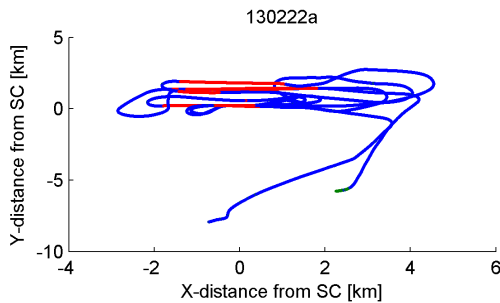


(a) Flight 130213b IGU

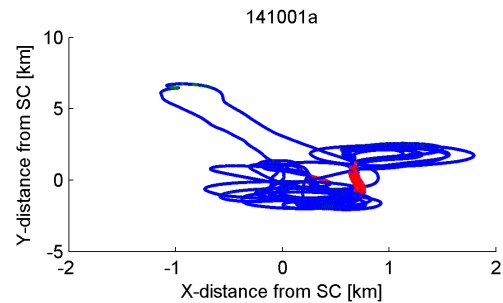


(b) Flight 130213c IGU

Figure A.1: Flight path in scene centred coordinates for AFT and FWD. The SAR-runs have been highlighted.

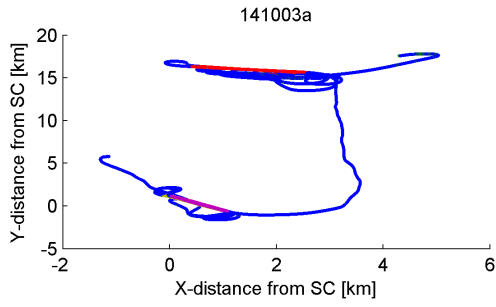


(a) Flight 130222a IGU

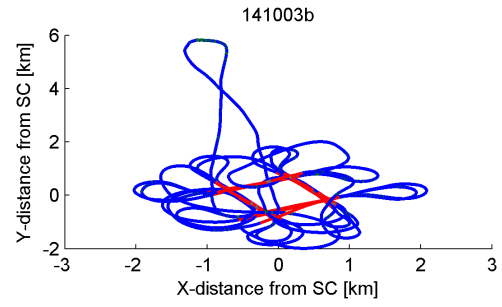


(b) Flight 141001a IGU

Figure A.2: Flight path in scene centred coordinates for AFT and FWD. The SAR-runs have been highlighted.

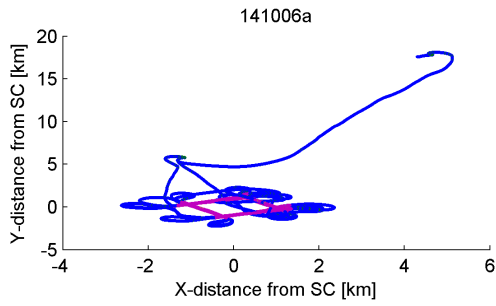


(a) Flight 141003a IGU

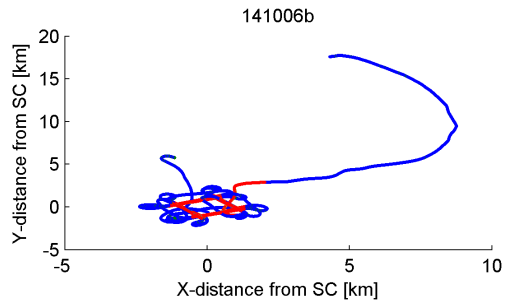


(b) Flight 141003b IGU

Figure A.3: Flight path in scene centred coordinates for AFT and FWD. The SAR-runs have been highlighted.

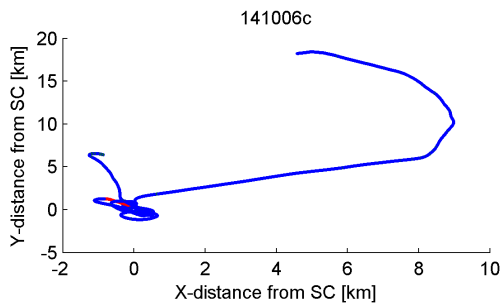


(a) Flight 141006a IGU

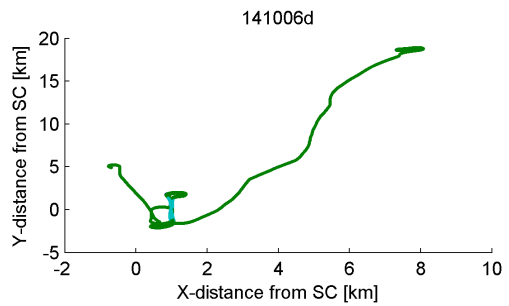


(b) Flight 141006b IGU

Figure A.4: Flight path in scene centred coordinates for AFT and FWD. The SAR-runs have been highlighted.

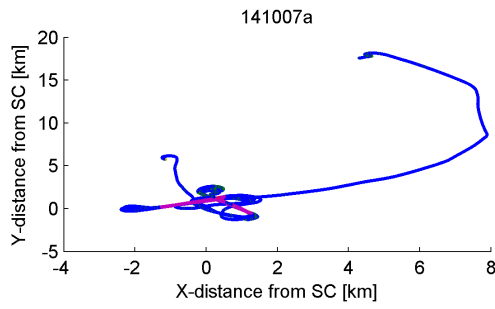


(a) Flight 141006c IGU

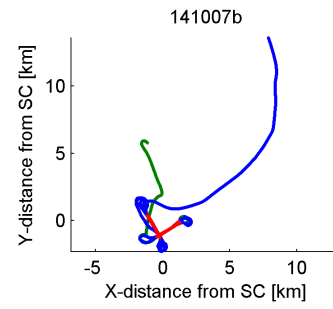


(b) Flight 141006d IGU

Figure A.5: Flight path in scene centred coordinates for AFT and FWD. The SAR-runs have been highlighted.



(a) Flight 141007a IGU

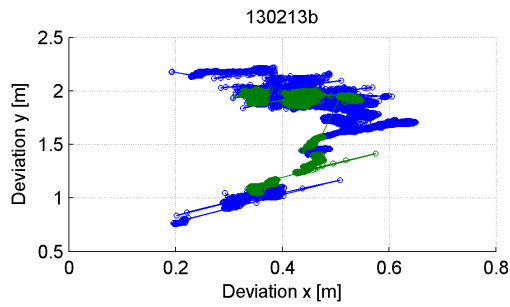


(b) Flight 141007b IGU

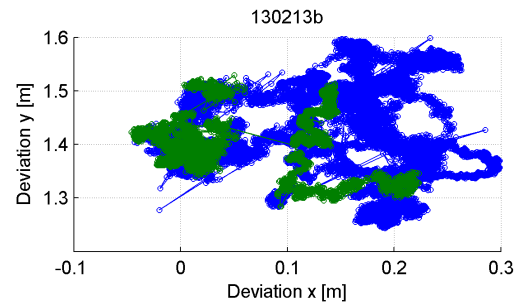
Figure A.6: Flight path in scene centred coordinates for AFT and FWD. The SAR-runs have been highlighted.

A.2.1 Deviation over time

The deviation between the recorded and the reference position over time for AFT and FWD Antenna. The runs have been highlighted. X, Y, Z.

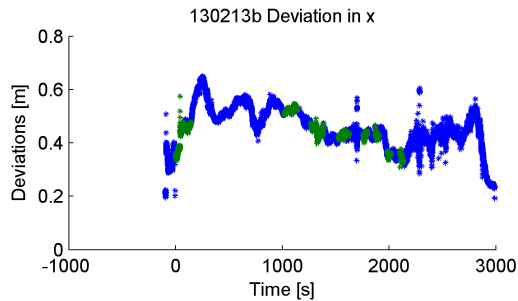


(a) AFT

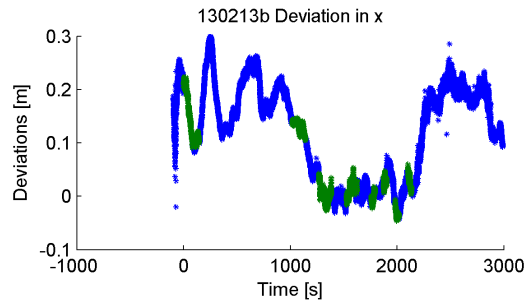


(b) FWD

Figure A.7: 130213b IGU

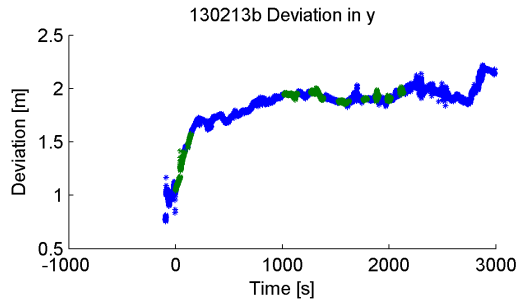


(a) AFT

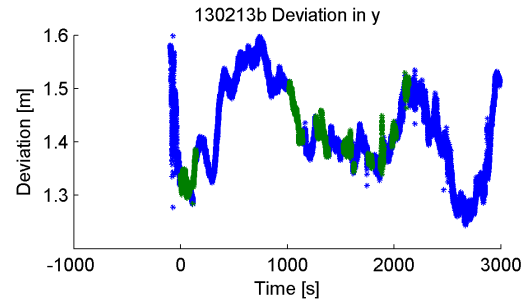


(b) FWD

Figure A.8: 130213b IGU

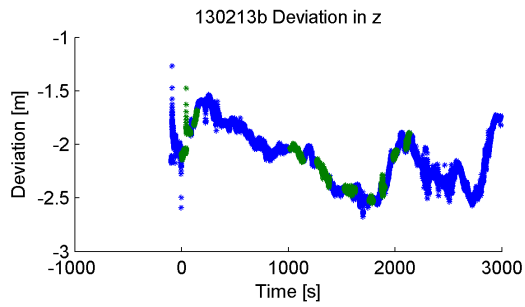


(a) AFT

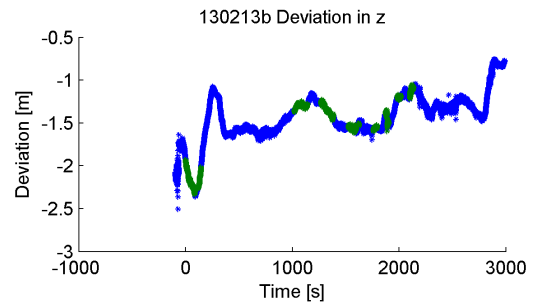


(b) FWD

Figure A.9: 130213b IGU

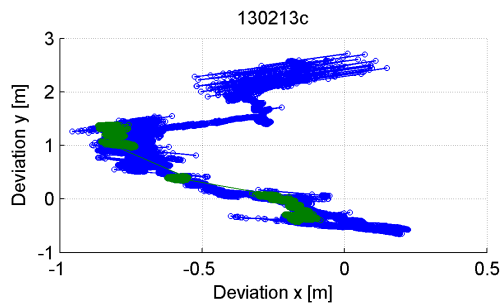


(a) AFT

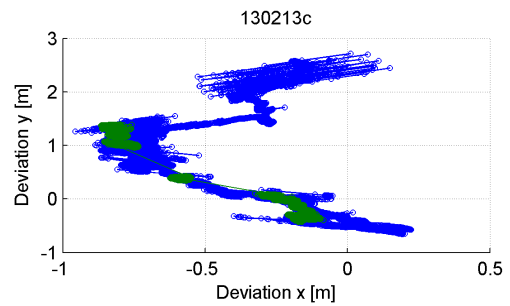


(b) FWD

Figure A.10: 130213b IGU

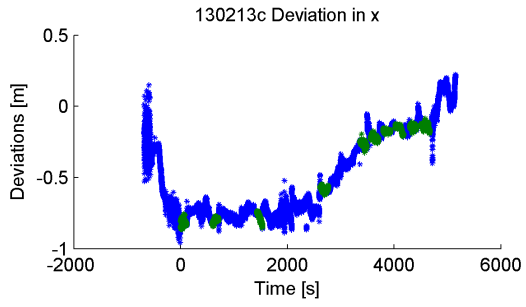


(a) AFT

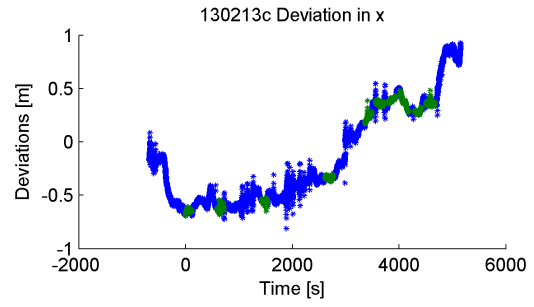


(b) FWD

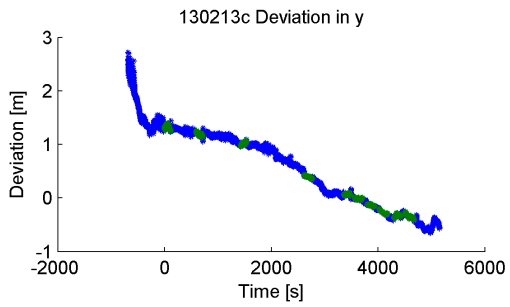
Figure A.11: 130213c IGU



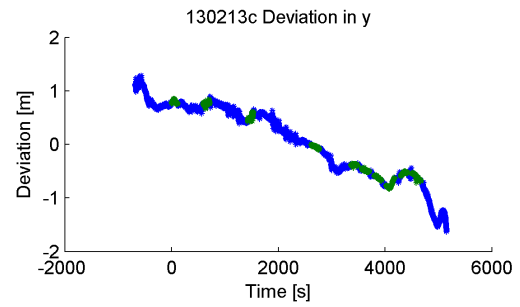
(a) AFT



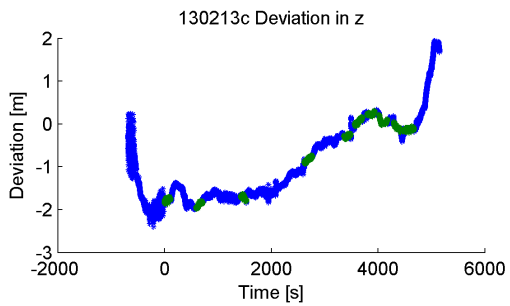
(b) FWD

Figure A.12: 130213c IGU


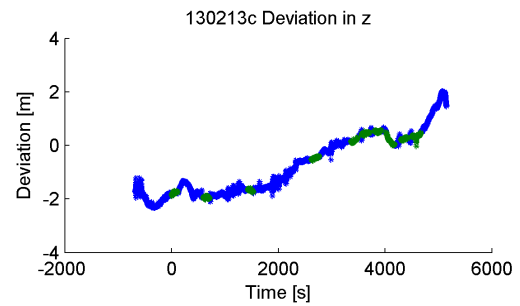
(a) AFT



(b) FWD

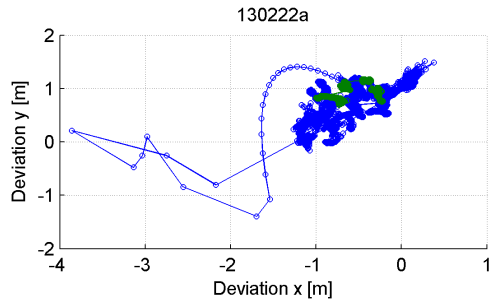
Figure A.13: 130213c IGU


(a) AFT

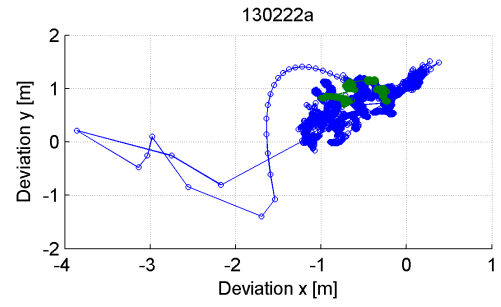


(b) FWD

Figure A.14: 130213c IGU

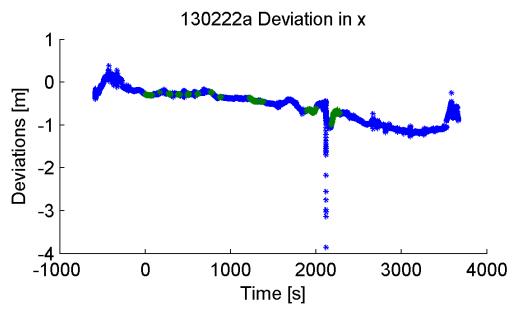


(a) AFT

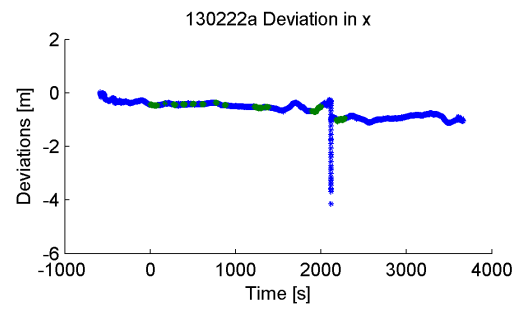


(b) FWD

Figure A.15: 130222a IGU

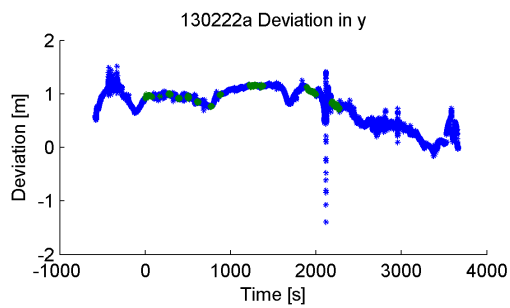


(a) AFT

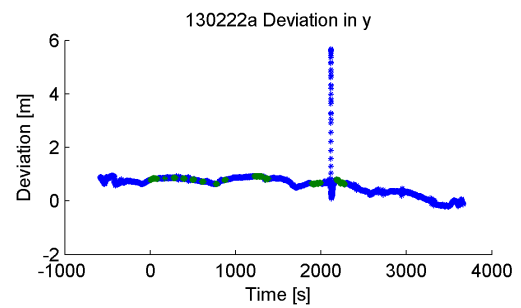


(b) FWD

Figure A.16: 130222a IGU

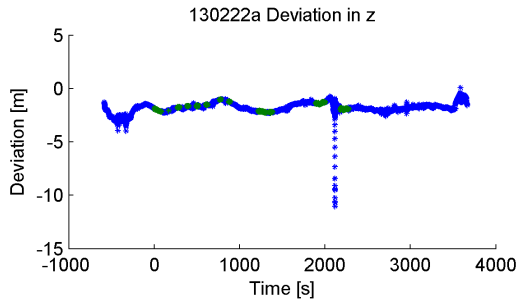


(a) AFT

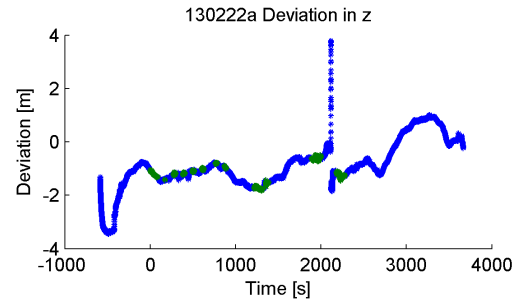


(b) FWD

Figure A.17: 130222a IGU

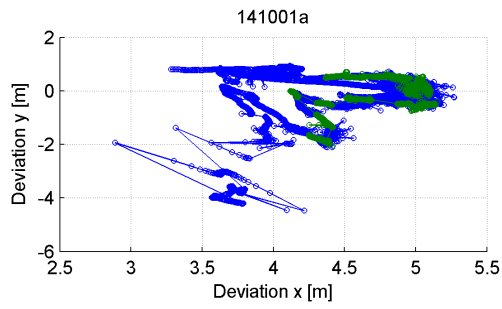


(a) AFT

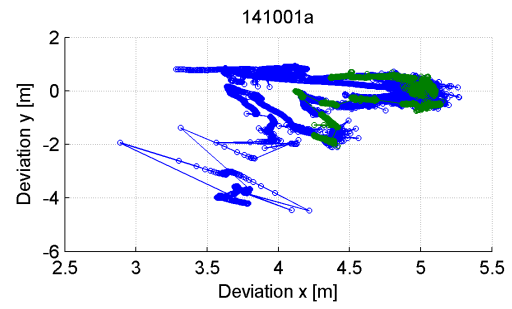


(b) FWD

Figure A.18: 130222a IGU

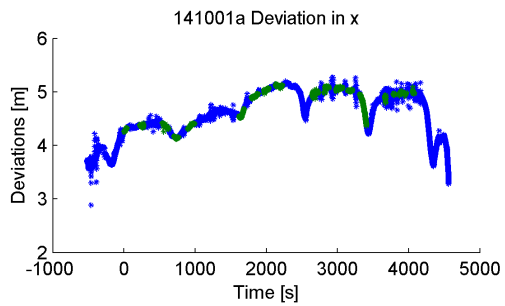


(a) AFT

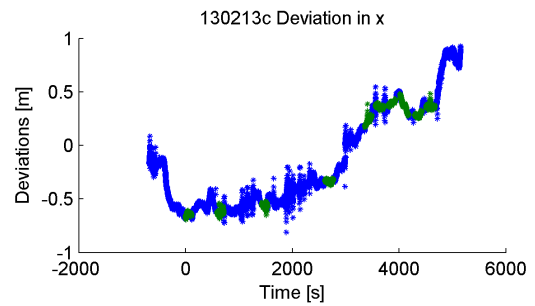


(b) FWD

Figure A.19: 141001a IGU

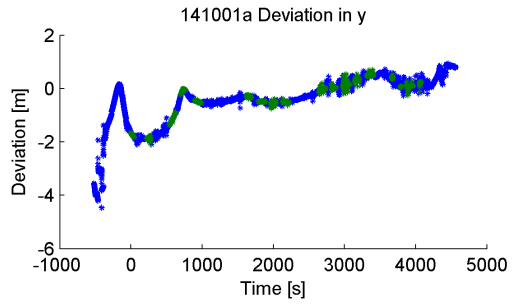


(a) AFT

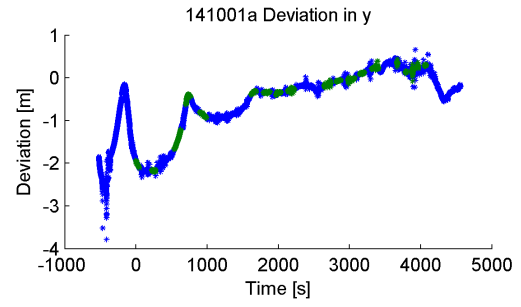


(b) FWD

Figure A.20: 141001a IGU

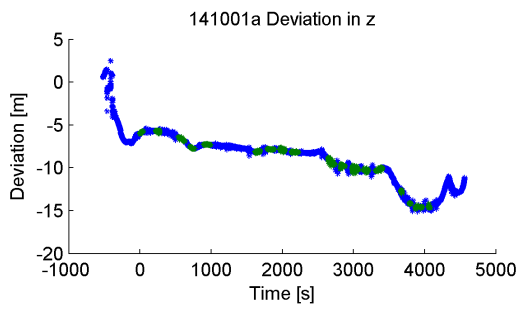


(a) AFT

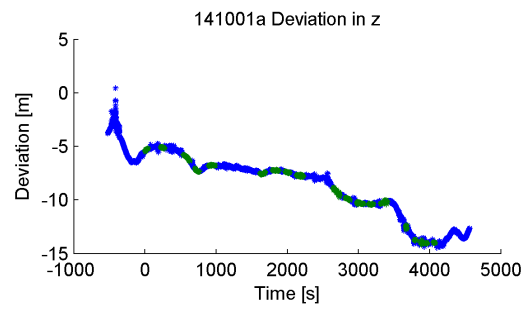


(b) FWD

Figure A.21: 141001a IGU

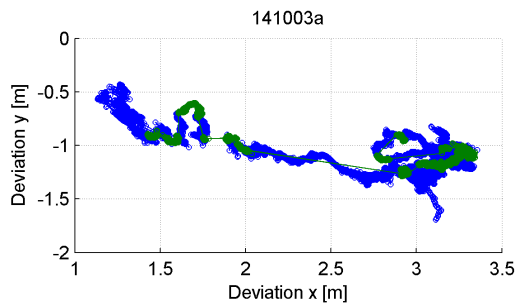


(a) AFT

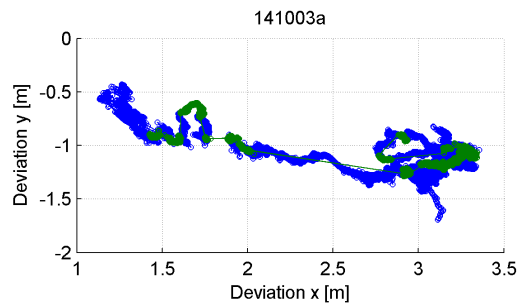


(b) FWD

Figure A.22: 141001a IGU

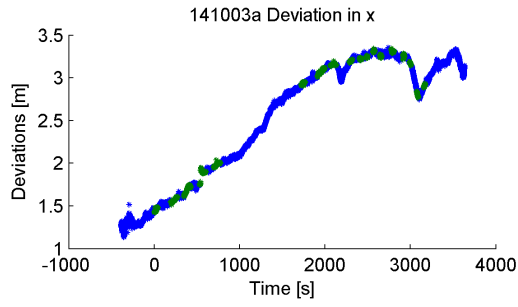


(a) AFT

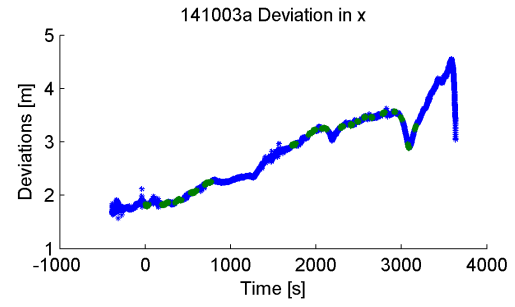


(b) FWD

Figure A.23: 141003a IGU

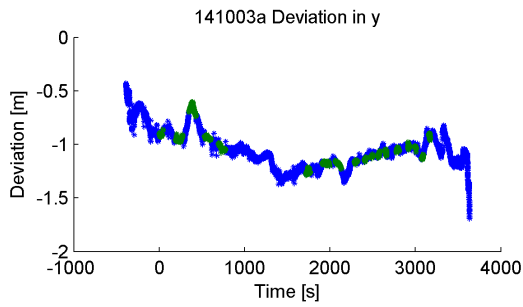


(a) AFT

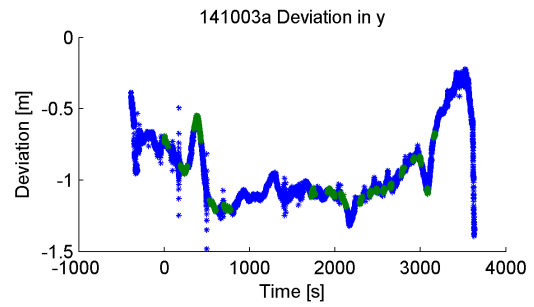


(b) FWD

Figure A.24: 141003a IGU

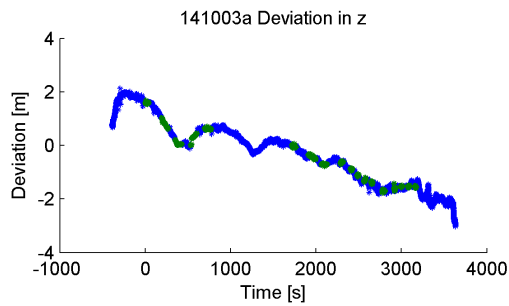


(a) AFT

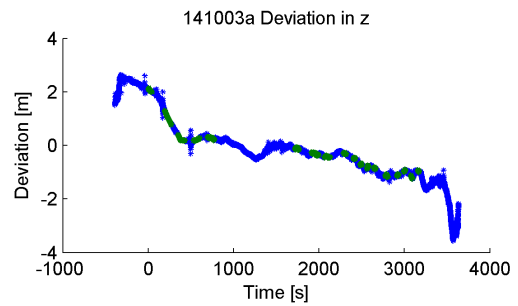


(b) FWD

Figure A.25: 141003a IGU

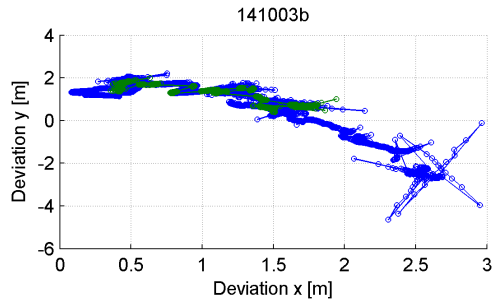


(a) AFT

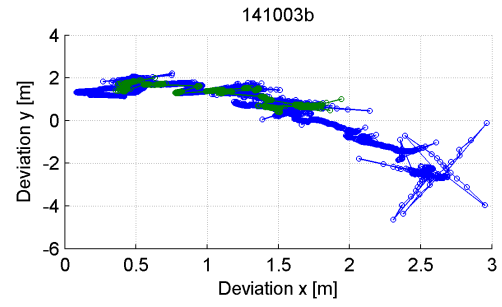


(b) FWD

Figure A.26: 141003a IGU

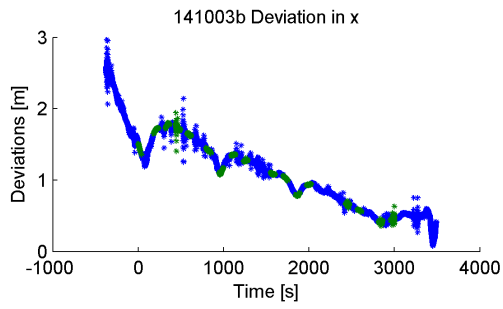


(a) AFT

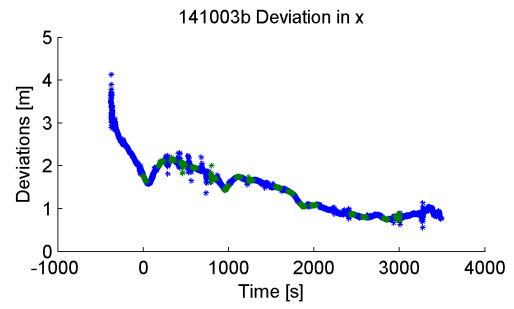


(b) FWD

Figure A.27: 141003b IGU

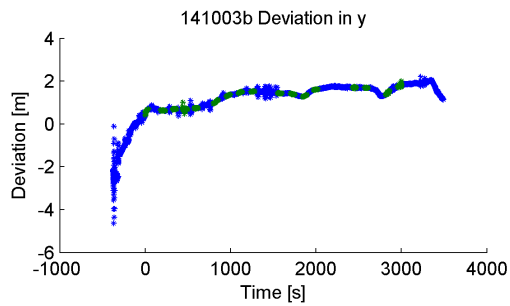


(a) AFT

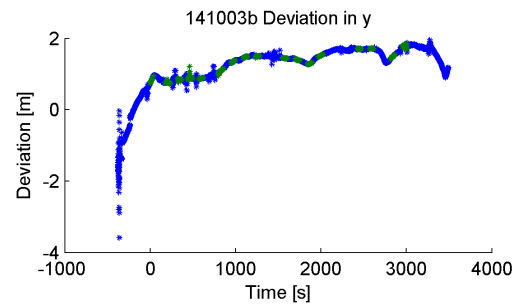


(b) FWD

Figure A.28: 141003b IGU

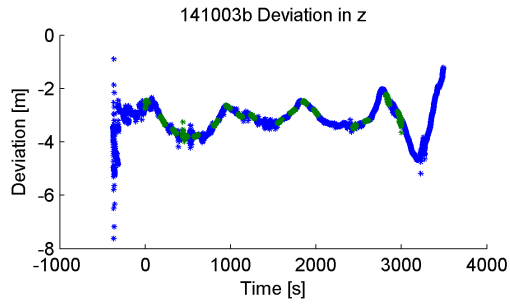


(a) AFT

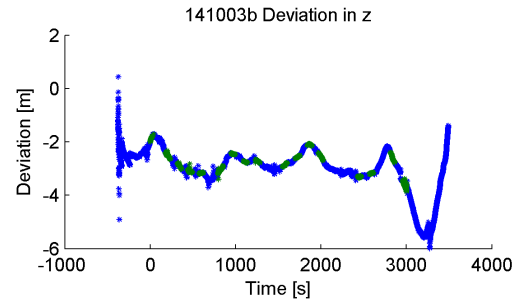


(b) FWD

Figure A.29: 141003b IGU

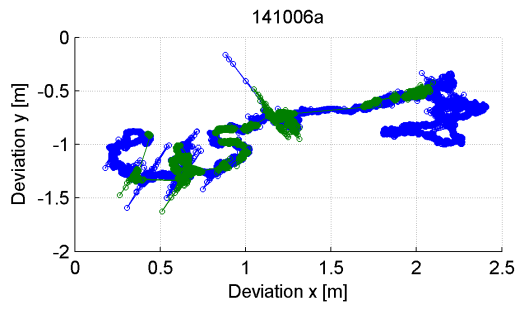


(a) AFT

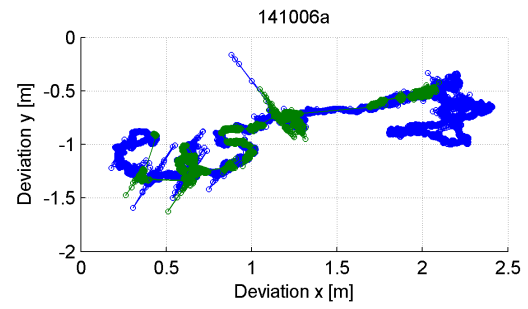


(b) FWD

Figure A.30: 141003b IGU

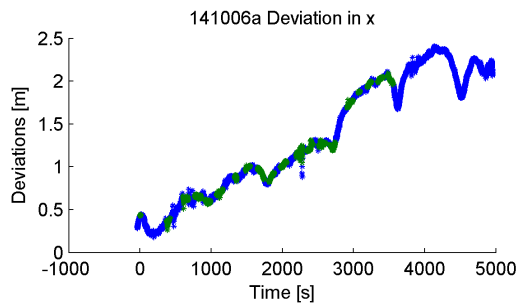


(a) AFT

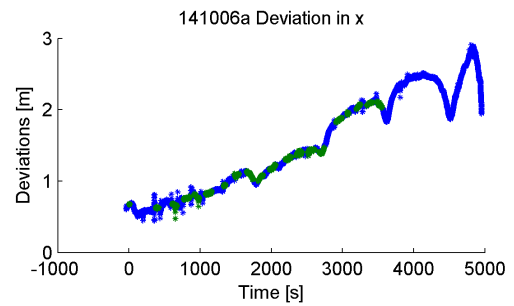


(b) FWD

Figure A.31: 141006a IGU

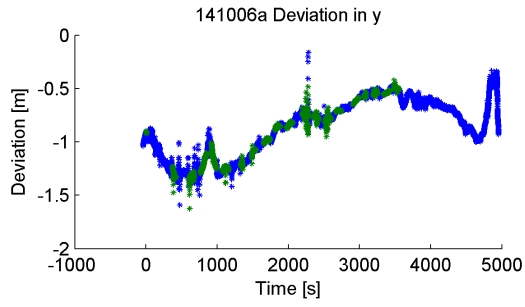


(a) AFT

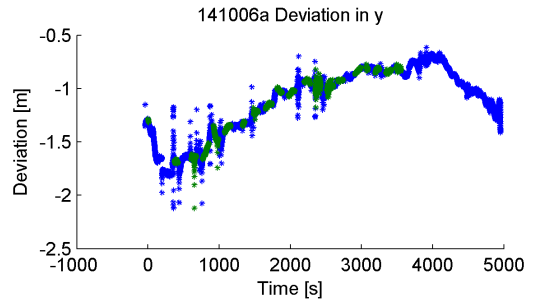


(b) FWD

Figure A.32: 141006a IGU

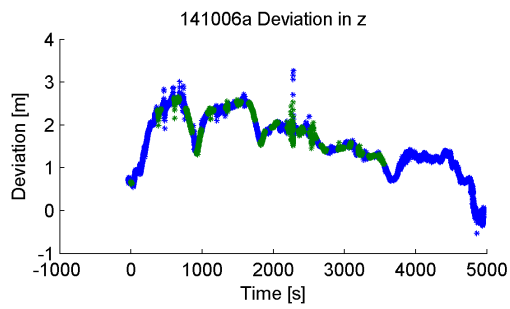


(a) AFT

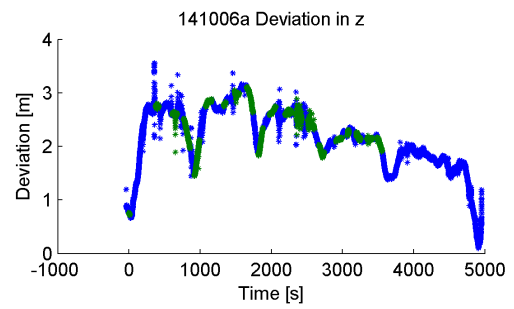


(b) FWD

Figure A.33: 141006aIGU

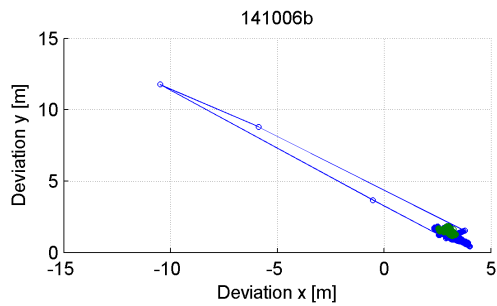


(a) AFT

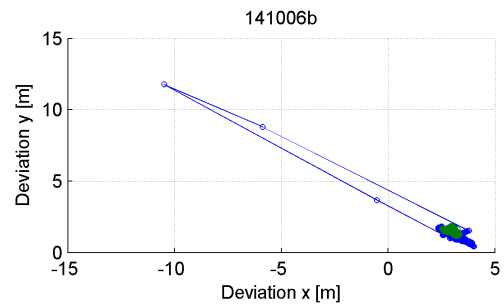


(b) FWD

Figure A.34: 141006a IGU

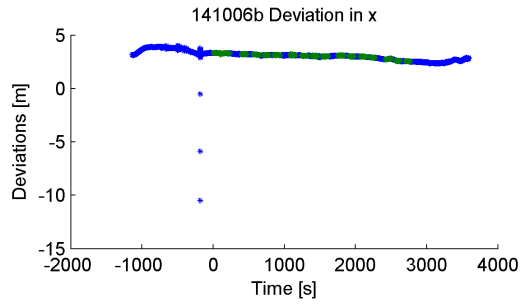


(a) AFT

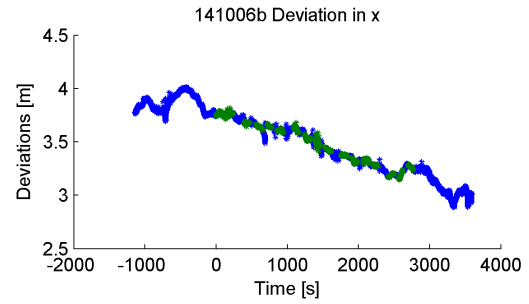


(b) FWD

Figure A.35: 141006b IGU

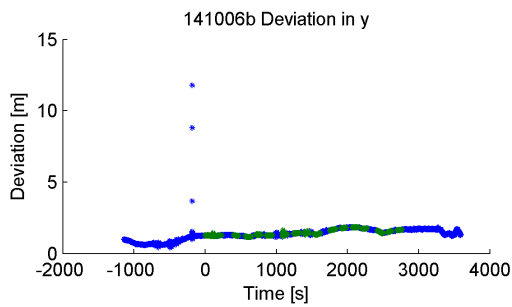


(a) AFT

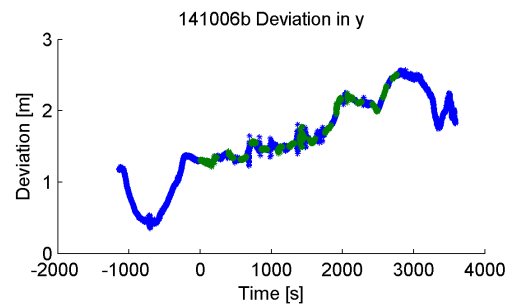


(b) FWD

Figure A.36: 141006b IGU

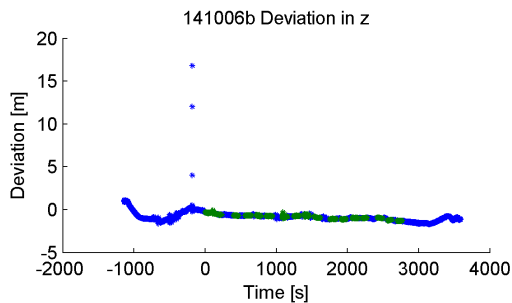


(a) AFT

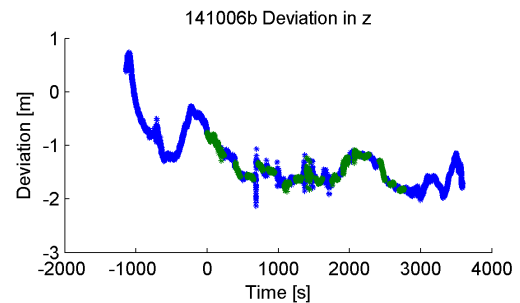


(b) FWD

Figure A.37: 141006b IGU

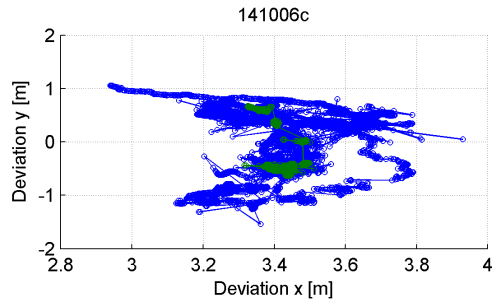


(a) AFT

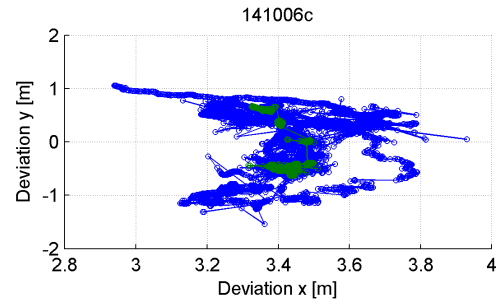


(b) FWD

Figure A.38: 141006b IGU

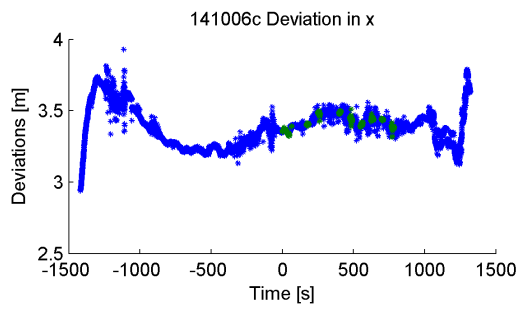


(a) AFT

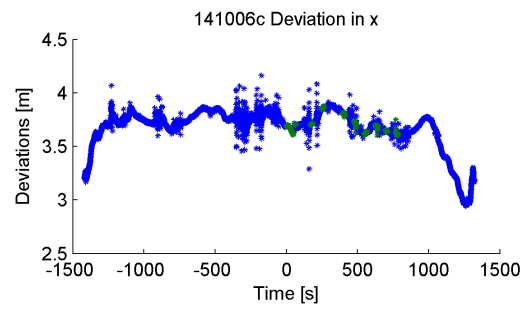


(b) FWD

Figure A.39: 141006c IGU

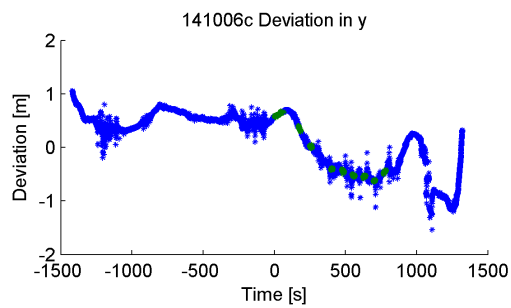


(a) AFT

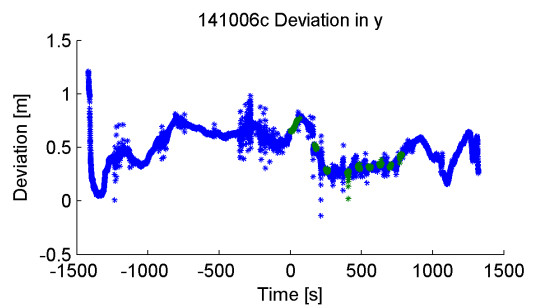


(b) FWD

Figure A.40: 141006c IGU

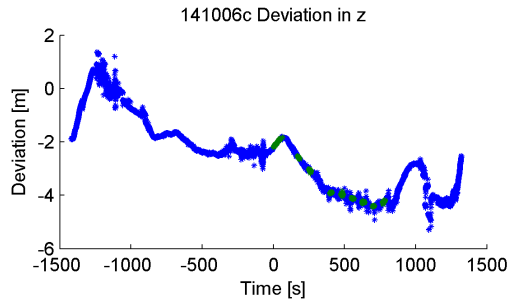


(a) AFT

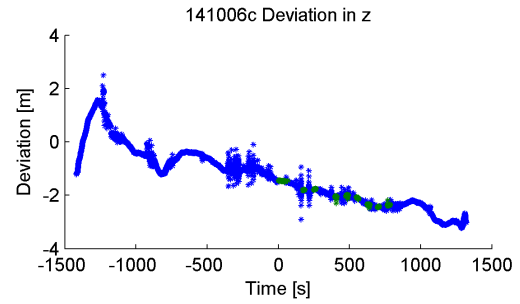


(b) FWD

Figure A.41: 141006c IGU

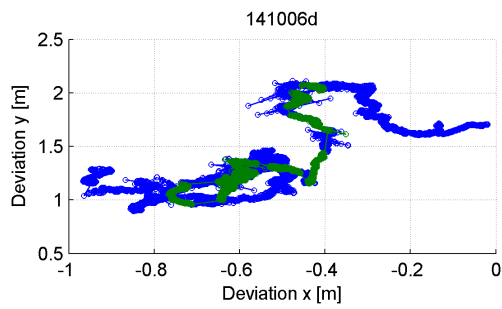


(a) AFT

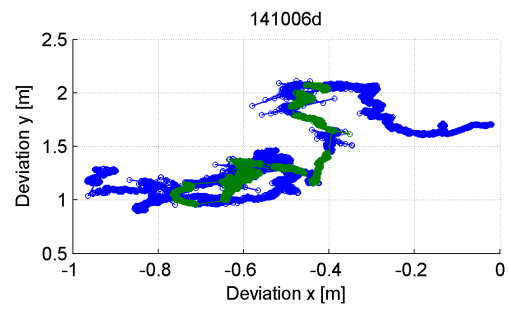


(b) FWD

Figure A.42: 141006c IGU

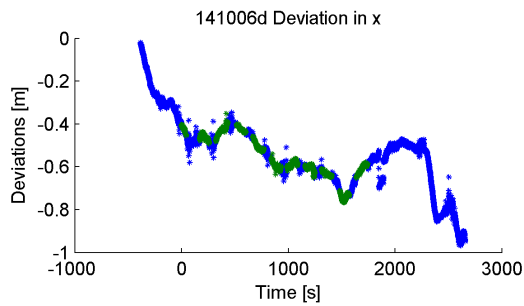


(a) AFT

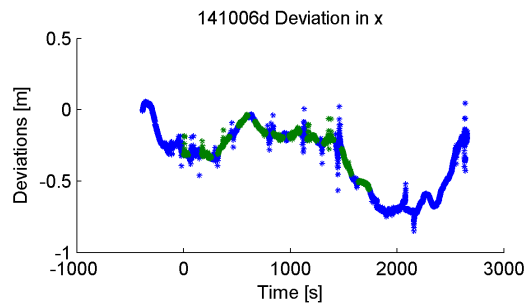


(b) FWD

Figure A.43: 141006d IGU

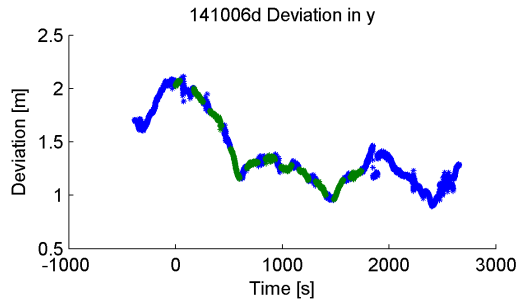


(a) AFT

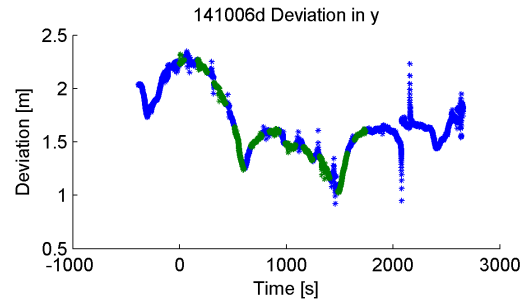


(b) FWD

Figure A.44: 141006d IGU

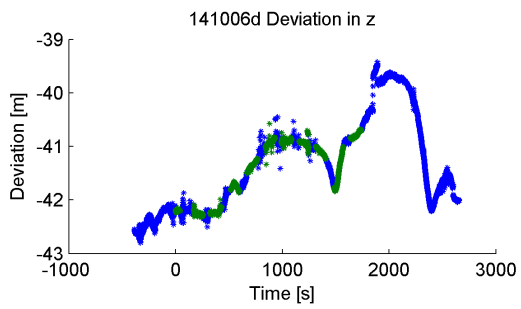


(a) AFT

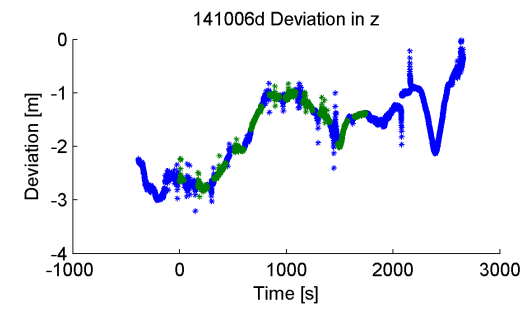


(b) FWD

Figure A.45: 141006d IGU

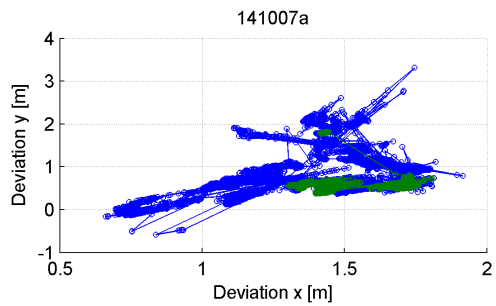


(a) AFT

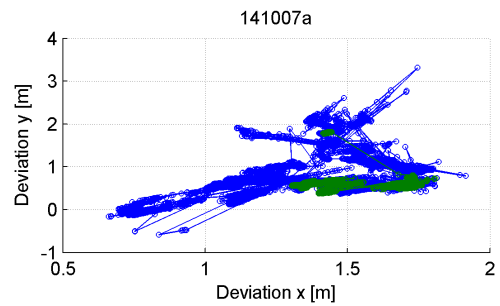


(b) FWD

Figure A.46: 141006d IGU

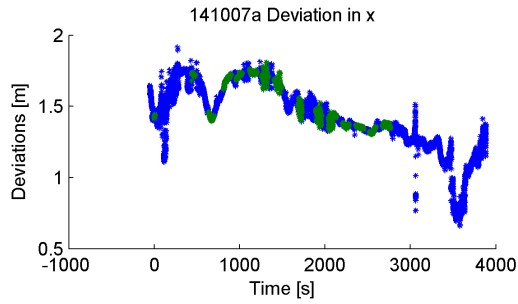


(a) AFT

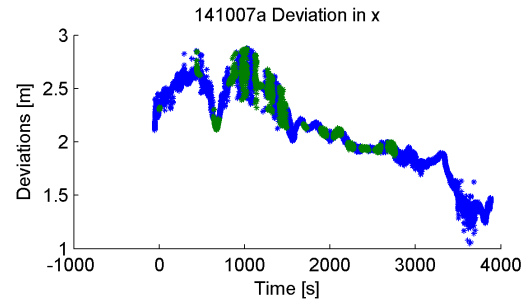


(b) FWD

Figure A.47: 141007a IGU

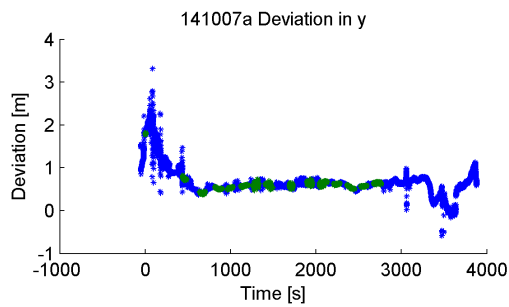


(a) AFT

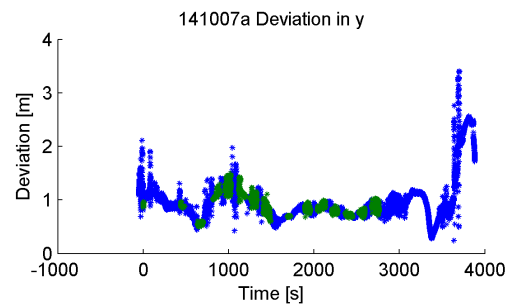


(b) FWD

Figure A.48: 141007a IGU

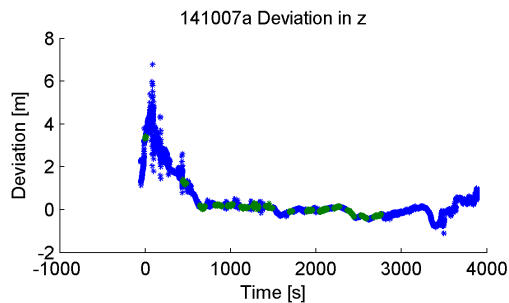


(a) AFT

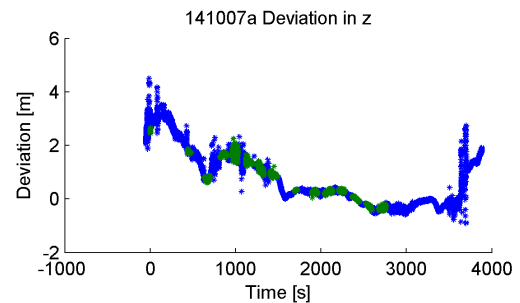


(b) FWD

Figure A.49: 141007a IGU

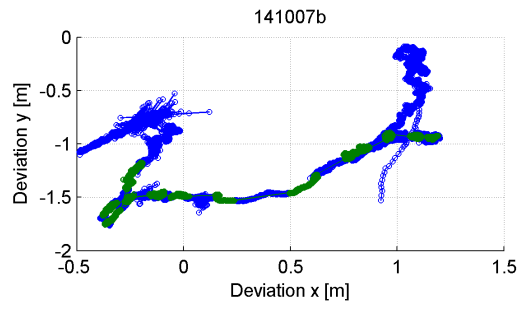


(a) AFT

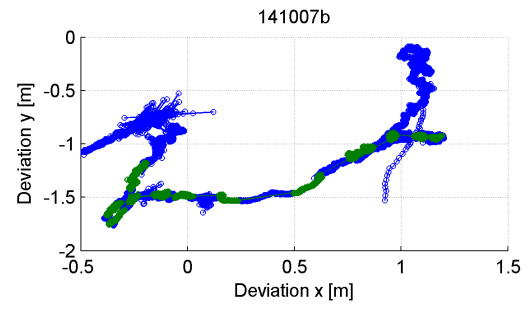


(b) FWD

Figure A.50: 141007a IGU

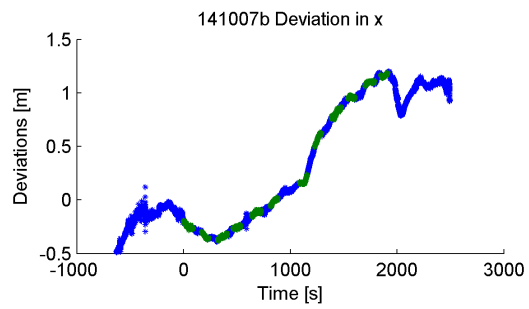


(a) AFT

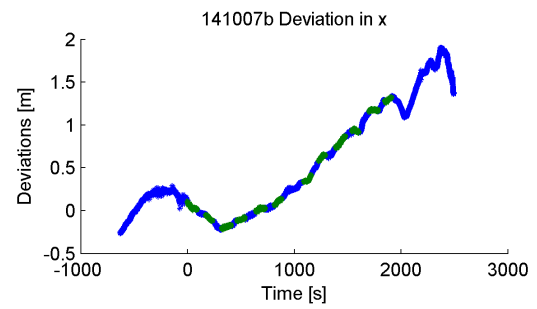


(b) FWD

Figure A.51: 141007b IGU

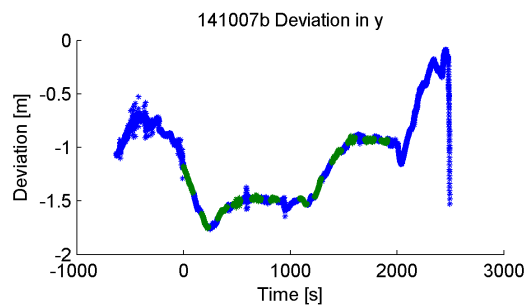


(a) AFT

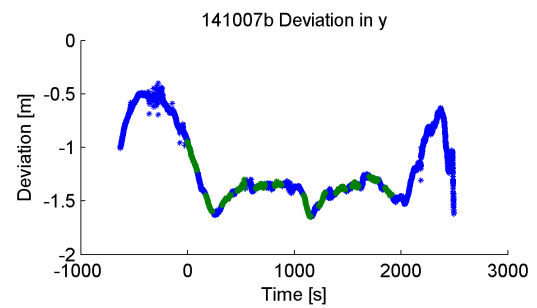


(b) FWD

Figure A.52: 141007b IGU

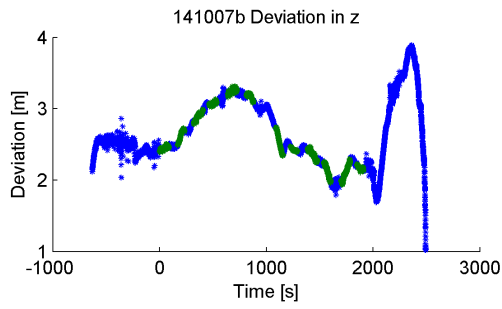


(a) AFT

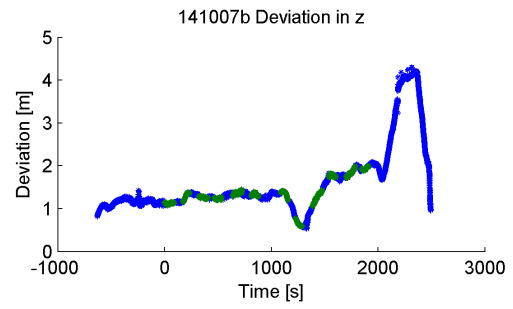


(b) FWD

Figure A.53: 141007b IGU



(a) AFT

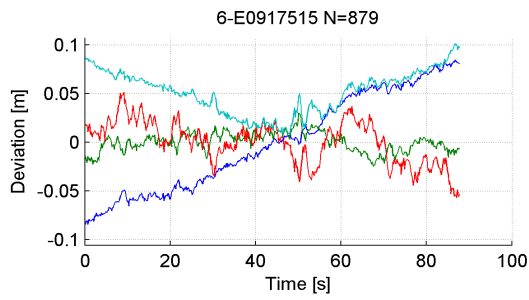


(b) FWD

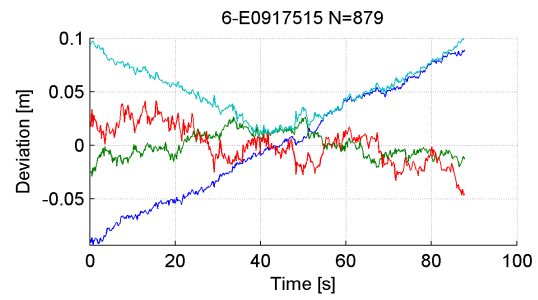
Figure A.54: 141007b IGU

Deviation for transformed runs

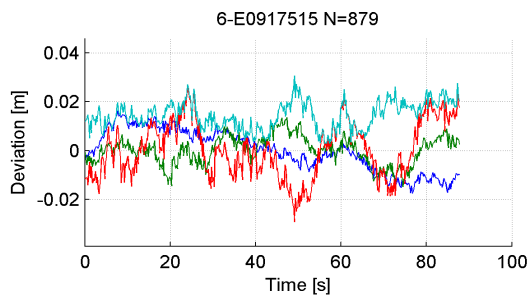
Blue is X direction, green is R direction, red is Z direction and cyan is the norm difference.



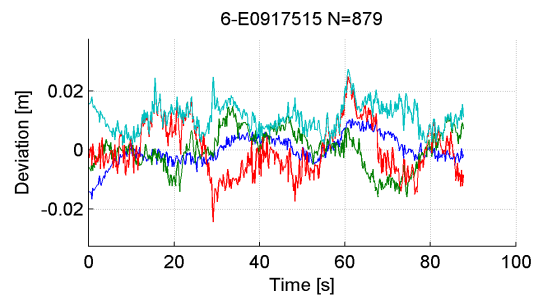
(a) IGU AFT



(b) IGU FWD



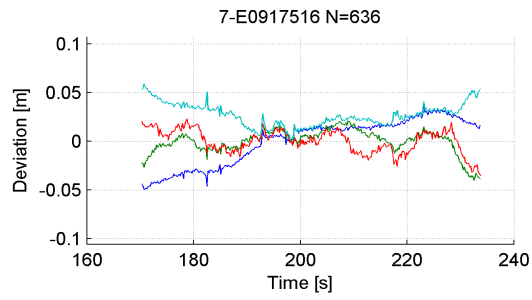
(c) IGS AFT



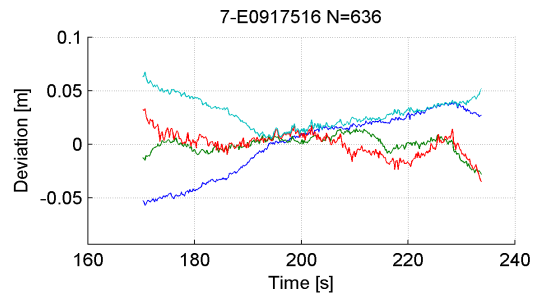
(d) IGS FWD

Figure A.55: Run E0917515

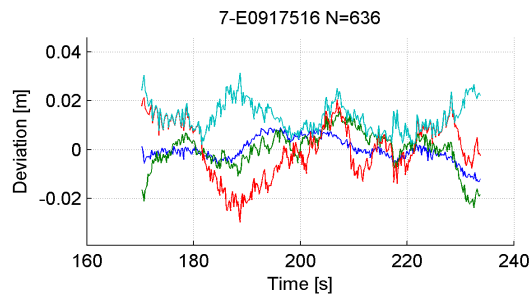
A. Extra Figures



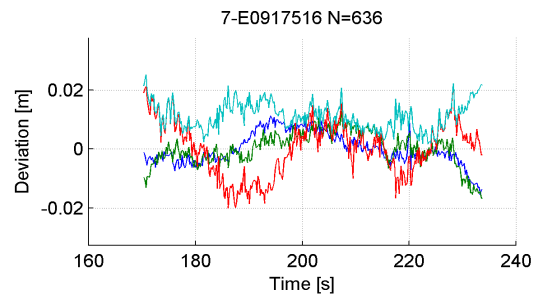
(a) IGU AFT



(b) IGU FWD

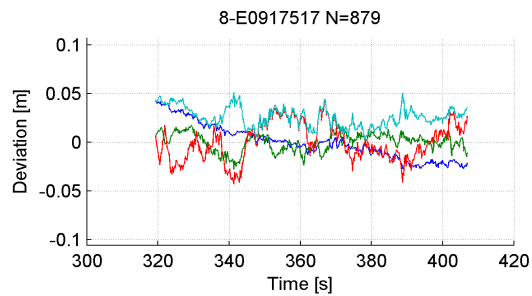


(c) IGS AFT

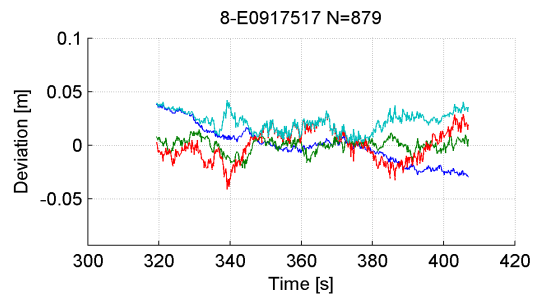


(d) IGS FWD

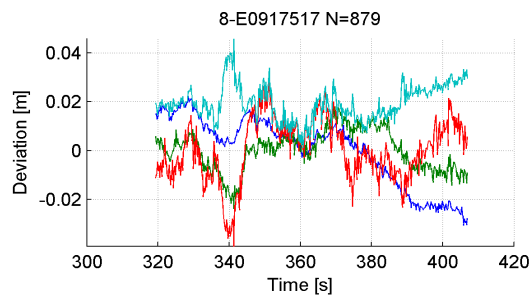
Figure A.56: Run E0917516



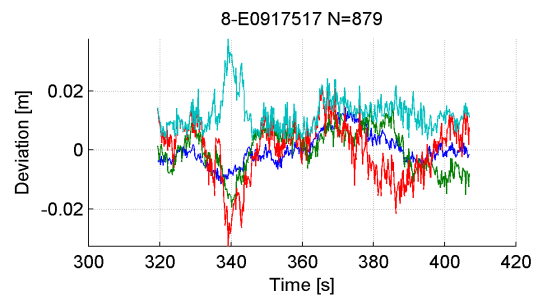
(a) IGU AFT



(b) IGU FWD

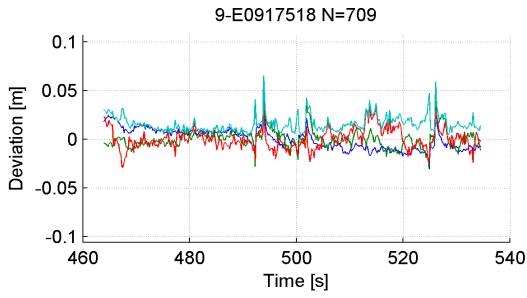


(c) IGS AFT

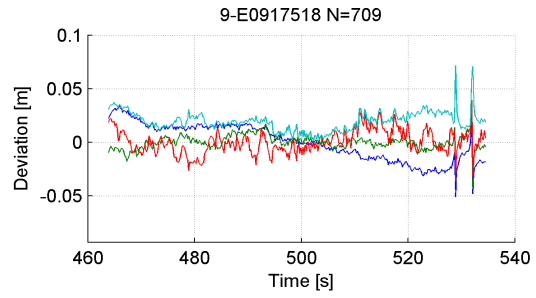


(d) IGS FWD

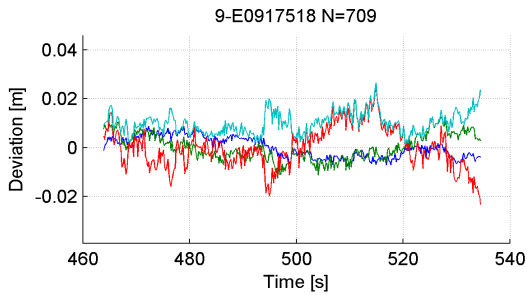
Figure A.57: Run E0917517



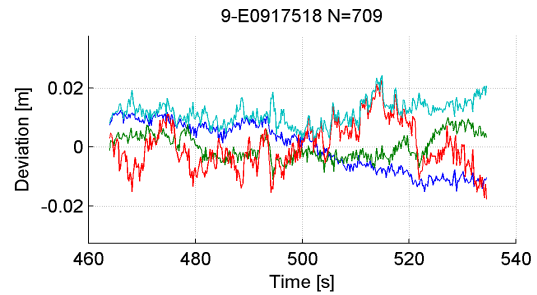
(a) IGU AFT



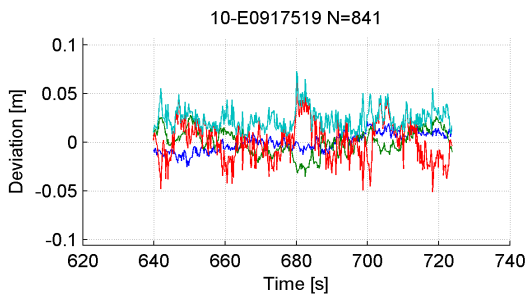
(b) IGU FWD



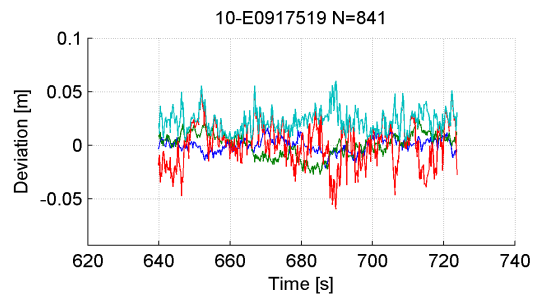
(c) IGS AFT



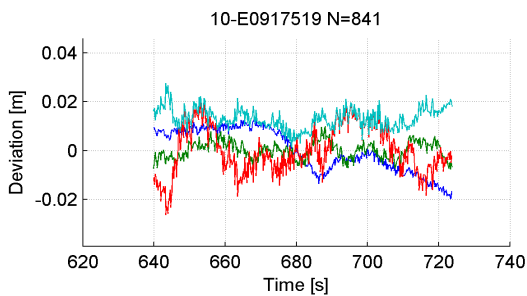
(d) IGS FWD

Figure A.58: Run E0917518


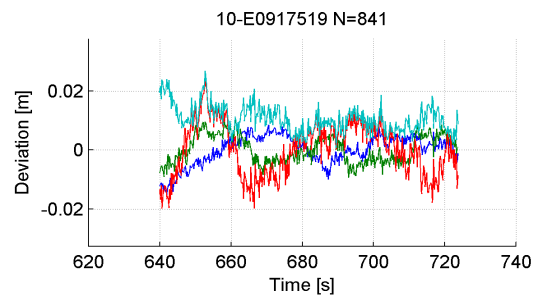
(a) IGU AFT



(b) IGU FWD



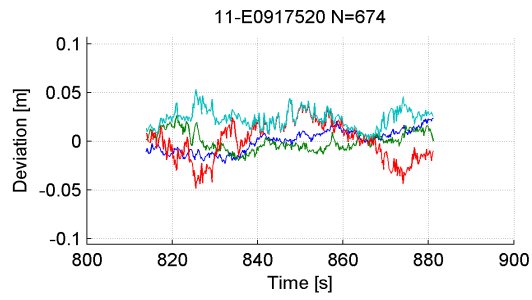
(c) IGS AFT



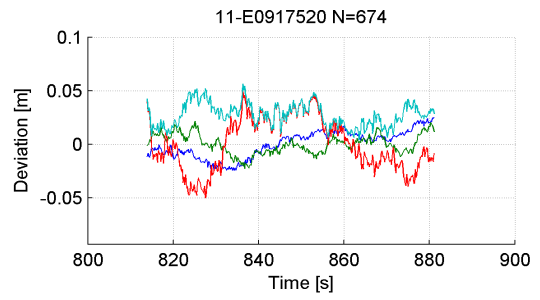
(d) IGS FWD

Figure A.59: Run E0917519

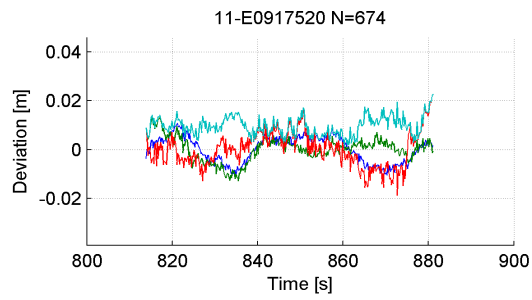
A. Extra Figures



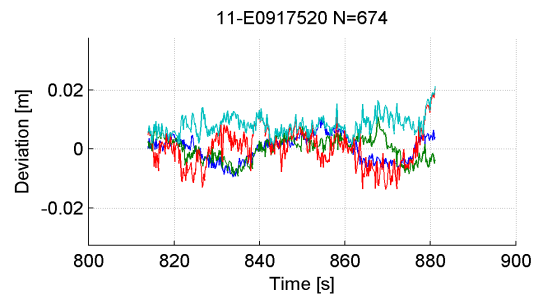
(a) IGU AFT



(b) IGU FWD

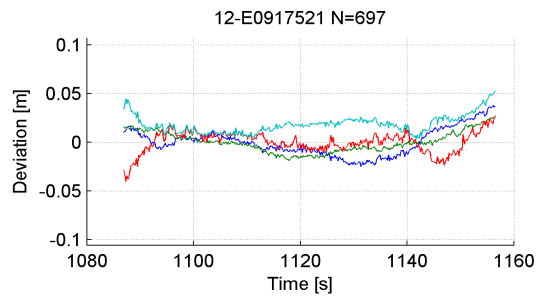


(c) IGS AFT

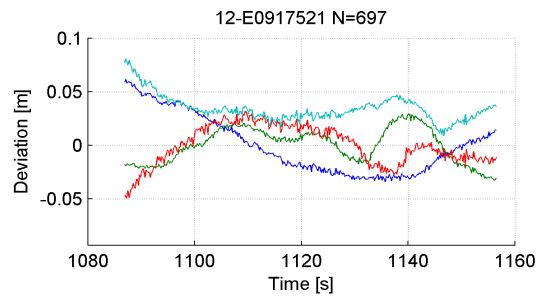


(d) IGS FWD

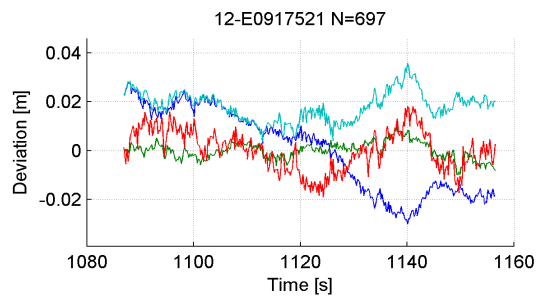
Figure A.60: Run E0917520



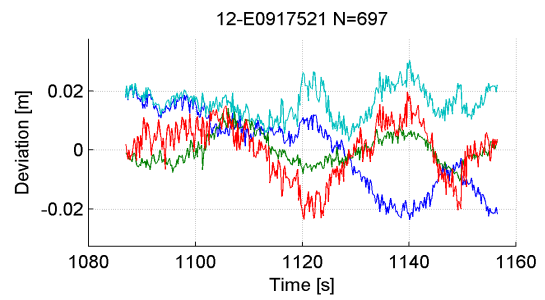
(a) IGU AFT



(b) IGU FWD

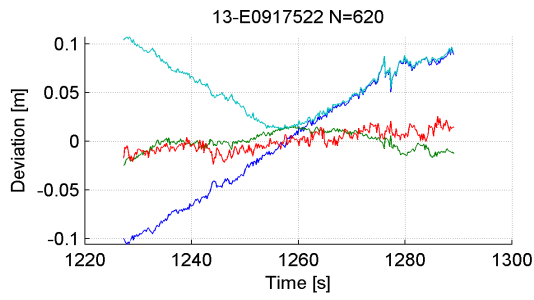


(c) IGS AFT

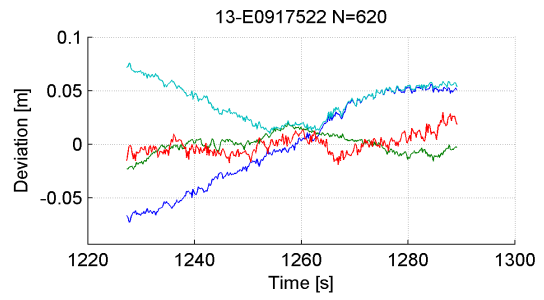


(d) IGS FWD

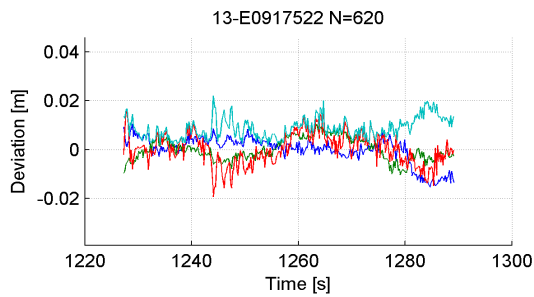
Figure A.61: Run E0917521



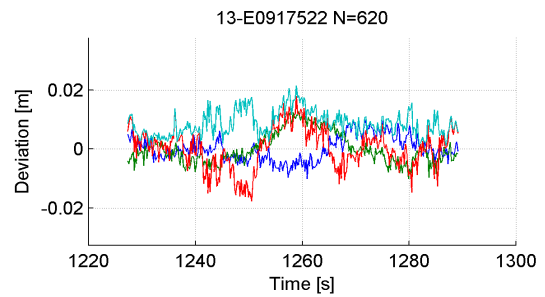
(a) IGU AFT



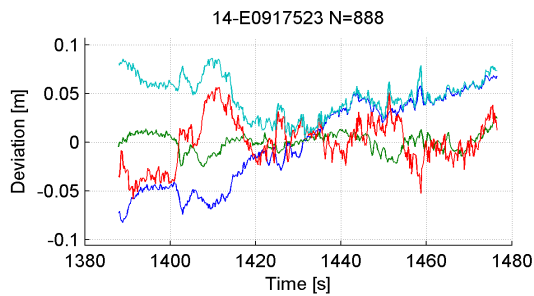
(b) IGU FWD



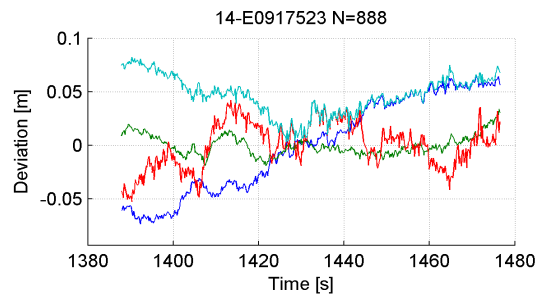
(c) IGS AFT



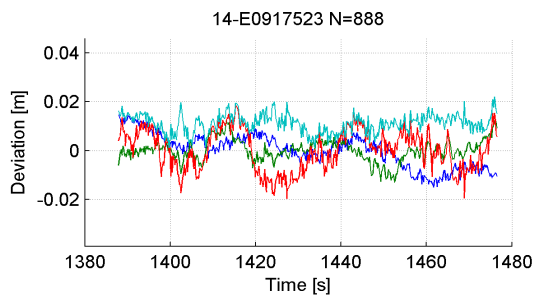
(d) IGS FWD

Figure A.62: Run E0917522


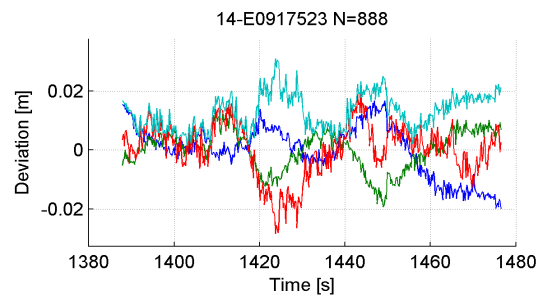
(a) IGU AFT



(b) IGU FWD



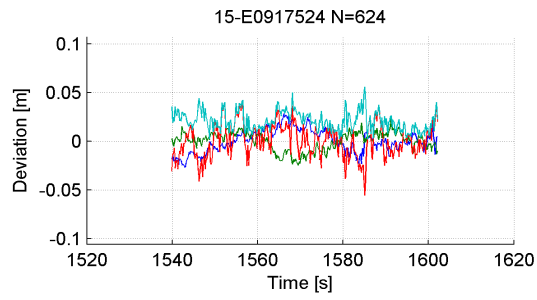
(c) IGS AFT



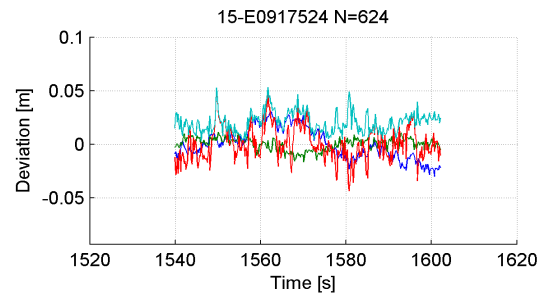
(d) IGS FWD

Figure A.63: Run E0917523

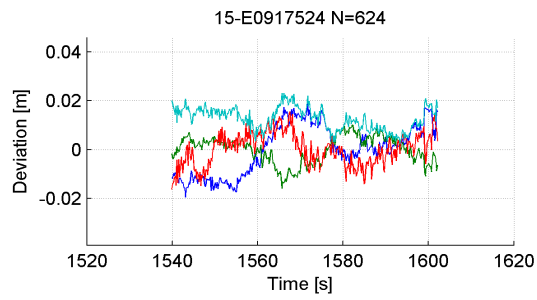
A. Extra Figures



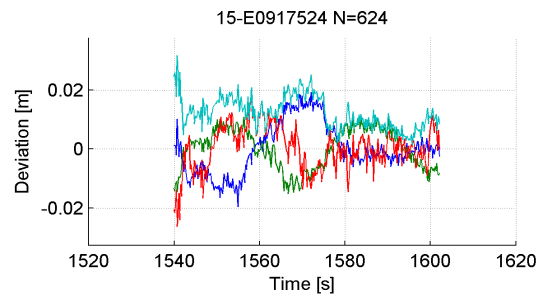
(a) IGU AFT



(b) IGU FWD

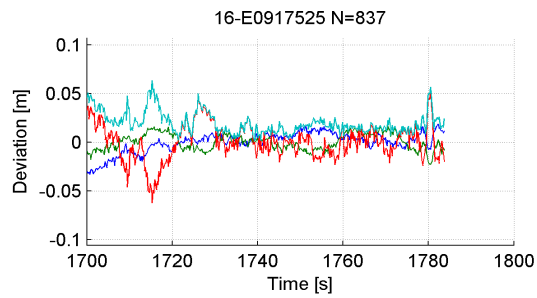


(c) IGS AFT

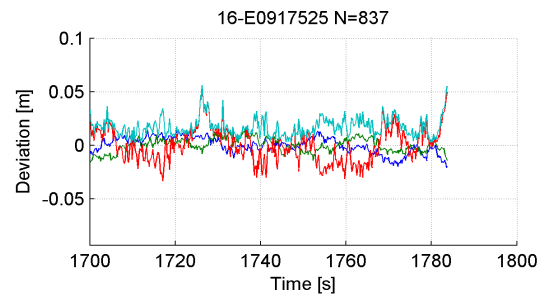


(d) IGS FWD

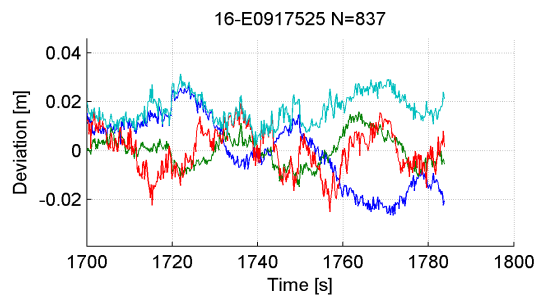
Figure A.64: Run E0917524



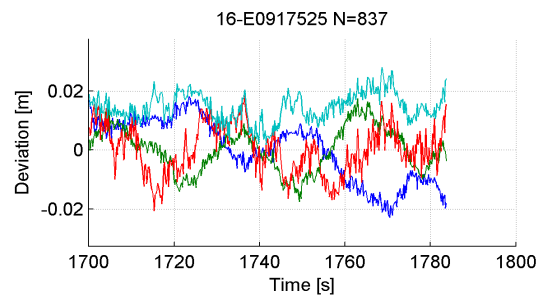
(a) IGU AFT



(b) IGU FWD

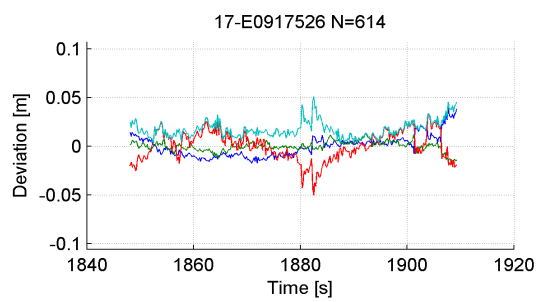


(c) IGS AFT

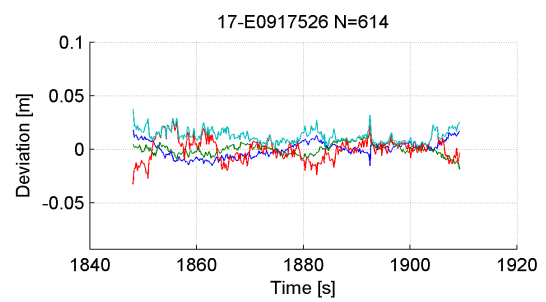


(d) IGS FWD

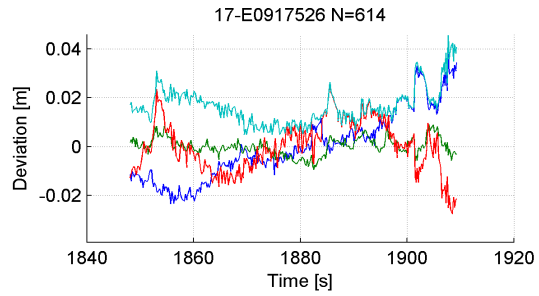
Figure A.65: Run E0917525



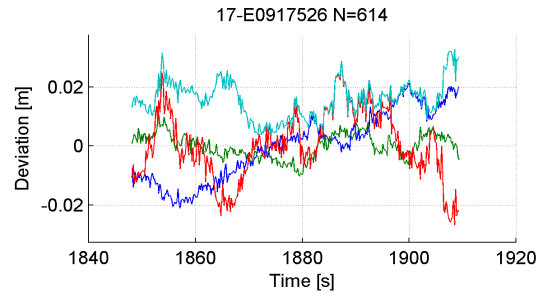
(a) IGU AFT



(b) IGU FWD



(c) IGS AFT



(d) IGS FWD

Figure A.66: Run E0917526

B

Extra Tables

B.1 Maximum and Standard Deviations for runs

B.1.1 IGU

Table B.1: Flight 141007b AFT IGU: Maximum and Standard deviation of the deviation of shape from the reference for the SAR-runs in mm.

Run	N	max(X)	max(R)	max(Z)	max(A)	Sd(X)	Sd(R)	Sd(Z)	Sd(A)
6-E0917515	879	84	30	51	101	50	10	22	56
7-E0917516	636	36	21	23	59	24	12	12	29
8-E0917517	879	43	18	43	51	18	9	19	28
9-E0917518	709	38	44	36	65	11	9	11	18
10-E0917519	841	22	28	67	73	9	13	21	26
11-E0917520	674	24	27	44	53	11	10	20	25
12-E0917521	697	38	26	28	53	14	10	11	21
13-E0917522	620	96	15	26	108	62	9	10	63
14-E0917523	888	69	26	57	86	44	9	24	51
15-E0917524	624	28	24	39	56	12	9	17	23
16-E0917525	837	18	17	52	64	10	8	18	23
17-E0917526	614	39	13	33	51	11	5	15	19

Table B.2: Flight 141007b FWD IGU: Maximum and Standard deviation of the deviation of shape from the reference for the SAR-runs in mm.

Run	N	max(X)	max(R)	max(Z)	max(A)	Sd(X)	Sd(R)	Sd(Z)	Sd(A)
6-E0917515	879	89	27	42	101	53	11	18	57
7-E0917516	636	39	15	33	68	30	8	11	33
8-E0917517	879	39	15	32	42	17	7	15	24
9-E0917518	709	34	39	35	72	17	7	11	22
10-E0917519	841	17	24	54	60	7	11	21	24
11-E0917520	674	25	22	49	56	13	9	25	29
12-E0917521	697	62	29	32	81	27	16	18	36
13-E0917522	620	56	20	30	76	42	9	9	44
14-E0917523	888	65	34	42	83	44	9	22	50
15-E0917524	624	30	12	53	53	15	6	16	22
16-E0917525	837	14	13	55	56	7	6	16	19
17-E0917526	614	18	15	28	38	7	5	10	14

Table B.3: Flight 141007a AFT IGU: Maximum and Standard deviation of the deviation of shape from the reference for the SAR-runs in mm.

Run	N	max(X)	max(R)	max(Z)	max(A)	Sd(X)	Sd(R)	Sd(Z)	Sd(A)
1-E0916500	55	72	28	41	92	35	18	22	45
6-E0916501	291	40	98	44	119	16	17	17	29
7-E0916502	11	4	5	10	13	4	7	7	11
8-E0916503	626	75	28	71	115	30	12	34	47
9-E0916504	835	43	68	30	75	14	22	17	31
10-E0916505	658	26	27	57	63	10	9	19	23
11-E0916506	838	26	20	57	61	10	12	17	24
12-E0916507	709	132	45	138	195	31	15	36	50
13-E0916508	856	143	30	31	230	23	15	15	32
14-E0916510	349	22	98	43	112	9	40	12	43
15-E0916509	647	35	131	54	133	11	39	17	44
16-E0916510	898	36	90	46	113	23	51	18	59
17-E0916511	693	11	32	23	43	4	11	11	16
18-E0916512	869	19	37	52	63	10	18	17	27
19-E0916513	688	21	37	27	40	8	14	9	19
20-E0916514	861	14	32	41	58	5	13	20	25

Table B.4: Flight 141007a FWD IGU: Maximum and Standard deviation of the deviation of shape from the reference for the SAR-runs in mm.

Run	N	max(X)	max(R)	max(Z)	max(A)	Sd(X)	Sd(R)	Sd(Z)	Sd(A)
1-E0916500	55	21	111	40	125	11	63	33	72
6-E0916501	291	89	41	164	215	18	27	35	47
7-E0916502	11	4	3	3	6	3	3	3	5
8-E0916503	626	127	57	121	186	40	28	40	63
9-E0916504	835	221	39	189	300	33	28	32	54
10-E0916505	658	249	178	396	575	87	61	148	182
11-E0916506	838	289	162	232	413	68	35	62	98
12-E0916507	709	240	104	257	355	89	40	73	121
13-E0916508	856	414	125	130	503	97	43	47	116
14-E0916510	349	20	20	31	32	6	9	12	16
15-E0916509	647	111	114	151	248	18	38	32	52
16-E0916510	898	25	88	140	154	15	30	39	52
17-E0916511	693	17	77	98	123	6	21	31	38
18-E0916512	869	17	58	49	76	7	14	16	23
19-E0916513	688	23	89	82	126	7	27	27	39
20-E0916514	861	33	143	140	231	12	51	50	72

Table B.5: Flight 141006d AFT IGU: Maximum and Standard deviation of the deviation of shape from the reference for the SAR-runs in mm.

Run	N	max(X)	max(R)	max(Z)	max(A)	Sd(X)	Sd(R)	Sd(Z)	Sd(A)
6-E0915501	318	25	11	30	39	13	5	12	18
7-E0915502	11	3	1	5	5	3	1	3	4
8-E0915503	860	106	33	79	166	33	9	26	42
9-E0915504	1089	64	24	98	235	36	8	28	46
10-E0915505	861	133	28	91	150	93	15	46	105
11-E0915506	1031	23	19	77	81	16	8	13	22
12-E0915507	895	92	38	330	352	13	7	31	35
13-E0915508	973	35	20	181	182	11	8	24	28
14-E0915509	881	44	37	155	265	29	10	52	61
15-E0915510	942	57	18	77	90	34	4	11	37
16-E0915511	891	83	32	49	146	57	19	32	68
17-E0915512	1035	36	23	41	54	18	9	17	26

Table B.6: Flight 141006d FWD IGU: Maximum and Standard deviation of the deviation of shape from the reference for the SAR-runs in mm.

Run	N	max(X)	max(R)	max(Z)	max(A)	Sd(X)	Sd(R)	Sd(Z)	Sd(A)
6-E0915501	318	16	131	374	395	7	24	64	69
7-E0915502	11	3	2	2	6	3	2	2	4
8-E0915503	860	114	20	200	234	27	10	31	42
9-E0915504	1089	96	24	59	349	59	8	28	66
10-E0915505	861	196	17	107	232	124	6	33	129
11-E0915506	1031	54	18	77	95	28	5	13	32
12-E0915507	895	41	21	172	186	13	5	18	23
13-E0915508	973	33	27	210	235	16	10	30	36
14-E0915509	881	82	25	178	206	38	14	28	49
15-E0915510	942	104	62	141	327	55	14	32	65
16-E0915511	891	197	22	78	212	118	13	34	124
17-E0915512	1035	53	24	27	54	23	6	10	25

Table B.7: Flight 141006c AFT IGU: Maximum and Standard deviation of the deviation of shape from the reference for the SAR-runs in mm.

Run	N	max(X)	max(R)	max(Z)	max(A)	Sd(X)	Sd(R)	Sd(Z)	Sd(A)
6-E0914216	497	19	60	28	69	7	28	11	31
7-E0914217	12	2	3	2	4	2	1	2	3
8-E0914218	154	24	44	17	50	11	22	7	26
9-E0914219	158	12	55	91	105	6	13	23	27
10-E0914220	149	16	12	20	23	7	6	7	12
11-E0914221	179	26	45	80	157	12	16	25	32
12-E0914222	172	20	27	18	34	9	12	7	17
13-E0914223	180	24	19	36	70	13	9	17	23
14-E0914218	153	16	14	16	23	6	5	7	11
15-E0914219	187	21	48	77	94	9	17	17	26

Table B.8: Flight 141006c FWD IGU: Maximum and Standard deviation of the deviation of shape from the reference for the SAR-runs in mm.

Run	N	max(X)	max(R)	max(Z)	max(A)	Sd(X)	Sd(R)	Sd(Z)	Sd(A)
6-E0914216	497	23	82	30	88	11	43	13	46
7-E0914217	12	3	6	3	7	3	4	2	5
8-E0914218	154	14	23	10	26	6	11	6	14
9-E0914219	158	13	22	19	26	6	9	8	14
10-E0914220	149	29	24	193	335	37	18	29	50
11-E0914221	179	14	78	148	169	7	11	22	26
12-E0914222	172	12	13	18	24	6	6	9	12
13-E0914223	180	18	85	123	150	8	12	18	23
14-E0914218	153	19	15	15	28	7	9	6	13
15-E0914219	187	36	15	19	238	8	18	24	31

Table B.9: Flight 141006b AFT IGU: Maximum and Standard deviation of the deviation of shape from the reference for the SAR-runs in mm.

Run	N	max(X)	max(R)	max(Z)	max(A)	Sd(X)	Sd(R)	Sd(Z)	Sd(A)
6-E0913502	1702	76	41	398	427	22	13	52	58
7-E0913502	229	15	17	54	59	8	9	20	23
8-E0913503	11	4	2	5	7	3	2	4	6
9-E0913504	704	34	39	42	57	11	18	13	24
10-E0913505	887	19	26	40	42	9	9	15	20
11-E0913506	657	49	32	55	100	20	13	34	41
12-E0913507	881	24	30	35	46	9	10	14	20
13-E0913508	709	121	408	205	577	26	55	55	82
14-E0913509	816	26	38	33	64	11	19	18	28
15-E0913510	706	32	198	161	301	7	26	30	40
16-E0913511	897	24	89	47	103	16	34	22	44
17-E0913512	876	43	33	39	62	23	11	15	30
18-E0913513	674	37	17	57	62	15	11	21	28
19-E0913514	840	21	33	51	66	9	9	20	24
20-E0913515	663	20	16	27	68	11	6	12	17
21-E0913516	812	22	23	31	46	8	11	11	17
22-E0913517	595	43	19	27	44	16	8	15	23
23-E0913518	640	17	11	32	33	6	5	12	14

Table B.10: Flight 141006b FWD IGU: Maximum and Standard deviation of the deviation of shape from the reference for the SAR-runs in mm.

Run	N	max(X)	max(R)	max(Z)	max(A)	Sd(X)	Sd(R)	Sd(Z)	Sd(A)
6-E0913502	1702	41	53	124	176	21	13	49	55
7-E0913502	229	43	52	109	156	10	14	22	28
8-E0913503	11	4	2	3	6	3	2	3	4
9-E0913504	704	51	69	45	102	11	17	11	23
10-E0913505	887	25	35	40	47	9	14	13	21
11-E0913506	657	18	20	26	43	8	8	11	16
12-E0913507	881	22	19	23	36	9	7	11	16
13-E0913508	709	104	41	106	157	15	17	21	31
14-E0913509	816	26	29	42	49	11	10	15	21
15-E0913510	706	40	220	242	324	8	34	43	55
16-E0913511	897	25	57	51	76	11	23	22	34
17-E0913512	876	57	27	35	83	25	12	14	31
18-E0913513	674	129	18	108	225	48	9	35	60
19-E0913514	840	78	36	64	180	12	11	21	26
20-E0913515	663	20	17	33	36	9	6	9	14
21-E0913516	812	19	20	25	36	8	10	14	19
22-E0913517	595	91	10	34	92	54	4	15	57
23-E0913518	640	14	10	23	24	5	3	9	11

Table B.11: Flight 141006a AFT IGU: Maximum and Standard deviation of the deviation of shape from the reference for the SAR-runs in mm.

Run	N	max(X)	max(R)	max(Z)	max(A)	Sd(X)	Sd(R)	Sd(Z)	Sd(A)
1-E0912501	89	19	10	10	38	12	5	5	14
6-E0912502	325	59	38	251	375	38	18	35	54
7-E0912503	11	2	1	1	4	2	2	1	3
8-E0912504	709	44	36	309	512	32	14	30	46
9-E0912505	894	58	82	47	95	27	47	22	58
10-E0912506	733	101	105	129	156	34	50	27	66
11-E0912507	843	32	23	182	252	18	11	25	32
12-E0912508	261	42	95	97	155	14	23	29	40
13-E0912508	603	18	48	51	151	9	18	25	32
14-E0912509	916	33	33	69	72	17	27	23	39
15-E0912510	691	30	50	42	110	16	28	28	42
16-E0912511	870	36	33	33	49	16	24	11	31
17-E0912512	834	101	72	704	715	20	14	98	101
18-E0912513	748	136	21	66	148	33	9	33	47
19-E0912514	908	104	13	322	345	28	7	99	103
20-E0912515	720	40	28	54	80	16	16	17	29
21-E0912516	836	50	64	126	142	31	9	14	35
22-E0912517	231	36	19	32	68	10	8	14	19
23-E0912517	602	39	52	120	142	25	16	27	40
24-E0912518	795	35	12	38	59	19	5	13	23
25-E0912519	704	111	44	49	124	27	7	11	30

Table B.12: Flight 141006a FWD IGU: Maximum and Standard deviation of the deviation of shape from the reference for the SAR-runs in mm.

Run	N	max(X)	max(R)	max(Z)	max(A)	Sd(X)	Sd(R)	Sd(Z)	Sd(A)
1-E0912501	89	25	5	10	26	13	3	4	14
6-E0912502	325	25	25	40	51	11	5	14	19
7-E0912503	11	4	6	8	10	3	4	5	7
8-E0912504	709	35	20	543	862	49	13	42	65
9-E0912505	894	41	48	38	63	18	31	15	38
10-E0912506	733	67	61	345	492	31	24	29	49
11-E0912507	843	25	27	39	55	10	15	19	26
12-E0912508	261	18	23	31	38	6	10	13	18
13-E0912508	603	26	56	132	179	7	15	24	30
14-E0912509	916	41	29	77	79	16	23	27	39
15-E0912510	691	26	28	44	103	10	13	27	32
16-E0912511	870	36	36	39	57	18	24	13	32
17-E0912512	834	32	25	53	66	13	9	22	27
18-E0912513	748	105	61	348	405	18	10	61	65
19-E0912514	908	57	24	228	232	16	5	43	46
20-E0912515	720	42	19	91	104	13	12	31	36
21-E0912516	836	44	14	23	55	23	6	10	26
22-E0912517	231	44	18	41	51	11	7	17	21
23-E0912517	602	38	24	46	83	25	9	20	33
24-E0912518	795	27	23	71	90	15	6	14	22
25-E0912519	704	45	20	35	88	22	6	10	25

Table B.13: Flight 141003b AFT IGU: Maximum and Standard deviation of the deviation of shape from the reference for the SAR-runs in mm.

Run	N	max(X)	max(R)	max(Z)	max(A)	Sd(X)	Sd(R)	Sd(Z)	Sd(A)
6-E0911502	239	71	76	84	250	54	59	46	93
7-E0911503	11	3	2	3	9	4	3	2	5
8-E0911504	580	21	38	27	47	10	16	13	23
9-E0911505	487	20	25	14	36	12	12	7	19
10-E0911506	541	522	329	110	653	45	48	40	77
11-E0911507	485	22	23	23	33	10	12	10	19
12-E0911508	569	15	29	36	45	8	14	13	21
13-E0911509	476	60	49	20	74	25	26	10	38
14-E0911510	501	20	20	19	58	8	15	10	20
15-E0911511	500	26	33	17	61	6	8	7	12
16-E0911512	551	13	14	15	21	6	5	8	11
17-E0911513	536	10	11	17	19	6	4	5	9
18-E0911514	531	29	22	19	52	19	13	11	26
19-E0911515	533	16	6	22	23	9	2	7	12
20-E0911516	416	67	22	50	106	19	6	16	26
21-E0911517	487	15	9	16	26	9	3	7	12
22-E0911518	485	76	79	145	192	41	15	34	55
23-E0911519	489	299	53	121	464	40	24	57	74

Table B.14: Flight 141003b FWD IGU: Maximum and Standard deviation of the deviation of shape from the reference for the SAR-runs in mm.

Run	N	max(X)	max(R)	max(Z)	max(A)	Sd(X)	Sd(R)	Sd(Z)	Sd(A)
6-E0911502	239	37	51	47	82	24	36	19	47
7-E0911503	11	2	4	4	6	2	3	3	4
8-E0911504	580	161	46	35	187	23	24	21	39
9-E0911505	487	15	21	20	145	7	11	12	18
10-E0911506	541	249	374	36	474	31	45	22	60
11-E0911507	485	21	25	14	30	8	12	6	16
12-E0911508	569	303	13	199	364	24	7	17	30
13-E0911509	476	60	49	14	77	27	29	7	41
14-E0911510	501	11	16	10	31	6	10	5	12
15-E0911511	500	102	19	93	139	10	9	10	16
16-E0911512	551	10	16	18	21	4	6	9	11
17-E0911513	536	11	10	15	21	7	5	5	9
18-E0911514	531	29	19	19	58	20	12	13	27
19-E0911515	533	28	10	17	31	16	5	7	18
20-E0911516	416	25	10	29	31	11	4	11	16
21-E0911517	487	8	9	15	18	5	4	6	9
22-E0911518	485	26	34	24	41	12	9	12	19
23-E0911519	489	100	110	248	319	22	17	40	49

Table B.15: Flight 141003a AFT IGU: Maximum and Standard deviation of the deviation of shape from the reference for the SAR-runs in mm.

Run	N	max(X)	max(R)	max(Z)	max(A)	Sd(X)	Sd(R)	Sd(Z)	Sd(A)
6-E0910602	335	51	30	40	96	12	11	18	24
7-E0910603	11	2	2	3	5	1	1	3	3
8-E0910604	787	30	43	122	129	12	13	17	25
9-E0910605	811	57	49	52	112	36	31	23	53
10-E0910606	748	100	84	128	167	50	37	56	84
11-E0910607	779	26	51	39	118	13	25	21	35
16-E0910408	374	22	33	57	102	10	12	30	34
17-E0910409	11	4	6	9	14	2	6	8	11
18-E0910410	855	39	34	64	76	22	18	23	37
19-E0910411	699	42	15	67	79	11	8	15	21
24-E0910412	232	13	17	47	51	5	10	21	24
25-E0910413	11	3	6	4	8	2	3	4	6
26-E0910414	210	15	16	63	64	6	9	23	26
27-E0910415	176	15	17	41	52	5	7	21	22
28-E0910416	188	22	27	48	61	10	9	22	26
29-E0910417	178	17	40	52	57	8	13	22	27
34-E0910418	220	38	34	77	86	13	12	23	29
35-E0910419	12	8	6	11	16	7	7	9	13
36-E0910420	182	27	36	95	180	18	18	52	58
37-E0910421	174	20	15	42	49	13	8	15	21
38-E0910422	184	42	26	41	55	22	10	20	32
39-E0910423	171	26	23	39	75	12	14	18	26

Table B.16: Flight 141003a FWD IGU: Maximum and Standard deviation of the deviation of shape from the reference for the SAR-runs in mm.

Run	N	max(X)	max(R)	max(Z)	max(A)	Sd(X)	Sd(R)	Sd(Z)	Sd(A)
6-E0910602	335	31	49	27	69	7	12	12	18
7-E0910603	11	3	5	2	6	2	3	2	4
8-E0910604	787	36	31	27	48	15	15	11	23
9-E0910605	811	62	34	51	134	43	24	24	55
10-E0910606	748	27	36	31	59	12	23	14	29
11-E0910607	779	22	37	59	67	11	14	14	23
16-E0910408	374	18	36	56	63	9	13	20	25
17-E0910409	11	5	5	8	13	4	4	7	9
18-E0910410	855	41	35	53	69	26	21	19	39
19-E0910411	699	16	39	45	52	8	7	20	22
24-E0910412	232	14	16	38	39	8	9	13	18
25-E0910413	11	7	5	5	8	4	3	4	7
26-E0910414	210	21	16	33	42	9	10	16	21
27-E0910415	176	9	15	40	48	4	7	17	19
28-E0910416	188	21	27	44	50	8	11	22	26
29-E0910417	178	18	26	47	48	7	10	17	21
34-E0910418	220	13	20	49	60	6	9	19	21
35-E0910419	12	2	5	5	9	2	4	5	7
36-E0910420	182	10	19	40	41	5	9	16	19
37-E0910421	174	24	22	33	49	11	8	16	21
38-E0910422	184	47	26	29	59	19	13	15	27
39-E0910423	171	27	19	26	50	20	12	12	26

Table B.17: Flight 141001a AFT IGU: Maximum and Standard deviation of the deviation of shape from the reference for the SAR-runs in mm.

Run	N	max(X)	max(R)	max(Z)	max(A)	Sd(X)	Sd(R)	Sd(Z)	Sd(A)
5-E0904201	349	67	15	74	101	37	8	16	41
6-E0904202	11	2	1	1	4	2	1	1	2
7-E0904203	537	60	37	226	260	19	12	37	43
8-E0904204	920	247	135	189	300	136	11	56	147
9-E0904205	642	58	31	63	164	57	13	27	64
10-E0904206	940	71	19	102	125	31	8	19	37
11-E0904207	685	38	43	130	164	19	26	34	47
12-E0904208	913	27	23	57	62	8	10	18	22
13-E0904209	667	95	36	280	288	34	10	61	71
14-E0904210	917	81	40	167	188	11	10	24	28
15-E0904211	937	57	106	546	558	30	13	63	71
16-E0904212	682	132	101	247	286	49	44	110	128
17-E0904213	948	219	42	575	615	44	11	112	121
18-E0904214	688	130	30	315	363	25	8	50	57
19-E0904215	968	92	76	342	350	27	36	64	78
24-E0904216	57	124	122	82	259	32	32	55	71
25-E0904217	11	137	57	23	165	89	55	20	107
26-E0904218	170	21	11	39	69	9	5	21	24
27-E0904219	242	154	132	206	377	42	39	45	73
28-E0904220	193	163	52	152	229	21	8	25	34
29-E0904221	261	24	16	54	542	36	14	51	64

Table B.18: Flight 141001a FWD IGU: Maximum and Standard deviation of the deviation of shape from the reference for the SAR-runs in mm.

Run	N	max(X)	max(R)	max(Z)	max(A)	Sd(X)	Sd(R)	Sd(Z)	Sd(A)
5-E0904201	349	72	13	62	98	38	8	24	46
6-E0904202	11	2	2	4	5	2	2	2	3
7-E0904203	537	33	17	56	64	12	7	19	23
8-E0904204	920	233	21	127	260	129	7	55	140
9-E0904205	642	54	29	54	187	57	13	26	64
10-E0904206	940	57	18	55	86	40	7	21	46
11-E0904207	685	43	38	40	137	23	25	32	47
12-E0904208	913	19	29	39	80	8	9	16	20
13-E0904209	667	31	15	49	53	20	6	17	27
14-E0904210	917	35	20	125	143	11	9	23	27
15-E0904211	937	39	49	246	252	17	10	40	45
16-E0904212	682	30	28	48	72	12	10	18	24
17-E0904213	948	51	23	158	160	20	8	25	33
18-E0904214	688	34	15	43	60	15	7	18	25
19-E0904215	968	63	47	331	337	15	26	47	55
24-E0904216	57	97	113	184	247	34	36	67	83
25-E0904217	11	2	4	15	16	1	4	9	10
26-E0904218	170	25	18	54	57	12	8	17	23
27-E0904219	242	111	103	217	345	27	25	45	58
28-E0904220	193	88	29	98	135	19	7	18	27
29-E0904221	261	24	15	21	36	10	6	12	16

Table B.19: Flight 130222a AFT IGU: Maximum and Standard deviation of the deviation of shape from the reference for the SAR-runs in mm.

Run	N	max(X)	max(R)	max(Z)	max(A)	Sd(X)	Sd(R)	Sd(Z)	Sd(A)
5-D0210235	837	21	21	109	111	6	12	18	23
6-D0210236	11	4	4	4	6	2	2	4	5
7-D0210237	250	21	16	55	65	9	9	18	22
8-D0210238	214	14	20	37	41	5	6	14	16
9-D0210239	220	24	45	103	117	7	11	24	27
10-D0210240	195	14	14	36	65	7	7	17	19
11-D0210241	209	19	10	24	30	11	4	11	16
12-D0210242	211	9	13	31	33	4	6	12	14
17-D0210245	937	64	23	78	88	27	10	22	36
18-D0210246	301	11	15	78	78	5	7	19	21
19-D0210247	1110	65	62	110	112	27	16	23	39
20-D0210248	966	113	66	120	268	81	26	41	95

Table B.20: Flight 130222a FWD IGU: Maximum and Standard deviation of the deviation of shape from the reference for the SAR-runs in mm.

Run	N	max(X)	max(R)	max(Z)	max(A)	Sd(X)	Sd(R)	Sd(Z)	Sd(A)
5-D0210235	837	28	31	37	66	12	13	13	22
6-D0210236	11	3	8	10	13	2	5	7	9
7-D0210237	250	25	25	58	67	9	8	22	26
8-D0210238	214	20	15	47	54	8	7	19	22
9-D0210239	220	11	16	52	53	5	7	17	19
10-D0210240	195	13	18	43	51	5	7	19	21
11-D0210241	209	13	9	28	28	6	4	9	12
12-D0210242	211	6	9	21	27	3	3	9	10
17-D0210245	937	43	23	75	82	18	8	21	29
18-D0210246	301	17	15	123	144	5	5	19	21
19-D0210247	1110	142	44	86	151	69	17	43	83
20-D0210248	966	57	64	109	134	27	36	45	63

Table B.21: Flight 130213c AFT IGU: Maximum and Standard deviation of the deviation of shape from the reference for the SAR-runs in mm.

Run	N	max(X)	max(R)	max(Z)	max(A)	Sd(X)	Sd(R)	Sd(Z)	Sd(A)
7-D0209503	1111	65	64	110	131	16	37	26	48
8-D0209504	1245	32	49	46	56	16	18	13	27
9-D0209505	1021	47	38	61	80	30	13	22	39
14-D0209512	1502	43	40	50	60	14	15	18	27
15-D0209511	1261	61	33	62	88	10	13	23	28
16-D0209506	1444	46	46	62	68	17	15	18	29
17-D0209507	1374	26	27	56	67	9	13	26	30
18-D0209508	1554	36	94	65	169	25	30	42	57
19-D0209509	1270	50	45	65	81	17	19	18	31
20-D0209510	1650	87	76	67	114	23	24	18	37

Table B.22: Flight 130213c FWD IGU: Maximum and Standard deviation of the deviation of shape from the reference for the SAR-runs in mm.

Run	N	max(X)	max(R)	max(Z)	max(A)	Sd(X)	Sd(R)	Sd(Z)	Sd(A)
7-D0209503	1111	31	62	68	97	15	28	23	39
8-D0209504	1245	89	79	75	133	13	16	25	33
9-D0209505	1021	40	71	49	138	15	24	23	37
14-D0209512	1502	33	37	54	57	14	15	16	26
15-D0209511	1261	150	59	39	203	14	20	19	31
16-D0209506	1444	44	86	47	138	14	17	14	26
17-D0209507	1374	27	36	63	72	10	13	32	36
18-D0209508	1554	58	124	59	158	26	41	31	57
19-D0209509	1270	61	36	53	79	19	15	18	30
20-D0209510	1650	223	49	322	409	20	26	30	44

Table B.23: Flight 130213b AFT IGU: Maximum and Standard deviation of the deviation of shape from the reference for the SAR-runs in mm.

Run	N	max(X)	max(R)	max(Z)	max(A)	Sd(X)	Sd(R)	Sd(Z)	Sd(A)
5-D0208409	835	211	85	529	557	123	15	66	141
6-D0208410	301	52	8	16	85	33	3	8	34
7-D0208411	1249	18	62	19	73	8	20	9	23
8-D0208412	1170	42	59	133	143	12	26	44	52
13-D0208625	704	21	23	38	55	8	8	15	19
14-D0208626	21	6	5	12	20	4	3	8	9
15-D0208627	366	20	14	28	32	11	5	9	15
16-D0208628	295	66	21	110	119	15	8	28	33
17-D0208629	341	19	18	42	46	9	9	16	20
18-D0208630	320	36	26	59	92	9	11	19	24

Table B.24: Flight 130213b FWD IGU: Maximum and Standard deviation of the deviation of shape from the reference for the SAR-runs in mm.

Run	N	max(X)	max(R)	max(Z)	max(A)	Sd(X)	Sd(R)	Sd(Z)	Sd(A)
5-D0208409	835	45	23	49	66	27	11	19	35
6-D0208410	301	34	13	28	73	22	6	15	27
7-D0208411	1249	43	50	29	75	22	18	17	33
8-D0208412	1170	53	57	94	129	13	22	46	53
13-D0208625	704	39	33	44	59	14	8	15	22
14-D0208626	21	7	8	13	14	5	4	6	9
15-D0208627	366	22	11	22	28	11	5	9	15
16-D0208628	295	66	24	94	159	19	9	33	39
17-D0208629	341	13	14	34	37	5	10	11	16
18-D0208630	320	32	20	54	64	10	11	18	23

B.1.2 IGS

Table B.25: Flight 141007b AFT IGS: Maximum and Standard deviation of the deviation of shape from the reference for the SAR-runs in mm.

Run	N	max(X)	max(R)	max(Z)	max(A)	Sd(X)	Sd(R)	Sd(Z)	Sd(A)
6-E0917515	879	16	14	26	31	9	6	11	15
7-E0917516	636	9	16	23	31	5	8	12	15
8-E0917517	879	22	19	32	46	14	8	13	21
9-E0917518	709	9	12	26	27	4	5	9	11
10-E0917519	841	13	10	21	28	9	4	10	14
11-E0917520	674	11	13	22	23	5	5	7	10
12-E0917521	697	28	10	18	36	17	3	8	19
13-E0917522	620	11	10	18	22	5	4	6	10
14-E0917523	888	15	12	18	22	7	4	8	12
15-E0917524	624	19	10	16	23	10	6	7	13
16-E0917525	837	27	16	19	31	14	6	9	18
17-E0917526	614	38	9	26	46	14	4	10	18

Table B.26: Flight 141007b FWD IGS: Maximum and Standard deviation of the deviation of shape from the reference for the SAR-runs in mm.

Run	N	max(X)	max(R)	max(Z)	max(A)	Sd(X)	Sd(R)	Sd(Z)	Sd(A)
6-E0917515	879	11	15	25	27	5	7	9	12
7-E0917516	636	11	13	22	25	5	6	9	12
8-E0917517	879	15	15	21	38	5	7	10	13
9-E0917518	709	13	10	23	24	8	4	8	12
10-E0917519	841	8	10	25	27	5	5	9	11
11-E0917520	674	10	11	21	21	4	4	6	9
12-E0917521	697	22	14	20	30	13	5	9	17
13-E0917522	620	10	13	18	21	4	5	7	10
14-E0917523	888	17	14	20	31	9	7	9	14
15-E0917524	624	19	11	20	32	8	7	8	13
16-E0917525	837	18	17	19	28	10	7	8	15
17-E0917526	614	21	11	28	33	12	4	12	17

Table B.27: Flight 141007a AFT IGS: Maximum and Standard deviation of the deviation of shape from the reference for the SAR-runs in mm.

Run	N	max(X)	max(R)	max(Z)	max(A)	Sd(X)	Sd(R)	Sd(Z)	Sd(A)
1-E0916500	55	48	31	11	58	23	14	5	27
6-E0916501	291	37	24	32	40	13	7	12	19
7-E0916502	11	2	3	6	8	2	4	4	6
8-E0916503	626	35	33	67	74	16	13	24	31
9-E0916504	835	27	23	36	49	12	9	18	23
10-E0916505	658	44	17	32	48	15	10	12	22
11-E0916506	838	22	21	37	41	9	8	12	17
12-E0916507	709	27	23	31	44	9	10	14	19
13-E0916508	856	31	26	33	48	15	18	14	27
14-E0916510	349	6	15	24	32	3	9	8	12
15-E0916509	647	15	19	29	35	5	8	13	16
16-E0916510	898	13	17	32	38	4	8	14	17
17-E0916511	693	9	14	27	29	3	6	11	13
18-E0916512	869	13	27	26	37	6	9	12	16
19-E0916513	688	15	30	27	37	6	14	12	19
20-E0916514	861	13	28	38	49	6	12	21	24

Table B.28: Flight 141007a FWD IGS: Maximum and Standard deviation of the deviation of shape from the reference for the SAR-runs in mm.

Run	N	max(X)	max(R)	max(Z)	max(A)	Sd(X)	Sd(R)	Sd(Z)	Sd(A)
1-E0916500	55	13	9	4	13	6	4	2	8
6-E0916501	291	21	12	16	33	9	5	9	13
7-E0916502	11	2	3	3	4	2	2	3	4
8-E0916503	626	118	36	72	167	26	11	25	38
9-E0916504	835	34	21	48	67	17	13	22	31
10-E0916505	658	83	28	109	133	27	11	30	41
11-E0916506	838	32	16	34	45	14	8	14	21
12-E0916507	709	35	23	29	63	14	11	18	25
13-E0916508	856	36	26	21	55	16	17	11	26
14-E0916510	349	5	25	12	26	3	11	4	12
15-E0916509	647	27	116	42	126	7	28	15	32
16-E0916510	898	22	46	49	96	9	15	12	21
17-E0916511	693	9	21	21	26	4	10	7	13
18-E0916512	869	19	43	24	52	9	15	13	22
19-E0916513	688	12	23	23	27	5	11	8	15
20-E0916514	861	21	37	29	57	12	20	15	27

Table B.29: Flight 141006d AFT IGS: Maximum and Standard deviation of the deviation of shape from the reference for the SAR-runs in mm.

Run	N	max(X)	max(R)	max(Z)	max(A)	Sd(X)	Sd(R)	Sd(Z)	Sd(A)
6-E0915501	318	12	11	20	21	4	6	8	11
7-E0915502	11	2	2	4	4	2	1	2	3
8-E0915503	860	19	7	35	41	9	3	13	17
9-E0915504	1089	17	15	39	39	6	9	13	16
10-E0915505	861	25	9	25	45	10	4	14	18
11-E0915506	1031	19	15	23	30	12	6	8	15
12-E0915507	895	23	9	22	30	8	4	10	13
13-E0915508	973	29	10	36	37	12	4	16	20
14-E0915509	881	12	16	19	26	6	9	9	13
15-E0915510	942	19	9	26	31	9	4	12	16
16-E0915511	891	9	10	25	36	4	4	13	14
17-E0915512	1035	27	13	34	56	8	5	16	19

Table B.30: Flight 141006d FWD IGS: Maximum and Standard deviation of the deviation of shape from the reference for the SAR-runs in mm.

Run	N	max(X)	max(R)	max(Z)	max(A)	Sd(X)	Sd(R)	Sd(Z)	Sd(A)
6-E0915501	318	20	11	24	29	8	5	8	13
7-E0915502	11	1	1	2	3	1	1	1	2
8-E0915503	860	21	7	36	42	9	3	13	16
9-E0915504	1089	18	16	44	45	5	8	14	17
10-E0915505	861	30	9	35	51	13	5	19	24
11-E0915506	1031	37	9	24	43	12	3	10	16
12-E0915507	895	29	11	38	48	13	4	13	19
13-E0915508	973	27	11	24	34	13	4	11	18
14-E0915509	881	13	23	25	26	7	11	9	15
15-E0915510	942	22	13	32	57	9	6	9	14
16-E0915511	891	18	11	35	36	7	5	15	17
17-E0915512	1035	22	10	46	81	8	5	13	16

Table B.31: Flight 141006c AFT IGS: Maximum and Standard deviation of the deviation of shape from the reference for the SAR-runs in mm.

Run	N	max(X)	max(R)	max(Z)	max(A)	Sd(X)	Sd(R)	Sd(Z)	Sd(A)
6-E0914216	497	9	30	11	31	4	9	5	11
7-E0914217	12	3	2	2	4	2	2	2	3
8-E0914218	154	19	11	15	33	7	7	7	12
9-E0914219	158	10	9	14	25	5	7	7	11
10-E0914220	149	13	11	16	20	5	4	7	9
11-E0914221	179	20	19	27	34	10	9	11	17
12-E0914222	172	15	19	12	24	7	8	6	12
13-E0914223	180	20	11	34	40	10	5	16	19
14-E0914218	153	19	14	9	28	5	6	5	9
15-E0914219	187	13	10	15	17	4	5	6	9

Table B.32: Flight 141006c FWD IGS: Maximum and Standard deviation of the deviation of shape from the reference for the SAR-runs in mm.

Run	N	max(X)	max(R)	max(Z)	max(A)	Sd(X)	Sd(R)	Sd(Z)	Sd(A)
6-E0914216	497	9	21	11	23	3	9	5	11
7-E0914217	12	2	2	2	3	2	1	1	2
8-E0914218	154	11	13	7	22	4	4	4	7
9-E0914219	158	17	17	11	24	5	5	6	9
10-E0914220	149	26	16	11	36	6	5	5	9
11-E0914221	179	13	11	18	23	6	5	8	11
12-E0914222	172	12	14	13	20	5	5	6	9
13-E0914223	180	16	13	20	29	5	4	8	11
14-E0914218	153	15	13	12	22	5	7	5	10
15-E0914219	187	9	8	12	12	3	3	4	6

Table B.33: Flight 141006b AFT IGS: Maximum and Standard deviation of the deviation of shape from the reference for the SAR-runs in mm.

Run	N	max(X)	max(R)	max(Z)	max(A)	Sd(X)	Sd(R)	Sd(Z)	Sd(A)
6-E0913502	1702	25	37	94	97	11	12	29	34
7-E0913502	229	12	10	21	26	6	5	8	11
8-E0913503	11	3	2	1	5	2	2	2	3
9-E0913504	704	32	17	19	38	12	8	9	17
10-E0913505	887	22	24	29	40	7	10	10	15
11-E0913506	657	42	24	43	70	17	10	25	32
12-E0913507	881	29	16	35	42	10	6	11	16
13-E0913508	709	18	53	51	87	6	12	16	21
14-E0913509	816	17	28	22	39	5	12	10	17
15-E0913510	706	11	21	38	41	5	9	13	16
16-E0913511	897	9	26	24	34	4	8	8	12
17-E0913512	876	20	17	46	54	9	5	23	25
18-E0913513	674	23	13	20	32	12	6	10	16
19-E0913514	840	11	15	29	35	4	6	11	14
20-E0913515	663	15	20	16	29	8	8	9	14
21-E0913516	812	27	18	24	35	13	7	10	18
22-E0913517	595	21	23	27	39	10	7	10	16
23-E0913518	640	13	11	20	27	6	5	11	13

Table B.34: Flight 141006b FWD IGS: Maximum and Standard deviation of the deviation of shape from the reference for the SAR-runs in mm.

Run	N	max(X)	max(R)	max(Z)	max(A)	Sd(X)	Sd(R)	Sd(Z)	Sd(A)
6-E0913502	1702	34	16	66	67	18	7	28	34
7-E0913502	229	12	11	14	18	5	5	7	10
8-E0913503	11	2	2	2	3	1	2	2	3
9-E0913504	704	18	18	56	72	7	4	8	12
10-E0913505	887	24	31	25	46	10	17	12	23
11-E0913506	657	21	17	26	42	8	5	12	15
12-E0913507	881	21	16	28	31	10	7	10	16
13-E0913508	709	37	31	66	90	7	13	17	23
14-E0913509	816	11	27	29	35	4	10	11	16
15-E0913510	706	16	53	58	63	5	9	14	17
16-E0913511	897	9	19	21	26	4	8	8	12
17-E0913512	876	21	13	33	57	9	5	23	25
18-E0913513	674	38	16	90	97	12	9	16	22
19-E0913514	840	24	13	27	37	12	6	12	18
20-E0913515	663	14	13	20	28	7	5	9	13
21-E0913516	812	16	18	20	39	5	9	11	15
22-E0913517	595	19	15	22	31	7	8	12	16
23-E0913518	640	26	12	27	37	12	6	15	20

Table B.35: Flight 141006a AFT IGS: Maximum and Standard deviation of the deviation of shape from the reference for the SAR-runs in mm.

Run	N	max(X)	max(R)	max(Z)	max(A)	Sd(X)	Sd(R)	Sd(Z)	Sd(A)
1-E0912501	89	23	13	12	34	15	6	6	17
6-E0912502	325	22	35	62	76	11	16	16	25
7-E0912503	11	2	3	2	5	2	3	1	3
8-E0912504	709	30	43	81	138	13	19	24	33
9-E0912505	894	30	32	39	54	11	15	18	25
10-E0912506	733	30	32	47	63	11	15	20	28
11-E0912507	843	24	35	45	66	12	14	19	26
12-E0912508	261	27	41	55	85	10	17	18	26
13-E0912508	603	32	18	38	52	14	7	19	25
14-E0912509	916	28	15	42	54	14	6	17	22
15-E0912510	691	28	16	28	38	12	7	14	20
16-E0912511	870	22	12	28	38	8	6	8	13
17-E0912512	834	24	9	63	64	8	4	15	17
18-E0912513	748	52	12	25	58	10	6	11	16
19-E0912514	908	22	14	28	33	8	7	8	14
20-E0912515	720	24	13	18	29	10	4	7	13
21-E0912516	836	16	25	28	38	8	7	7	13
22-E0912517	231	12	14	11	18	6	7	5	11
23-E0912517	602	31	28	38	48	17	14	14	26
24-E0912518	795	18	9	13	28	11	4	5	13
25-E0912519	704	19	15	15	25	6	5	6	10

Table B.36: Flight 141006a FWD IGS: Maximum and Standard deviation of the deviation of shape from the reference for the SAR-runs in mm.

Run	N	max(X)	max(R)	max(Z)	max(A)	Sd(X)	Sd(R)	Sd(Z)	Sd(A)
1-E0912501	89	22	9	28	32	8	4	14	16
6-E0912502	325	14	20	36	44	7	11	11	17
7-E0912503	11	2	4	2	4	2	2	2	3
8-E0912504	709	25	42	121	173	15	17	22	32
9-E0912505	894	22	24	33	34	8	12	13	20
10-E0912506	733	23	36	95	117	11	18	13	25
11-E0912507	843	26	29	30	44	9	14	13	21
12-E0912508	261	14	13	15	28	6	7	6	11
13-E0912508	603	38	21	93	130	15	11	23	30
14-E0912509	916	25	15	48	54	12	6	17	22
15-E0912510	691	24	22	25	41	11	11	11	19
16-E0912511	870	25	12	32	46	10	6	10	15
17-E0912512	834	20	10	29	29	9	4	11	15
18-E0912513	748	23	17	28	53	11	7	10	17
19-E0912514	908	52	23	39	65	10	8	11	16
20-E0912515	720	20	10	17	30	8	4	9	13
21-E0912516	836	20	17	24	27	10	6	6	13
22-E0912517	231	12	13	11	20	6	8	6	11
23-E0912517	602	25	26	30	39	13	11	12	21
24-E0912518	795	18	15	16	24	10	5	6	13
25-E0912519	704	29	14	22	29	13	6	6	15

Table B.37: Flight 141003b AFT IGS: Maximum and Standard deviation of the deviation of shape from the reference for the SAR-runs in mm.

Run	N	max(X)	max(R)	max(Z)	max(A)	Sd(X)	Sd(R)	Sd(Z)	Sd(A)
6-E0911502	239	22	14	38	57	11	7	13	19
7-E0911503	11	4	3	4	8	3	3	3	5
8-E0911504	580	18	11	19	30	8	7	9	14
9-E0911505	487	12	11	21	23	5	5	8	11
10-E0911506	541	25	23	39	53	13	10	11	20
11-E0911507	485	19	19	18	28	6	8	7	12
12-E0911508	569	10	20	15	26	7	10	6	13
13-E0911509	476	7	11	16	17	3	4	4	6
14-E0911510	501	14	17	11	34	6	11	6	14
15-E0911511	500	12	11	14	23	7	5	5	10
16-E0911512	551	16	13	22	22	7	4	11	14
17-E0911513	536	13	9	16	22	7	5	7	11
18-E0911514	531	12	10	17	19	6	5	7	10
19-E0911515	533	16	6	12	17	7	2	5	9
20-E0911516	416	17	8	12	33	15	4	6	16
21-E0911517	487	9	9	15	25	7	4	5	9
22-E0911518	485	9	35	46	68	5	8	9	13
23-E0911519	489	16	8	26	28	11	4	8	14

Table B.38: Flight 141003b FWD IGS: Maximum and Standard deviation of the deviation of shape from the reference for the SAR-runs in mm.

Run	N	max(X)	max(R)	max(Z)	max(A)	Sd(X)	Sd(R)	Sd(Z)	Sd(A)
6-E0911502	239	11	8	22	30	5	5	10	12
7-E0911503	11	3	2	3	4	2	2	2	3
8-E0911504	580	19	11	19	25	7	6	8	12
9-E0911505	487	9	11	14	20	5	4	6	9
10-E0911506	541	24	19	36	70	13	11	12	20
11-E0911507	485	11	11	14	27	5	5	6	9
12-E0911508	569	9	8	19	19	4	4	6	8
13-E0911509	476	6	15	10	17	3	6	4	8
14-E0911510	501	9	10	9	17	4	5	5	9
15-E0911511	500	12	12	14	23	7	5	6	10
16-E0911512	551	12	10	26	26	5	5	11	13
17-E0911513	536	11	9	17	23	7	5	7	11
18-E0911514	531	12	9	16	18	6	4	6	10
19-E0911515	533	10	7	12	12	5	3	5	7
20-E0911516	416	24	13	14	32	14	6	7	17
21-E0911517	487	8	13	13	24	3	8	5	10
22-E0911518	485	15	17	14	24	8	10	8	15
23-E0911519	489	8	12	21	26	4	8	10	13

Table B.39: Flight 141003a AFT IGS: Maximum and Standard deviation of the deviation of shape from the reference for the SAR-runs in mm.

Run	N	max(X)	max(R)	max(Z)	max(A)	Sd(X)	Sd(R)	Sd(Z)	Sd(A)
6-E0910602	335	14	24	23	28	6	14	7	17
7-E0910603	11	2	2	1	4	1	2	1	2
8-E0910604	787	21	53	31	55	11	23	13	29
9-E0910605	811	15	26	29	43	8	12	13	19
10-E0910606	748	9	33	18	33	5	11	8	15
11-E0910607	779	16	18	19	26	6	9	10	14
16-E0910408	374	15	12	26	32	6	5	11	14
17-E0910409	11	1	1	4	6	1	1	4	4
18-E0910410	855	16	24	30	39	9	10	12	18
19-E0910411	699	18	21	41	45	7	8	17	20
24-E0910412	232	13	9	25	31	5	5	10	13
25-E0910413	11	3	4	2	5	2	2	1	3
26-E0910414	210	9	11	38	39	5	5	14	16
27-E0910415	176	18	7	30	36	7	4	12	15
28-E0910416	188	22	17	20	41	13	7	13	19
29-E0910417	178	10	9	18	20	4	4	9	11
34-E0910418	220	39	22	47	62	18	7	15	25
35-E0910419	12	5	6	6	9	4	4	5	7
36-E0910420	182	22	49	72	202	22	19	51	59
37-E0910421	174	20	9	31	44	8	5	11	14
38-E0910422	184	24	15	49	52	11	7	21	24
39-E0910423	171	13	10	28	63	6	7	15	18

Table B.40: Flight 141003a FWD IGS: Maximum and Standard deviation of the deviation of shape from the reference for the SAR-runs in mm.

Run	N	max(X)	max(R)	max(Z)	max(A)	Sd(X)	Sd(R)	Sd(Z)	Sd(A)
6-E0910602	335	15	15	15	23	5	8	5	11
7-E0910603	11	2	1	3	4	1	1	2	3
8-E0910604	787	20	36	25	38	8	17	12	22
9-E0910605	811	12	19	29	50	7	9	15	19
10-E0910606	748	11	20	17	23	5	11	8	14
11-E0910607	779	12	22	21	29	5	7	9	12
16-E0910408	374	15	10	23	24	6	4	10	12
17-E0910409	11	4	2	1	4	2	2	1	3
18-E0910410	855	15	23	31	33	6	8	11	15
19-E0910411	699	25	31	55	62	12	11	20	25
24-E0910412	232	17	14	20	25	9	6	9	14
25-E0910413	11	2	2	6	7	2	1	4	4
26-E0910414	210	19	9	29	35	6	6	11	14
27-E0910415	176	14	15	20	27	8	4	9	12
28-E0910416	188	18	17	31	37	10	7	12	18
29-E0910417	178	13	11	28	29	7	5	10	13
34-E0910418	220	25	13	29	53	14	6	14	20
35-E0910419	12	2	2	8	8	1	2	5	6
36-E0910420	182	21	17	30	37	9	6	12	16
37-E0910421	174	15	15	23	30	6	5	10	13
38-E0910422	184	26	14	35	49	13	8	19	25
39-E0910423	171	25	9	22	30	11	4	10	16

Table B.41: Flight 141001a AFT IGS: Maximum and Standard deviation of the deviation of shape from the reference for the SAR-runs in mm.

Run	N	max(X)	max(R)	max(Z)	max(A)	Sd(X)	Sd(R)	Sd(Z)	Sd(A)
5-E0904201	349	24	14	20	35	15	7	9	19
6-E0904202	11	2	1	1	4	2	1	1	2
7-E0904203	537	13	17	28	31	6	7	16	18
8-E0904204	920	14	9	31	35	5	3	12	14
9-E0904205	642	29	10	27	30	9	3	10	14
10-E0904206	940	19	9	23	30	9	4	10	14
11-E0904207	685	12	15	77	164	5	6	19	21
12-E0904208	913	27	19	40	48	13	9	13	20
13-E0904209	667	27	12	52	85	11	6	14	18
14-E0904210	917	19	23	26	46	9	12	10	18
15-E0904211	937	21	23	40	50	12	11	21	26
16-E0904212	682	38	19	55	70	12	8	12	19
17-E0904213	948	38	26	50	100	16	11	25	32
18-E0904214	688	26	26	83	90	9	12	28	31
19-E0904215	968	27	35	47	55	13	11	19	26
24-E0904216	57	9	5	27	28	4	4	9	10
25-E0904217	11	1	2	8	9	1	2	6	6
26-E0904218	170	15	9	43	55	9	5	19	22
27-E0904219	242	20	14	33	38	9	7	13	17
28-E0904220	193	10	9	41	46	6	5	14	16
29-E0904221	261	14	14	23	30	6	10	11	16

Table B.42: Flight 141001a FWD IGS: Maximum and Standard deviation of the deviation of shape from the reference for the SAR-runs in mm.

Run	N	max(X)	max(R)	max(Z)	max(A)	Sd(X)	Sd(R)	Sd(Z)	Sd(A)
5-E0904201	349	20	8	19	38	15	3	8	17
6-E0904202	11	2	2	2	4	2	2	1	3
7-E0904203	537	14	15	22	27	6	6	12	15
8-E0904204	920	16	12	33	34	7	5	12	15
9-E0904205	642	20	9	22	29	6	4	9	11
10-E0904206	940	25	16	41	42	15	6	11	19
11-E0904207	685	14	14	32	36	6	6	13	16
12-E0904208	913	23	14	26	35	9	9	10	16
13-E0904209	667	21	15	28	42	13	8	15	21
14-E0904210	917	13	18	43	60	5	11	10	16
15-E0904211	937	19	24	45	58	8	12	17	22
16-E0904212	682	21	42	60	78	9	12	20	25
17-E0904213	948	30	24	44	58	14	11	16	24
18-E0904214	688	23	27	59	66	10	13	24	29
19-E0904215	968	22	20	51	54	8	10	16	20
24-E0904216	57	6	7	19	19	5	3	11	12
25-E0904217	11	4	2	13	13	2	3	8	9
26-E0904218	170	21	8	37	38	8	4	12	15
27-E0904219	242	19	13	20	27	11	8	7	15
28-E0904220	193	11	15	36	36	5	5	13	15
29-E0904221	261	30	12	29	37	12	7	15	20

Table B.43: Flight 130222a AFT IGS: Maximum and Standard deviation of the deviation of shape from the reference for the SAR-runs in mm.

Run	N	max(X)	max(R)	max(Z)	max(A)	Sd(X)	Sd(R)	Sd(Z)	Sd(A)
5-D0210235	837	20	17	37	44	8	6	15	18
6-D0210236	11	3	3	6	6	2	2	3	4
7-D0210237	250	16	8	25	30	9	4	8	13
8-D0210238	214	12	7	15	20	6	3	7	10
9-D0210239	220	8	10	27	35	4	4	11	12
10-D0210240	195	11	9	13	27	6	3	7	10
11-D0210241	209	5	9	24	26	2	4	13	13
12-D0210242	211	6	10	23	23	3	5	7	9
17-D0210245	937	24	12	53	55	9	5	16	19
18-D0210246	301	12	8	24	27	7	4	12	15
19-D0210247	1110	30	20	39	64	18	8	20	28
20-D0210248	966	15	35	50	51	8	14	16	23

Table B.44: Flight 130222a FWD IGS: Maximum and Standard deviation of the deviation of shape from the reference for the SAR-runs in mm.

Run	N	max(X)	max(R)	max(Z)	max(A)	Sd(X)	Sd(R)	Sd(Z)	Sd(A)
5-D0210235	837	20	21	50	55	8	6	14	17
6-D0210236	11	2	4	5	8	2	3	4	5
7-D0210237	250	11	12	25	27	6	4	10	13
8-D0210238	214	18	8	25	28	10	3	9	14
9-D0210239	220	9	9	20	22	4	4	8	9
10-D0210240	195	7	8	21	22	3	3	8	9
11-D0210241	209	7	8	31	31	3	4	9	10
12-D0210242	211	6	7	13	20	3	3	6	7
17-D0210245	937	19	10	58	60	9	4	15	18
18-D0210246	301	14	9	18	27	11	3	7	13
19-D0210247	1110	45	22	35	65	31	7	14	34
20-D0210248	966	19	26	47	58	15	14	23	30

Table B.45: Flight 130213c AFT IGS: Maximum and Standard deviation of the deviation of shape from the reference for the SAR-runs in mm.

Run	N	max(X)	max(R)	max(Z)	max(A)	Sd(X)	Sd(R)	Sd(Z)	Sd(A)
7-D0209503	1111	22	34	27	48	10	13	14	21
8-D0209504	1245	20	34	37	53	11	11	13	20
9-D0209505	1021	23	32	45	73	14	13	23	30
14-D0209512	1502	11	17	33	35	4	6	13	15
15-D0209511	1261	12	16	34	38	4	5	16	17
16-D0209506	1444	21	41	32	43	10	10	11	18
17-D0209507	1374	15	21	26	36	6	11	9	15
18-D0209508	1554	14	23	37	39	6	9	12	16
19-D0209509	1270	23	17	29	45	9	8	11	16
20-D0209510	1650	29	30	27	37	11	11	9	18

Table B.46: Flight 130213c FWD IGS: Maximum and Standard deviation of the deviation of shape from the reference for the SAR-runs in mm.

Run	N	max(X)	max(R)	max(Z)	max(A)	Sd(X)	Sd(R)	Sd(Z)	Sd(A)
7-D0209503	1111	30	33	30	46	11	12	15	22
8-D0209504	1245	27	31	42	53	10	12	20	25
9-D0209505	1021	34	34	51	67	10	12	19	24
14-D0209512	1502	10	15	32	33	4	5	12	14
15-D0209511	1261	10	16	27	32	4	5	12	14
16-D0209506	1444	20	34	35	38	8	9	11	16
17-D0209507	1374	13	20	25	31	4	9	9	13
18-D0209508	1554	16	19	33	39	6	7	12	15
19-D0209509	1270	15	22	42	45	7	11	14	19
20-D0209510	1650	27	25	31	44	9	8	9	15

Table B.47: Flight 130213b AFT IGS: Maximum and Standard deviation of the deviation of shape from the reference for the SAR-runs in mm.

Run	N	max(X)	max(R)	max(Z)	max(A)	Sd(X)	Sd(R)	Sd(Z)	Sd(A)
5-D0208409	835	20	12	32	42	12	5	15	20
6-D0208410	301	8	8	18	31	5	4	9	11
7-D0208411	1249	14	44	13	58	7	13	5	16
8-D0208412	1170	33	24	54	58	14	12	19	27
13-D0208625	704	11	12	22	22	5	4	8	11
14-D0208626	21	4	3	3	8	2	2	2	4
15-D0208627	366	17	9	14	19	6	3	5	9
16-D0208628	295	36	9	34	58	17	3	13	21
17-D0208629	341	17	17	39	43	8	9	14	18
18-D0208630	320	20	24	34	81	5	9	15	18

Table B.48: Flight 130213b FWD IGS: Maximum and Standard deviation of the deviation of shape from the reference for the SAR-runs in mm.

Run	N	max(X)	max(R)	max(Z)	max(A)	Sd(X)	Sd(R)	Sd(Z)	Sd(A)
5-D0208409	835	29	25	66	73	13	11	33	37
6-D0208410	301	11	14	39	62	6	9	23	25
7-D0208411	1249	46	25	21	55	9	12	10	18
8-D0208412	1170	42	32	40	58	11	14	13	22
13-D0208625	704	17	10	37	48	8	5	12	15
14-D0208626	21	10	6	9	34	6	5	8	11
15-D0208627	366	16	8	18	20	8	3	7	11
16-D0208628	295	32	12	26	39	16	4	11	20
17-D0208629	341	15	12	28	29	4	5	9	11
18-D0208630	320	22	17	42	44	9	9	13	18

C

Example files

C.1 RTKLIB PPP configuration files

conf095.conf

```
# rtkpost options (2016/06/09 13:56:43, v.2.4.3 b8)

pos1-posmode      =ppp-kine # (0: single, 1: dgps, 2: kinematic, 3: static, 4: movingbase, 5: fixed, 6:
    ppp-kine, 7: ppp-static, 8: ppp-fixed)
pos1-frequency    =l1+l2 # (1: l1, 2: l1+l2, 3: l1+l2+l5, 4: l1+l5)
pos1-soltype      =combined # (0: forward, 1: backward, 2: combined)
pos1-elmask       =5 # (deg)
pos1-snrmask_r    =off # (0: off, 1: on)
pos1-snrmask_b    =off # (0: off, 1: on)
pos1-snrmask_L1   =0,0,0,0,0,0,0,0,0,0
pos1-snrmask_L2   =0,0,0,0,0,0,0,0,0,0
pos1-snrmask_L5   =0,0,0,0,0,0,0,0,0,0
pos1-dynamics     =on # (0: off, 1: on)
pos1-tidecorr     =off # (0: off, 1: on, 2: ot1)
pos1-ionoopt      =dual-freq # (0: off, 1: brdc, 2: sbas, 3: dual-freq, 4: est-stec, 5: ionex-tec, 6: qzs-
    brdc, 7: qzs-lex, 8: stec)
pos1-tropopt      =est-ztd # (0: off, 1: saas, 2: sbas, 3: est-ztd, 4: est-ztdgrad, 5: ztd)
pos1-sateph       =precise # (0: brdc, 1: precise, 2: brdc+sbas, 3: brdc+ssrapc, 4: brdc+ssrcom)
pos1-posopt1      =on # (0: off, 1: on)
pos1-posopt2      =off # (0: off, 1: on)
pos1-posopt3      =off # (0: off, 1: on, 2: precise)
pos1-posopt4      =off # (0: off, 1: on)
pos1-posopt5      =off # (0: off, 1: on)
pos1-posopt6      =off # (0: off, 1: on)
pos1-exclsats     = # (prn ...)
pos1-navsys       =1 # (1: gps+2: sbas+4: glo+8: gal+16: qzs+32: comp)
pos2-armode       =off # (0: off, 1: continuous, 2: instantaneous, 3: fix-and-hold)
pos2-gloarmode    =on # (0: off, 1: on, 2: autocal)
pos2-bdsarmode    =on # (0: off, 1: on)
pos2-arthres      =3
pos2-arthres1     =0.9999
pos2-arthres2     =0.25
pos2-arthres3     =0.1
pos2-arthres4     =0.05
pos2-arlockcnt    =0
pos2-arelmask     =0 # (deg)
pos2-arminfix     =10
pos2-armaxiter    =1
pos2-elmaskhold   =0 # (deg)
pos2-aroutcnt     =5
pos2-maxage       =30 # (s)
pos2-syncsol      =off # (0: off, 1: on)
pos2-slipthres    =0.05 # (m)
pos2-rejionno     =30 # (m)
pos2-rejgdop      =30
pos2-niter        =1
pos2-baselen      =0 # (m)
pos2-basesig      =0 # (m)
out-solformat     =llh # (0: llh, 1: xyz, 2: enu, 3: nmea)
out-outhead       =on # (0: off, 1: on)
out-outopt        =on # (0: off, 1: on)
out-timesys       =gpst # (0: gpst, 1: utc, 2: jst)
out-timeform      =tow # (0: tow, 1: hms)
out-timendec      =6 # (deg, 1: dms)
out-degform       =deg # (0: deg, 1: dms)
out-fieldsep      =
out-height        =ellipsoidal # (0: ellipsoidal, 1: geodetic)
out-geoid         =internal # (0: internal, 1: egm96, 2: egm08_2.5, 3: egm08_1, 4: gsi2000)
out-solstatic     =all # (0: all, 1: single)
out-nmeaintv1     =0 # (s)
out-nmeaintv2     =0 # (s)
out-outstat       =off # (0: off, 1: state, 2: residual)
stats-eratio1     =300
stats-eratio2     =300
stats-errphase    =0.003 # (m)
stats-errphaseel  =0.003 # (m)
stats-errphasebl  =0 # (m/10km)
```

```

stats-errdoppler =10 # (Hz)
stats-stdbbias =30 # (m)
stats-stdiono =0.03 # (m)
stats-stdtrop =0.3 # (m)
stats-prnaccelh =10 # (m/s^2)
stats-prnaccelv =10 # (m/s^2)
stats-prnbias =0.0001 # (m)
stats-prniono =1000 # (m)
stats-prntrop =1e-06 # (m)
stats-prnpos =0 # (m)
stats-clkstabil =5e-12 # (s/s)
ant1-postype =11h # (0:11h,1:xyz,2:single,3:posfile,4:rinxhead,5:rtcm)
ant1-pos1 =90 # (deg|m)
ant1-pos2 =0 # (deg|m)
ant1-pos3 =-6335367.6285 # (m|m)
ant1-anttype =
ant1-antdele =0 # (m)
ant1-antdeln =0 # (m)
ant1-antdelu =0 # (m)
ant2-postype =11h # (0:11h,1:xyz,2:single,3:posfile,4:rinxhead,5:rtcm)
ant2-pos1 =90 # (deg|m)
ant2-pos2 =0 # (deg|m)
ant2-pos3 =-6335367.6285 # (m|m)
ant2-anttype =
ant2-antdele =0 # (m)
ant2-antdeln =0 # (m)
ant2-antdelu =0 # (m)
misc-timeinterp =off # (0:off,1:on)
misc-sbasatsel =0 # (0:all)
misc-rnxopt1 =
misc-rnxopt2 =
misc-pppopt =
file-satantfile =../download/igs08.atx
file-rcvantfile =../download/igs08.atx
file-staposfile =
file-geoidfile =
file-ionofile =
file-dcbfile =
file-eopfile =
file-blqfile =
file-tempdir =
file-geexefile =
file-solstatfile =
file-tracefile =

```


C.2 RTKLIB FBL configuration file

bconf329.conf

```
# rtkpost options (2016/06/21 12:52:48, v.2.4.3 b10)

pos1-posmode      =movingbase # (0:single,1:dgps,2:kinematic,3:static,4:movingbase,5:fixed,6:
  ppp-kinematic,7:ppp-static,8:ppp-fixed)
pos1-frequency    =l1+l2      # (1:l1,2:l1+l2,3:l1+l2+l5,4:l1+l5)
pos1-soltype      =combined    # (0:forward,1:backward,2:combined)
pos1-elmask       =5          # (deg)
pos1-snrmask_r    =off         # (0:off,1:on)
pos1-snrmask_b    =off         # (0:off,1:on)
pos1-snrmask_L1   =0,0,0,0,0,0,0,0
pos1-snrmask_L2   =0,0,0,0,0,0,0,0
pos1-snrmask_L5   =0,0,0,0,0,0,0,0
pos1-dynamics     =off         # (0:off,1:on)
pos1-tidecorr     =off         # (0:off,1:on,2:otl)
pos1-ionoopt      =brdc        # (0:off,1:brdc,2:sbas,3:dual-freq,4:est-stec,5:ionex-tec,6:qzs-
  brdc,7:qzs-lex,8:stec)
pos1-tropopt      =saas        # (0:off,1:saas,2:sbas,3:est-ztd,4:est-ztdgrad,5:ztd)
pos1-sateph       =brdc        # (0:brdc,1:precise,2:brdc+sbas,3:brdc+ssrapc,4:brdc+ssrcom)
pos1-posopt1      =off         # (0:off,1:on)
pos1-posopt2      =off         # (0:off,1:on)
pos1-posopt3      =off         # (0:off,1:on,2:precise)
pos1-posopt4      =off         # (0:off,1:on)
pos1-posopt5      =off         # (0:off,1:on)
pos1-posopt6      =off         # (0:off,1:on)
pos1-exclsats     =            # (prn ...)
pos1-navsys       =1          # (1:gps+2:sbas+4:glo+8:gal+16:qzs+32:comp)
pos2-armode       =fix-and-hold # (0:off,1:continuous,2:instantaneous,3:fix-and-hold)
pos2-gloarmode    =off         # (0:off,1:on,2:autocal)
pos2-bdsarmode    =off         # (0:off,1:on)
pos2-arthres      =3          #
pos2-arthres1     =0.9999
pos2-arthres2     =0.25
pos2-arthres3     =0.1
pos2-arthres4     =0.05
pos2-arlockcnt    =0
pos2-arelmask     =0          # (deg)
pos2-arminfix     =5
pos2-armaxiter    =1
pos2-elmaskhold   =0          # (deg)
pos2-aroutcnt     =5
pos2-maxage       =30         # (s)
pos2-syncsol      =off         # (0:off,1:on)
pos2-slipthres    =0.05      # (m)
pos2-rejionno     =30         # (m)
pos2-rejgdop      =30
pos2-niter        =2
pos2-baselen      =1.18      # (m)
pos2-basesig      =0.07      # (m)
out-solformat     =enu        # (0:llh,1:xyz,2:enu,3:nmea)
out-outhead       =on         # (0:off,1:on)
out-outopt        =on         # (0:off,1:on)
out-timesys       =gpst       # (0:gpst,1:utc,2:jst)
out-timeform      =tow        # (0:tow,1:hms)
out-timendec      =2
out-degform       =deg        # (0:deg,1:dms)
out-fieldsep      =
out-height        =ellipsoidal # (0:ellipsoidal,1:geodetic)
out-geoid         =internal   # (0:internal,1:egm96,2:egm08_2.5,3:egm08_1,4:gsi2000)
out-solstatic     =all        # (0:all,1:single)
out-nmeaintv1     =0          # (s)
out-nmeaintv2     =0          # (s)
out-outstat       =off         # (0:off,1:state,2:residual)
stats-eratio1     =100
stats-eratio2     =100
stats-errphase    =0.003      # (m)
stats-errphaseel  =0.003      # (m)
stats-errphasebl  =0          # (m/10km)
stats-errdoppler  =10         # (Hz)
stats-stdbias     =30         # (m)
stats-stdiono     =0.03       # (m)
stats-stdtrop     =0.3        # (m)
stats-prnacclh    =10         # (m/s^2)
stats-prnacclv    =10         # (m/s^2)
stats-prnbias     =0.0001     # (m)
stats-prniono     =0.001      # (m)
stats-prntrop     =0.0001     # (m)
stats-prnpos      =0          # (m)
stats-clkstabil   =5e-12     # (s/s)
ant1-postype      =llh        # (0:llh,1:xyz,2:single,3:posfile,4:rinxhead,5:rtcm)
ant1-pos1         =90         # (deg|m)
ant1-pos2         =0          # (deg|m)
ant1-pos3         =-6335367.6285 # (m|m)
ant1-anttype      =
ant1-antdele      =0          # (m)
ant1-antdeln      =0          # (m)
ant1-antdelu      =0          # (m)
ant2-postype      =single     # (0:llh,1:xyz,2:single,3:posfile,4:rinxhead,5:rtcm)
ant2-pos1         =0          # (deg|m)
```

```
ant2-pos2      =0      # (deg|m)
ant2-pos3      =0      # (m|m)
ant2-anttype   =
ant2-antdele   =0      # (m)
ant2-antdeln   =0      # (m)
ant2-antdelu   =0      # (m)
misc-timeinterp =off    # (0: off , 1: on)
misc-sbasatsel =0      # (0: all)
misc-rnxopt1   =
misc-rnxopt2   =
misc-pppopt    =
file-satantfile =C:\Users\u030881\PPP\V07\download\ngs08.atx
file-rcvantfile =
file-staposfile =
file-geoidfile =
file-ionofile  =
file-dcbfile   =
file-eopfile   =
file-blqfile   =
file-tempdir   =
file-geexefile =
file-solstatfile =
file-tracefile =
```

C.3 Rinex .obs file

AFT1007b.obs

2.10 OBSERVATION DATA M (MIXED)										RINEX VERSION / TYPE	
RTKCONV 2.4.3 b8 20160331 151155 UTC										PGM / RUN BY / DATE	
log: C:\Users\u030881\PPP\V07\input-data\2014-10-07\AFT100										COMMENT	
format: Javad										COMMENT	
										MARKER NAME	
										MARKER NUMBER	
										OBSERVER / AGENCY	
										REC # / TYPE / VERS	
										ANT # / TYPE	
										APPROX POSITION XYZ	
										ANTENNA: DELTA H/E/N	
										WAVELENGTH FACT L1/2	
3225226.7781	0.0000	903907.2607	0.0000	5409758.1076	0.0000					S2# / TYPES OF OBSERV	
1	1									# / TYPES OF OBSERV	
10	C1	L1	D1	S1	P1	C2	L2	D2		TIME OF FIRST OBS	
	P2									TIME OF LAST OBS	
2014	10	7	10	38	16.90000000		GPS			END OF HEADER	
2014	10	7	11	37	38.50000000		GPS				
14	10	7	10	38	16.90000000	0	12G21G27G29G26G	3G	8G	7G16G15G18G19G22	
21335901.925		112120923.308				902.453			39.000	21335900.771	
		87366955.013				703.209			31.500	21335908.152	
21683240.838		113946205.244				4057.779			38.750	21683240.547	
21683251.720		88789250.791				3161.901			32.750	21683250.353	
24512827.006		128815783.215				-1907.131			38.250	24512826.865	
24512841.102		100375939.059				-1486.064			29.000	24512841.030	
24159405.952		126958551.241				3241.878			35.000		
22188705.966		116602438.151				-1354.678			39.750	22188705.519	
		90859045.708				-1055.598			26.250	22188714.162	
23213161.649		121985990.777				1566.787			38.250	23213161.361	
		95054016.774				1220.873			27.000	23213172.357	
23995784.928		126098700.622				2619.708			40.750	23995784.616	
23995793.001		98258729.343				2041.366			24.750	23995792.399	
21075958.960		110754916.008				883.925			35.750	21075958.484	
		86302529.135				688.782			32.000	21075966.173	
24884725.414		130770123.691				4134.307			33.500	24884727.911	
24884739.513		101898801.633				3221.554			21.750	24884739.537	
22409413.836		117762266.419				3754.781			44.750	22409412.451	
		91762805.202				2925.767			32.500	22409421.792	
24074119.375		126510358.959				5155.920			46.250	24074117.876	
		98579497.615				4017.633			31.750	24074128.018	
24322807.205		127817228.173				5194.990			41.750	24322806.908	
		99597843.190				4048.056			24.250	24322818.837	
14	10	7	10	38	17.00000000	0	12G21G27G29G26G	3G	8G	7G16G15G18G19G22	
21335884.930		112120833.062				902.440			38.500	21335883.563	
		87366884.691				703.212			31.250	21335890.980	
21683163.491		113945799.452				4057.846			39.000	21683163.278	
21683174.590		88788934.592				3161.932			32.250	21683173.312	
24512863.353		128815973.924				-1907.093			38.500	24512863.077	
24512877.560		100376087.659				-1486.018			28.500	24512877.128	
24159344.144		126958227.003				3242.174			34.750		
22188731.748		116602573.627				-1354.716			39.500	22188730.992	
		90859151.271				-1055.600			26.250	22188740.049	
23213132.188		121985834.073				1566.916			38.500	23213131.450	
		95053894.661				1221.038			27.000	23213141.736	
23995734.943		126098438.667				2619.541			41.000	23995734.509	
23995743.664		98258525.227				2041.203			24.750	23995742.591	
21075942.343		110754827.599				884.007			35.500	21075941.671	
		86302460.243				688.853			32.000	21075949.571	
24884646.796		130769710.254				4134.332			34.000	24884649.027	
24884660.647		101898479.476				3221.546			21.750	24884660.902	
22409342.455		117761890.950				3754.725			44.750	22409340.680	
		91762512.617				2925.807			32.500	22409349.917	
24074021.220		126509843.394				5155.759			46.500	24074019.898	
		98579095.876				4017.497			31.750	24074030.088	
24322708.195		127816708.663				5195.096			41.750	24322708.103	
		99597438.384				4048.086			24.250	24322720.004	

C.4 RTKLIB .pos file

AFT1007b.pos

```
% program      : RTKLIB ver.2.4.3
% inp file     : ..\input-data\2014-10-07\AFT1007b.obs
% inp file     : ..\input-data\2014-10-07\AFT1007b.nav
% inp file     : ..\download\2014-10-07\igs18132.clk_30s
% inp file     : ..\download\2014-10-07\igs18132.sp3
% obs start    : 2014/10/07 10:38:17.0 GPST (week1813 211097.0s)
% obs end      : 2014/10/07 11:37:38.0 GPST (week1813 214658.0s)
% pos mode     : ppp-kinematic
% solution     : combined
% elev mask    : 5.0 deg
% dynamics     : on
% tidecorr     : off
% tropo opt    : est ztd
% ephemeris    : precise
% antennal     : ( 0.0000 0.0000 0.0000)
%
% (lat/lon/height=WGS84/ellipsoidal,Q=1:fix,2:float,3:sbas,4:dgps,5:single,6:ppp,ns=# of
  satellites)
% GPST
% sdn(m) sdeu(m) sdun(m) age(s) ratio
1813 211096.999510 58.407900943 15.656148533 75.5406 6 10 0.0334 0.0262 0.0475
    0.0219 0.0167 0.0178 0.00 0.0
1813 211097.099510 58.407900938 15.656148542 75.5409 6 10 0.0333 0.0261 0.0475
    0.0218 0.0166 0.0178 0.00 0.0
1813 211097.199510 58.407900929 15.656148532 75.5431 6 10 0.0333 0.0261 0.0474
    0.0218 0.0166 0.0178 0.00 0.0
1813 211097.299510 58.407900964 15.656148563 75.5424 6 10 0.0332 0.0260 0.0474
    0.0217 0.0166 0.0177 0.00 0.0
1813 211097.399510 58.407900957 15.656148577 75.5485 6 10 0.0333 0.0261 0.0473
    0.0217 0.0165 0.0177 0.00 0.0
1813 211097.499511 58.407900972 15.656148552 75.5458 6 10 0.0332 0.0261 0.0472
    0.0216 0.0165 0.0177 0.00 0.0
1813 211097.599511 58.407900975 15.656148568 75.5444 6 10 0.0332 0.0260 0.0471
    0.0217 0.0165 0.0176 0.00 0.0
1813 211097.699511 58.407900953 15.656148527 75.5477 6 10 0.0331 0.0260 0.0471
    0.0216 0.0164 0.0177 0.00 0.0
```